DOCTORAL (PHD) DISSERTATION

DOI:10.18136/PE.2023.832

Numerical and Experimental Investigation of Radon and Progeny in Residential Areas

Written by

Mohammademad Adelikhah

Doctoral School of Chemistry and Environmental Sciences

Supervisor:

Dr. Tibor Kovács (Ph.D)

University of Pannonia

Institute of Radiochemistry and Radioecology, Research Centre for Biochemical, Environmental and Chemical Engineering

Veszprém

2023

Numerical and Experimental Investigation of Radon and Progeny in Residential Areas

Thesis for obtaining a Ph.D. degree in
the Doctoral School of Chemistry and Environmental Sciences of the University of Pannonia, Institute of Radiochemistry and Radioecology, Research Centre for Biochemical, Environmental and Chemical Engineering

Written by:

Mohammademad Adelikhah

Supervisor:
Dr. Tibor Kovács (Ph.D)

Propose acceptance (yes / no) .....
Dr. Tibor Kovács

As reviewer, I propose acceptance of the thesis:

Name of reviewer: ..... yes / no .....
(reviewer)

Name of reviewer: ..... yes / no .....
(reviewer)

The PhD-candidate has achieved..... % at the public discussion

Veszprém/Keszthely, ...

….....
(Chairman of the Committee)

The grade of the PhD diploma ..... (.....%)

Veszprém/Keszthely, ...

.....
(Chairman of UDHC)

Numerical and Experimental Investigation of Radon and Progeny in Residential Areas

by
Mohammademad Adelikhah

Supervisor:
Dr. Tibor Kovács

Abstract

Studies on indoor radon and thoron exposure as well as naturally occurring radionuclide content in building materials are of particular interest because possible human exposure to natural background radiation and constitutes the largest source of radiation exposure to the public. Due to the lack of data concerning the indoor radon and thoron concentrations in the confined areas in IRAN and also limited information about the radionuclide activity concentrations of building materials, it makes the author to carry out a new comprehensive radiological survey in some parts of Iran to identify the potential radiation exposure where there is no such data available. Therefore, this thesis is divided into 3 major parts: A) Measuring the indoor radon and thoron concentrations in the thermal spas of Dehloran as well as NORM concentrations in soil and ^{226}Ra concentrations in water samples of Dehloran, B) Calculating the annual committed effective dose of Mashhad inhabitant caused by the inhalation of radon and thoron and consequently generate the indoor radon maps of Mashhad city by ArcGIS software over a grid of 1×1 km by applying different interpolation techniques to increase public awareness of environmental radioactivity and C) assessment of gamma-ray emitters in building materials and the estimated exposure to indoor gamma radiation from the materials in two part of Iran including HNBRA of Mahallat, and Semnan Province.

The indoor radon concentrations in the thermal baths were measured to be between 1880±410 and 2450±530 Bq/m^3 and the radon concentrations in the spa galleries were measured to be between 790±135 and 1050±120 Bq/m^3, however, thoron concentrations were below the detection limit. The results of dissolved ^{226}Ra in water samples from different thermal baths were approximated to also be 0.42±0.20 Bq/l. The activity concentrations of three major naturally occurring radionuclides in soil samples were also measured to be 101±8 to 240±12, 276±7 to 322±12 and 20±7 to 80±10 Bq/kg for ^{40}K, ^{226}Ra and ^{228}Ra, respectively. Higher activity concentrations of ^{226}Ra and ^{228}Ra were recorded in soil samples irrigated with hot spring water.

Regarding indoor radon and thoron concertation in Mashhad dwellings, in the winter, indoor radon concentrations measured between 75±11 to 376±24 Bq/m^3 whereas indoor thoron concentrations ranged from below the LLD to 166±10 Bq/m^3, while radon and thoron concentrations in summer fell between 50±11 and 305±24 Bq/m^3 and from

below the LLD to 122±10 Bq/m^3, respectively. The corresponding annual average effective dose was estimated to be 3.7±0.5 mSv/year. The soil-gas radon concentrations fell within the range from 1.07±0.28 to 8.02±0.65 kBq/m^3.

In case of radioactivity in studied building materials from Semnan, the activity concentrations of ^{226}Ra, ^{232}Th, and ^{40}K varied from 6.7±1 to 43.6±9, 5.9±1 to 60±11, and 28.5±3 to 1085±113 Bq/kg with averages of 26.8±5, 22.7±4, and 322.4±4 Bq/kg. In addition, for building materials of Mahallat HNBR, the activity of ^{232}Th, ^{226}Ra and ^{40}K were within the ranges from 18±3 to 44±10 Bq/kg, 22±5 to 53±14 Bq/kg and 82±18 to 428±79 Bq/kg, respectively. Consequently, it can be concluded that most results fell below the average values for building materials worldwide, therefore, in terms of their inhabitants, buildings constructed from such materials are radiologically safe. The results draw attention to the use of granite, brick, ceramic, and tile in the construction of dwellings. RESRAD-BUILD computer code was used to estimate the contribution of corresponding building materials towards indoor external and internal doses received by inhabitants in Mahallat in a standard model room for three different case studies using different compositions of basic building materials. Maximum effective dose rates of between 504 and 1433 μSv/year were calculated in the second case study, tiled cement floor. The highest external and radon doses were also calculated to be 369 and 1064 μSv, respectively.

This work also aimed to develop and predict the thoron distribution profile inside the RRI thoron calibration chamber for different configuration of inlet and outlet as well as flow rates by applying the CFD technique regarding SSNTDs calibration for long-term indoor exposure of thoron concentration. The results showed that the applicability of thoron chamber for the purposes of calibrating monitoring instruments. Furthermore, CFD-based predictions are in strong agreement with the results from experimental and analytical models due to the corresponding appreciable relative deviation (with a maximum of approximately 9%).

مطالعات بر روی قرار گرفتن در معرض رادون و تورون داخلی و همچنین محتوای رادیونوکلید طبیعی در مصالح ساختمانی از اهمیت ویژه ای برخوردار است، زیرا قرار گرفتن احتمالی انسان در برابر تشعشعات پس زمینه طبیعی است و بزرگترین منبع قرار گرفتن در معرض تشعشع برای عموم نیز میباشد. با توجه به فقدان اطلاعات در مورد غلظت رادون و تورون داخلی در ایران و همچنین اطلاعات محدود در مورد غلظت فعالیت رادیونوکلئید در مصالح ساختمانی، نگارنده را بر آن می دارد تا یک بررسی جامع رادیولوژیکی جدید در برخی از نقاط ایران برای شناسایی قرار گرفتن در معرض تابش بالقوه در مکانهایی که چنین داده ای در دسترس نیست، انجام دهد. بنابراین، این پایان نامه به 3 بخش عمده تقسیم می شود: الف) اندازه گیری غلظت رادون و تورون داخلی در آبگرم دهلران و همچنین غلظت NORM در خاک و غلظت Ra -226 در نمونه های آب دهلران، ب) محاسبه غلظت دوز موثر سالانه ساکنان شهر مشهد ناشی از استنشاق رادون و تورون و درنتیجه تولید نقشه‌های رادون داخل منازل شهر مشهد توسط نرم‌افزار ArcGIS در شبکه‌ای 1×1 کیلومتر با بکارگیری تکنیک‌های مختلف درون‌یابی برای افزایش آگاهی عمومی ازرادیواکتیویته محیطی. و ج) ارزیابی پرتوهای گاما در مصالح ساختمانی و برآورد قرار گرفتن در معرض تابش گامای داخلی از این مواد در دو شهر محلات و استان سمنان.

غلظت رادون داخل اتاق حمام‌های آبگرم بین 410±1880 و 530±2450 Bq/m^3 و غلظت رادون در گالری‌های آبگرم بین 135±790 و 1050±120 Bq/m^3 اندازه‌گیری شد، با این حال، غلظت تورن کمتر از حد تشخیص بود. نتایج غلظت Ra-226 محلول در نمونه های آب از حمام های مختلف نیز 0.42±0.20 Bq/l بود. غلظت فعالیت سه رادیونوکلئید اصلی طبیعی در نمونه‌های خاک نیز 8±101 تا 12±240، 7±276 تا 12±322 و 7±20 تا 10±80 Bq/kg برای K-40، Ra-228 و Ra-226 اندازه‌گیری شد. بدین ترتیب غلظت فعالیت بالاتر Ra-228 و Ra-226 در نمونه های خاک آبیاری شده با آب چشمه گرم ثبت شد.

درباره غلظت گاز رادون و تورون در خانه‌های مشهد، در فصل زمستان، غلظت رادون در داخل خانه بین 11±75 تا 24±376 Bq/m^3 اندازه‌گیری شد، در حالی که غلظت تورون از زیر LLD تا 10±166 Bq/m^3 بود. در حالی که غلظت رادون و تورون در تابستان به ترتیب بین 11±50 و 24±305 Bq/m^3 و از زیر LLD به 10±122 Bq/m^3 کاهش یافت. میانگین دوز موثر سالانه مربوطه 0.5±3.7 mSv/year برآورد شد. غلظت رادون خاک-گاز در محدوده 0.28 ± 1.07 تا 0.65 ± 8.02 kBq/m^3 قرار گرفت.

در مورد رادیواکتیویته در مصالح ساختمانی مورد مطالعه از سمنان، غلظت فعالیت Ra-226 ، Th-232 و K-40 از 1±6.7 تا 9±43.6، 1±5.9 تا 11±60، و 3±28.5 تا 1085±113 Bq/kg متغیر بود. با میانگین های 5±26.8، 4±22.7 و 4±322.4 Bq/kg. همچنین برای مصالح ساختمانی شهر محلات، فعالیت 232-Th، Ra-226 و K-40 در محدوده 3±18 تا 10±44 Bq/kg، 5±22 تا 14±53 Bq/kg و 18±82 Bq/kg تا 428 قرار داشت. در نتیجه، می توان نتیجه گرفت که اکثر نتایج کمتر از مقادیر متوسط مصالح ساختمانی در سراسر جهان است، بنابراین، برای ساکنان آنها، ساختمان های ساخته شده از چنین مصالحی از نظر رادیولوژیکی ایمن هستند. این نتایج توجه را به استفاده از گرانیت، آجر، سرامیک و کاشی در ساخت و ساز خانه جلب می کند. کد محاسباتی RESRAD-BUILD برای تخمین سهم مصالح ساختمانی متناظر با دوزهای داخلی و خارجی داخلی دریافتی توسط ساکنان محلات در یک اتاق مدل استاندارد برای سه مطالعه موردی مختلف با استفاده از ترکیبات مختلف مصالح ساختمانی مورد استفاده قرار گرفت. حداکثر میزان دوز مؤثر بین 504 و 1433 µSv/year در مطالعه موردی دوم، کف سیمانی کاشی شده محاسبه شد. بالاترین دوز خارجی و رادون نیز به ترتیب 369 و 1064 میکروسیورت محاسبه شد.

این پژوهش همچنین با بکارگیری تکنیک CFD در رابطه با کالیبراسیون SSNTDs برای قرار گرفتن در معرض طولانی مدت غلظت تورون در محیط داخلی، با هدف توسعه و پیش‌بینی نمایه توزیع تورون در اتاقک کالیبراسیون تورون RRI برای پیکربندی‌های مختلف ورودی و خروجی و همچنین نرخ‌های جریان انجام شد. نتایج نشان داد که محفظه تورون برای کالیبره کردن ابزارهای پایش قابل استفاده است. علاوه بر این، پیش‌بینی‌های مبتنی بر CFD با نتایج حاصل از مدل‌های تجربی و تحلیلی به دلیل انحراف نسبی قابل‌ملاحظه متناظر (با حداکثر تقریباً 9٪) مطابقت قوی دارند.

Table of Contents

List of Tables

List of Figures

List of Abbreviations and acronyms

NORM	Naturally Occurring Radioactive Materials
HNBRA	High Natural Background Radiation Areas
UNSCEAR	United Nations Scientific Committee on the Effects of Atomic Radiation
WHO	World Health Organization
IAEA	International Atomic Energy Agency
ICRP	International Commission on Radiological Protection
Air kerma	The number of individual x-ray photons per unit area
TLD	Thermo-Luminescence dosimeter
CFD	Computational Fluid Dynamics
RRI	Radiochemistry and Radioecology Institute
SSNTDs	Solid-State Nuclear Track Detectors
FVM	Finite Volume Method
IDW	Inverse Distance Weighting
OK	Ordinary Kriging
EBK	Empirical Bayesian Kriging
JRC	The Joint Research Centre
LLD	Lower Limit of Detection
ELCR	Excess Lifetime Cancer Risk
LCC	Lung Cancer Cases per year per million people
MDL	Minimum Detectable Limit
NCRP	National Council on Radiation Protection & Measurements
IAQ	indoor air quality
PCA	principal component analyses
CA	Cluster Analysis
AEOI	Atomic Energy Organization of Iran

Acknowledgments

This work is carried out as a part of the research activities in Institute of Radiochemistry and Radioecology, Research Centre for Biochemical, Environmental and Chemical Engineering. I would like to express my deepest thankfulness to my supervisor Dr. Tibor Kovács, the laboratory director and my thesis director, for entrusting me with this subject, as well as for his encouragement, invaluable advice, motivation and regular monitoring. Thank you for all the time you have given me, your guidance and your encouragement during these four years.

I owe special thanks to Dr. Stanislaw Chalupnik, for his kindness, availability, and support. Also, I would like to praise all the research fellows, Dr. Amin Shahrokhi and Dr. Edit Tóth-Bodrogi, whom I had the opportunity to exchange ideas and knowledge. I would have to thank them for their patience and assistance.

It is impossible to extend enough thanks to my family, especially my parents, brother and sisters who gave me the encouragement I needed throughout this process. Finally, this work would have been a much more difficult feat without my lovely wife. Thank you for your unwavering support and for reminding me to take breaks and have fun.

INTRODUCTION

1.1 WHAT IS RADIATION?

Radiation can be described as energy or particles from a source that travel through space or other mediums. Light and the microwaves and radio waves used for wireless communications are all forms of radiation. Radiation includes particles and electromagnetic waves that are emitted by some materials and carry energy. Radiation is classified as being either non-ionizing or ionizing. Non-ionizing radiation refers to types of radiation that do not carry enough energy to ionize atoms, includes: radiofrequency waves, microwaves, infrared, visible light; While, ionizing radiation is a type of radiation that can detach electrons from, or ionize, other atoms as they pass through matter. It consists of some forms of electromagnetic radiation such as high energy ultraviolet radiation, X-rays, neutrons, gamma rays, and particle radiation such as: alpha and beta particles.

Indeed, humans are constantly affected by ionizing radiations, which originate from both naturally occurring sources, referred to as "background" radiation, and artificial sources of ionizing radiation also called man-made sources. Natural sources of ionizing radiation include radiation in the environment from rocks and soil, internal radiation and radon as well as cosmic radiation from space particularly at high altitude; however, others radiation come from medical and nuclear medicine (X-ray machines, CT scanners, Mammography, Baggage X-ray screening devices), military purposes, consumer products, nuclear power plants and unplanned events such as power plant accidents are classified as artificial sources of ionizing radiation. Figure 1 shows a schematic view of these differences.

Regardless of where or how an ionizing radiation-related incident happens, three types of radiation-induced injury can occur: irradiation, external and internal contamination with radioactive materials and incorporation of radioactive material. Irradiation occurs when all or part of the body is exposed to penetrating radiation from an external source. This is the same process that occurs during an ordinary chest X-ray. Following irradiation, an individual is not radioactive, cannot spread radioactive contamination, and can be treated like any other patient. The second and third types of radiation injury involve external or internal contamination with radioactive materials. Contamination means that radioactive materials are spread to an unintended location. An external surface of the body, such as the skin, can become contaminated and, if radioactive materials get inside the body through the respiratory system, the gastrointestinal system, or

via wounds, the contaminant can become deposited internally. If a patient is internally contaminated, the body may incorporate the radioactive material. Incorporation refers to the uptake of radioactive materials by body cells, tissues, and target organs such as bone, liver, thyroid, or kidney. In general, radioactive materials are distributed throughout the body based upon their chemical properties. Incorporation cannot occur unless internal contamination has occurred.

On the other hand, given the current system of radiological protection developed by International Commission on Radiological Protection (ICRP) and implemented by national regulatory bodies, we have 'existing', 'planned', and 'emergency' exposure situations. First of all, planned exposure situations, result from the deliberate introduction and operation of radiation sources with specific purposes, as is the case with the medical use of radiation for diagnosis or treatment of patients, or the use of radiation in industry or research. Second one, existing exposures, is where exposure to radiation already exists, and a decision on control must be taken for instance, exposure to radon in homes or workplaces or exposure to natural background radiation from the environment. The last type, emergency exposure situations, result from unexpected events requiring prompt response such as nuclear accidents or malicious acts.

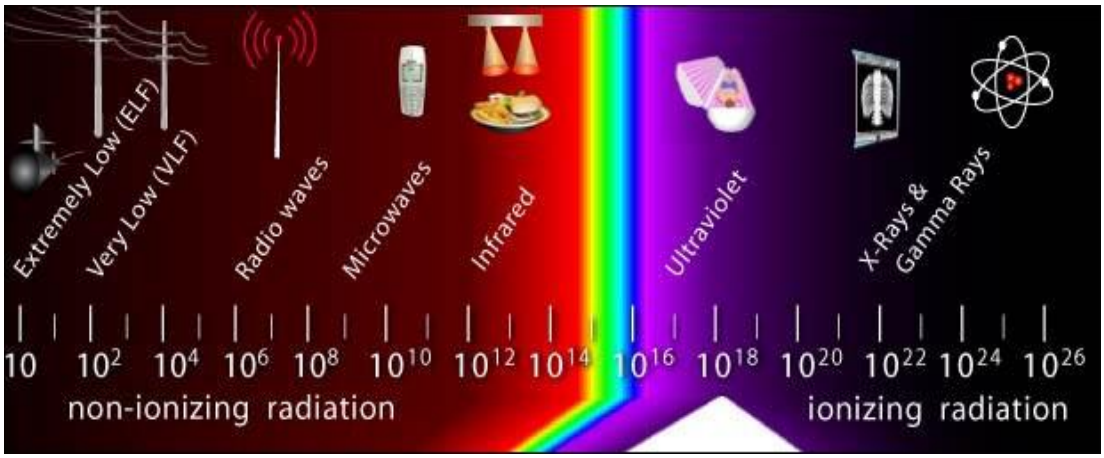

Figure 1. A schematic view of non-ionizing and ionizing radiation (OSHA, 2008)

1.2 HEALTH EFFECTS OF IONIZING RADIATION

Radiation damage to tissue and/or organs depends on the dose of radiation received, or the absorbed dose which is expressed in a unit called the gray (Gy). The potential damage from an absorbed dose depends on the type of radiation and the sensitivity of different tissues and organs. The effective dose is used to measure ionizing radiation

in terms of the potential for causing harm. The sievert (Sv) is the unit of effective dose that takes into account the type of radiation and sensitivity of tissues and organs. In addition to the amount of radiation (dose), it is often useful to express the rate at which this dose is delivered (dose rate), such as micro sieverts per hour (μSv/hour) or millisievert per year (mSv/year). Beyond certain thresholds, radiation can impair the functioning of tissues and/or organs and can produce acute effects such as skin redness, hair loss, radiation burns, or acute radiation syndrome. These effects are more severe at higher doses and higher dose rates. If the radiation dose is low and/or it is delivered over a long period of time (low dose rate), the risk is substantially lower because there is a greater likelihood of repairing the damage. There is still a risk of long-term effects such as cancer, however, that may appear years or even decades later. Effects of this type will not always occur, but their likelihood is proportional to the radiation dose. This risk is higher for children and adolescents, as they are significantly more sensitive to radiation exposure than adults (IAEA, 2004; WHO, 2009).

1.3 NATURAL BACKGROUND RADIATION

Natural background radiation is all around us. Background radiation varies from place to place and over time, depending on the amount of naturally-occurring radioactive elements in soil, water, air and building materials. Cosmic radiation from the sun, our galaxy, and beyond is constantly around us and contributes to natural background radiation. Generally, the natural dose rates from cosmic rays depend strongly on the altitude and slightly on the latitude. The latitude effect is due to the charged particle nature of the primary cosmic rays, and the effect of the earth's magnetic field, which tends to direct ions away from the equator and toward the poles (Shahbazi-Gahrouei, 2003).

Furthermore, uranium and thorium naturally found in the earth are called primordial radionuclides and are the source of terrestrial radiation. Terrestrial radiation levels vary by location, but areas with higher concentrations of uranium and thorium in surface soils generally have higher dose levels. All rocks and soils contain some trace amount of natural radioactivity and can sometimes be ingested or inhaled if disturbed. Radon and thoron are the gases that can concentrate indoors and be inhaled, along with their decay products. We can also ingest radioactivity from the food we eat and the water we drink. A small fraction of background radiation comes from human activities. Trace

amounts of radioactive elements have dispersed in the environment from nuclear weapons tests and accidents like the one at the Chernobyl nuclear power plant in Ukraine or Fukushima in Japan. Radioactive materials used in industry and even in some consumer products are also a source of small amounts of background radiation. Figure 2 shows the percentage of background radiation dose received annually from various natural sources (ICRP, 2007; Schauer and Linton, 2009).

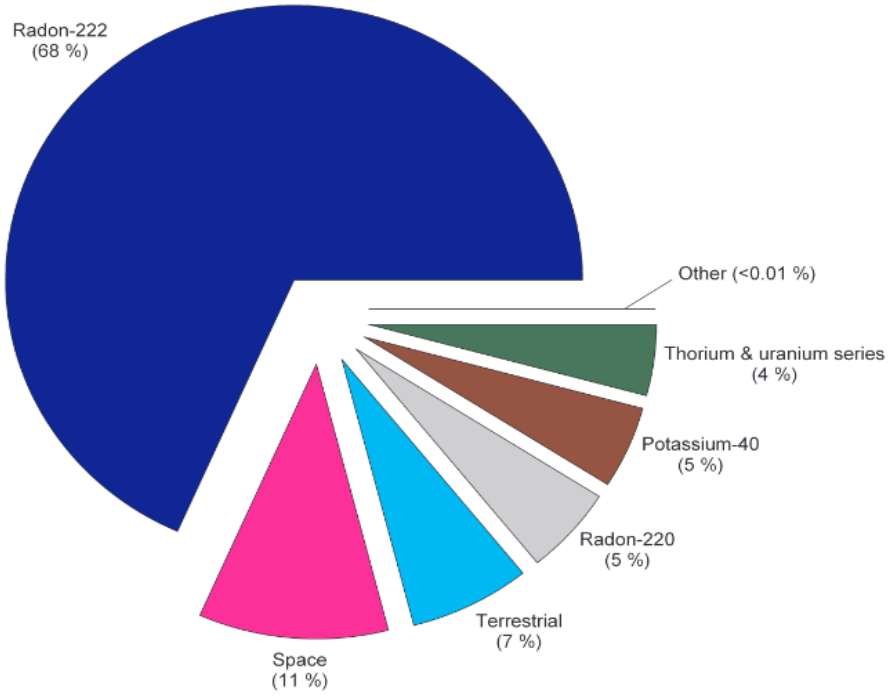

Figure 2. Background radiation dose received annually from various natural sources (ICRP, 2007)

The annual effective radiation dose from natural and man-made sources for the world's population is about 3 mSv (UNSCEAR, 2000, 2008). On average, 80% of the annual dose of background radiation that a person receives is due to naturally occurring terrestrial and cosmic radiation sources which can vary depending on the geology and altitude where people live ranging between 1 and 10 mSv/year, but can be even more than 50 mSv/year. Table 1 presents the latest the United Nations Scientific Committee on the Effects of Atomic Radiation (UNSCEAR) estimates of global radiation doses from different sources (UNSCEAR, 2008).

Table 1. Annual average doses and ranges of individual doses by source

Source of exposure		Annual effective dose (mSv)	
		Average	**Range**
Cosmic radiation	Directly ionizing and photon component	0.28	--
	Neutron component	0.1	--
	Cosmogenic radionuclides	0.01	--
Total cosmic and cosmogenic		0.39	0.3-1.0
External terrestrial radiation	Outdoors	0.07	--
	Indoors	0.41	--
Total external terrestrial radiation		0.48	0.3-1.0
Inhalation	Uranium and thorium series	0.006	--
	Radon	1.15	--
	Thoron	0.1	--
Total inhalation exposure		1.26	0.2-10
Ingestion	K-40	0.17	--
	Uranium and thorium series	0.12	--
Total ingestion exposure		0.29	0.2-10
Total		**2.4**	**1.0-13**

Several places are well-known in Iran (Ramsar and Mahallat), India (Kerala and Madras), China (Yangjiang), Brazil (Guarapari), Indonesia (Mamuju) and Europe where natural background radiation gives an annual dose of much higher than that of those in other parts of the world due to the radon, thoron and their short half-life decay products and also because of soil there is rich in radioactive materials such as radium, thorium and uranium. These areas are called High Natural Background Radiation Areas (HNBRA). However, based on epidemiological studies there is no evidence of increased cancers or other health problems arising from these high natural levels (Preston et al., 2007; Nair et al., 2009). The information available in the literature indicates that little attention or concern has been paid to the health of the public themselves being at risk due to living in such areas. Also, there is little information available on any remedial action undertaken in such areas. The following figure shows the location of high background radiation areas around the world.

In accordance with the findings of UNSCEAR, the annual effective doses received by inhabitants in HNBRAs are classified as: low (<5 mSv/year), medium (5-10 mSv/year), high (20-50 mSv/year) and very high (>50 mSv/year) (UNSCEAR, 2000). This classification is based on the recommended dose level prescribed by the International Commission on Radiological Protection (ICRP) and the worldwide average dose level for the general public (2.4 mSv/year) (UNSCEAR, 2000; Valentin, 2007; Shetty and Narayana, 2010; Mortazavi and Mozdarani, 2012; EU BSS, 2014).

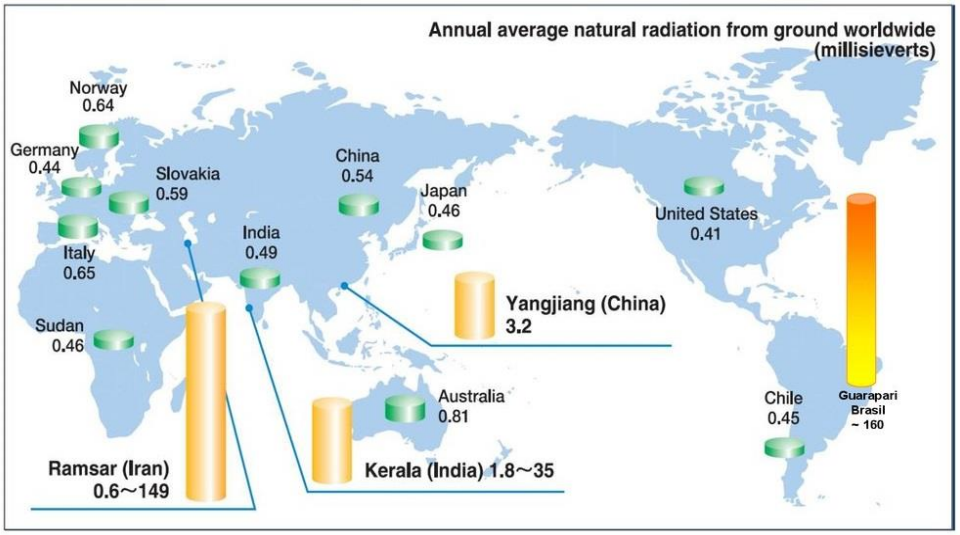

Figure 3. Location of HNBRAs around the world (prepared based on the 2008 UNSCEAR report and Environmental Radiation in Daily life, 2011)

1.4 MOST STUDIED WORLD HNBR AREAS

Kerala in India: The maximum value of the annual effective dose in this region is estimated to be 13 mSv, mostly from ^{232}Th contribution to air kerma (Hosoda et al., 2015). As for internal exposure, the geometric mean of the annual effective dose due to radon and thoron was calculated as 0.10 and 0.44 mSv, respectively (Omori et al., 2016). The presence of monazite and other heavy minerals such as zircon, rutile, and ilmenite cause high radiation levels in this area.

Yangjiang in China: The annual effective dose received from external radiation was measured to be 0.6–1.8 mSv (Omori et al., 2016). Meanwhile, Wei et al. reported that the annual dose of external radiation by thermoluminescence dosimeter (TLD) was 2.1 mSv (Wei and Yuan, 1998). The internal radiation dose due to radon and thoron were also measured to be 3.1, 2.2 mSv, respectively (Kudo et al., 2015). Besides that, Wei et al. estimates the annual internal effective dose received by residents in Yangjiang from all sources (^{40}K, ^{87}Rb, ^{228}Ra, ^{226}Ra, ^{222}Rn, radon progeny and thoron progeny) to be 4.3 mSv. The presence of monazites is a major element in the high radiation exposure in Yangjiang (Wei and Yuan, 1998).

Guarapari in Brazil: The existence of monazite sand on black sand beaches is the main cause of increased radiation exposure in this region, which also contains rare earth elements (Hendry et al., 2009; Boice et al., 2010). Hence, it is recorded that radiation exposure in the area reaches 50 μGy/h (Aliyu and Ramli, 2015). In 2003, Anjos and

his colleagues have also reported that the Guarapari radiation dose ranges from 3.5 to 10 mSv/year (Anjos et al., 2003).

Mamuju in Indonesia: Based on the survey carried out by Sukadana in 2015, the Mamuju area is heavily influenced by the rock formation of the Adang volcano (Sukadana et al., 2015). Syaeful et al. reported that the highest uranium content, which is ~ 1000 Bq/kg, in soil was observed using a NaI (Tl) scintillation spectrometer in Mamuju (Syaeful et al., 2014). In 2021, Hosoda et al. also reported the villagers of Botteng, Mamuju received an average annual effective dose of 27 mSv (Hosoda et al., 2021). Meanwhile, the value of the annual effective dose reported by Nugraha et al. in 2021, is 31 mSv which is13 times higher than the world average annual effective dose (Nugraha et al., 2021).

Ramsar in Iran: a northern city of Iran, has HNBR areas in an impressive natural landscape located at the foot of the Elburz mountains and overlooking the Caspian Sea. According to UNSCEAR 2000 report, Ramsar has some inhabited areas with the highest known natural radiation levels in the world. The effective dose equivalents in very high background radiation areas of Ramsar in particular in Talesh Mahalleh, are a few times higher than the ICRP-recommended radiation dose limits for radiation workers. Inhabitants who live in some houses in this area receive annual doses as high as 132 mSv from external terrestrial sources.

The radioactivity of the HNBRAs of Ramsar is due to ^{226}Ra and its decay products, which have been brought to the surface by the waters of hot springs. The area has over 50 active and dynamic hot springs which continuously pump warm water containing ^{226}Ra into the surrounding areas. There are more than 9 hot springs with different concentrations of radium in Ramsar that are used as spas by both tourists and residents (Ghiassi-nejad et al., 2002). According to the results of the surveys performed to date the radioactivity seems primarily to be due to the radium dissolved in mineral water and secondarily to travertine deposits having elevated levels of thorium combined with lesser concentrations of uranium (Sohrabi, 1993). Due to extraordinary levels of natural radiation in these areas, in some cases 55-200 times higher than normal background areas, some experts have suggested that dwellings having such high levels of natural radiation need urgent remedial actions (Sohrabi, 1997). In spite of this, many inhabitants still live in their unaltered paternal dwellings. Sohrabi and Esmaili et al. reported

that the annual effective dose is 0.6-132 mSv with a mean of 6 mSv and an indoor radon level of around 31 kBq/m^3 (Sohrabi, 2013).

Mahallat in Iran: with a population of approximately 53 thousand and surface area of 37 km^2, is one of the oldest towns in Iran. It is located in Markazi Province in north-western Iran (N 32° 54', E 50° 27') and is surrounded by mountains. Mahallat is recognized as a HNBRA (UNSCEAR, 2000). It contains several sources of spring water with high levels of radioactivity known as Abegarm-e-Mahallat, a region to the north-east of Mahallat. In Mahallat, the igneous bedrocks are rich in uranium, which decays into ^{226}Ra as a soluble in groundwater but in the presence of dissolved calcium carbonate ($CaCO_3$) precipitates out as radium carbonate ($RaCO_3$) houses (Mortazavi and Mozdarani, 2012). Thus, $RaCO_3$ may ultimately occur as a component of building materials, utilized to construct local. According to the UNSCEAR, 2000, the absorbed dose rate in this area was estimated to fall within the range of 800 to 4000 nGy/h (including cosmic and terrestrial radiation), which is at least fifteen times higher than the worldwide average of 55 nGy/h (UNSCEAR, 2000; Sohrabi et al., 1996). Some preliminary measurements of the radon level in dwellings in the investigated area were conducted a few years ago (Shahrokhi et al., 2015). The radon concentration measured was as high as 350 Bq/m^3 and corresponding annual effective doses from that area were as high as 13.6 mSv/year.

1.5 RADON/THORON AND ITS HEALTH RISK

Radon and thoron are gaseous radioactive materials produced through radioactive decay of a radium ore. They enter the human body through inhalation. Radon results from decay of Radium-226 produced in a decay chain (uranium series) that starts from uranium, and thoron results from decay of Radium-224 produced in a decay chain (thorium series) that starts from Thorium-232. Radon has a half-life of approximately 3.8 days and thoron has a half-life of approximately 55 seconds. Radon, thoron and their progeny can be regarded as the largest contributor of the annual effective dose for public in the world (50% of the total public dose) (UNSCEAR, 2000, 2008). Moreover, exposure to radon and its decay products is the second most common cause of lung cancer after tobacco smoking (WHO, 2009). Based on the WHO report in 2009, the worldwide proportion of lung cancer due to radon is 3-14% which is depending on the concentration of exposure, period of exposure and other committed risk factors.

The health risks related to radon and thoron exposure primarily arises in indoor environments while outdoor levels are generally low. Because radon and thoron diffuse into the air from the ground, building materials, etc., people inhale radon and thoron in their lives on a daily basis. Inhaled radon reaches the lungs and emits α-particles, causing internal exposure of the lungs. However, radon is not harmful by itself, as its short-lived decay products are responsible for most of the hazard. Indeed, Short-lived decay products of radon (Po-218 and Po-214) immediately deposit onto the tissue of the lungs, thereby densely ionizing alpha particles emitted by deposited decay products and interacting with biological tissue causing cellular tissue and DNA damage (U.S. Environmental Protection Agency, 2003; Lecomte, et al., 2014).

Transport mechanism of radon/thoron into indoor environment: it is produced in mineral grains by the radioactive decay of ^{226}Ra, emanated into the void spaces between the grains, transported by diffusion and advection/convection, and eventually exhaled from the soil into boreholes where it is detected. Moreover, cracks in concrete floors and walls, drainage pipes, connecting parts of buildings, heating, ventilation, and air conditioning ducts are the possible routes that radon can enter to the indoor environment. Figure 4 illustrates the transfer mechanism to inhale by an inhabitant simply.

On the other hand, elevated concentrations of radon and thoron are generally considered to increase the risk of lung cancer based on epidemiological data (Darby et al., 2005) and, given the acceptance of the linear non-threshold model (ICRP, 2007), even low doses have significant cumulative effect when considering the human population. Although radon has negative effects on human health, there is a different believe that it also has some healing characteristics during the speleotherapeutic treatment of different diseases, because of its natural presence in the atmosphere of caves, but this therapeutic effect of radon with first published results indicates that radon has nothing to do with curing different diseases (Nagy et al., 2009). Regarding the thoron, in the past, exposure to thoron was often ignored due to its very short half-life which was believed to prevent its indoor accumulation. It is already known that thoron and its progenies can significantly contribute to the radiation dose in certain environments (UNSCEAR, 2008). Therefore, it is important to identify these environments.

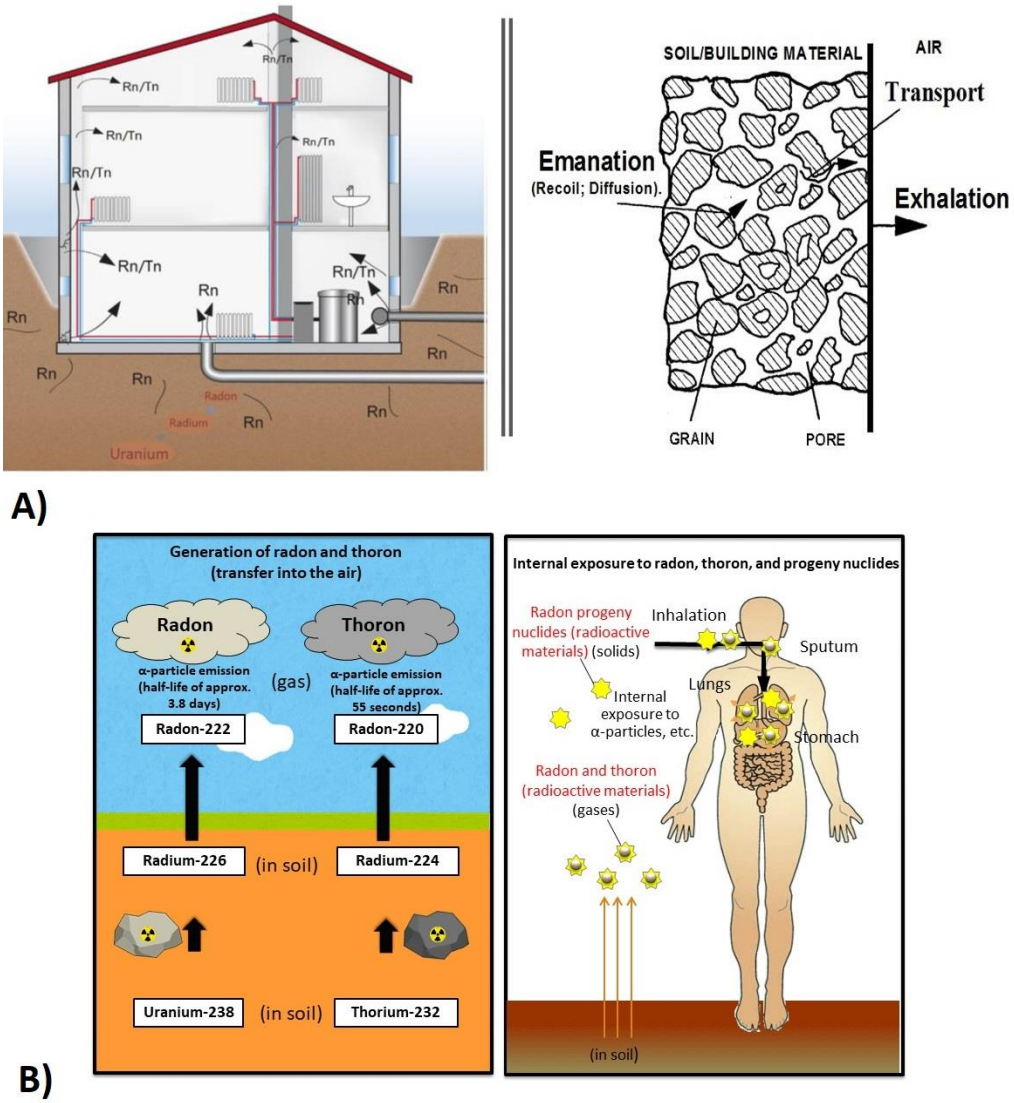

Figure 4. A) Radon and thoron entry paths into the residential environment and the mechanism, B) Internal exposure to radon and thoron through inhalation (JCN,2021)

1.6 RADON RECOMMENDATION LEVEL

National and international agencies operating under different directives have been responsible for addressing the health risk associated with indoor radon/thorn and for addressing its regulation. A national reference level for radon represents the maximum accepted radon concentration in a residential dwelling and is an important component of a national program. For dwelling with radon concentrations above these levels remedial actions may be recommended or required. When setting a reference level, various national factors such as the distribution of radon, the number of existing homes with high radon concentrations, the arithmetic mean indoor radon level and the prevalence of smoking should be taken into consideration.

In view of the latest scientific data, WHO proposes a reference level of 100 Bq/m^3 to minimize health hazards due to indoor radon exposure (WHO, 2009). However, if this level cannot be reached under the prevailing country-specific conditions, the chosen reference level should not exceed 300 Bq/m^3 which represents approximately 10 mSv/year according to recent calculations by the ICRP (ICRP, 2017). ICRP is one of the principal sources of guidance for radiation-protection policies for most international bodies. These recommendations are also consistent with the International Basic Safety Standards, 2014, co-sponsored by WHO and other international organizations (BSS, 2014). EPA also adopted a nonregulatory approach to the problem and recommended a primary action level of 150 Bq/m^3 (4 pCi/L) as the point above which mitigation is always advised to reduce radon in existing buildings (EPA, 2003).

According to IAEA basic safety standards for protection against ionizing radiation, the guidelines specific to indoor radon are based on the ICRP recommendation 126 (ICRP, 2014). The upper reference level of 300 Bq/m^3 for radon exposures in homes, as recommended in Publications 115 and 126 (ICRP, 2010, 2014), is established internationally and incorporated into the most recent Basic Safety Standards. For the optimized action levels, account should be taken of the benefits and costs assessed in the remedial action plan (IAEA, 2014).

1.7 RADIOACTIVITY IN BUILDING MATERILAS

As mentioned before, humans are exposed to background radiation from both natural and artificial sources on a daily basis; however, more than 80% of our entire exposure to ionizing radiation is from natural sources (UNSCEAR, 2000). The main contributor of human exposure is radon and its decay products, building materials can be also a source of external exposure to ionizing radiation (UNSCEAR, 2000; EU BSS, 2014). The inhalation of radon, thoron and their decay products contribute to the internal exposure, while the external exposure comes from the gamma emitting radionuclides. Therefore, it should be obligatory to monitor building materials as a secondary potential source of emitting indoor gamma radiation, however, the introduction of additional sources of enhanced radioactivity into such an environment would not be preferable. Moreover, according to the new European Union Basic Safety Standards (Council Directive 2013/59/EURATOM), the radioactivity index of building materials was restricted to less than 1 (to correspond to a reference level of external gamma dose -1

mSv/year - before being released to the market) (European Commission, 1999; UNSCEAR, 2000; EU BSS, 2014; Nuccetelli et al., 2015).

All building materials mostly constitute rock and soil; these two raw materials include natural radioactive isotopes such as ^{232}Th and ^{238}U decay series and ^{40}K. All can be sources of both internal and external radiation exposures. Several studies have been carried out to estimate the radiological hazards and annual dose contribution of natural radioactivity in building materials. Performing a radiological impact assessment for building materials to estimate and control the radiological effects on the public and on the environment is very critical and sensitive effort due the criteria of sustainable development. The assessment of the radiological impacts should be based on measured data which data could be the input parameter for models for environmental transfer process and radiation dose assessment. Hence, radiation protection standards have been introduced by difference organizations (ICRP, 1994; European commission, 1999; UNSCEAR, 2000, 2008; Council of the European union, 2014). The ^{226}Ra, ^{232}Th and ^{40}K worldwide activity concentrations for soils and building materials are given in the reports of UNSCEAR, these are 32, 45, 412 Bq/kg and 50, 50, 500 Bq/kg, respectively (UNSCEAR, 2000, 2008).

1.8 SIGNIFICANCE AND SCOPE OF THE WORK

Since the issue of radiological impact to the public plays a key role in radioecological research, determining the population's exposure to radiation from building materials is really important because almost 80% of human life is spent indoors. In terms of radiation and health physics, exposure to such sources of radiation is a major public health concern, especially in high natural background radiation Areas.

In Iran, the dose limit for workers, established in national regulations (ISIRI, 2005), is equal to 5 mSv/year, therefore, it was important to estimate doses for the staff members of the spa, caves and son on as the most critical group. Furthermore, the doses that patients and tourists are exposed to should be estimated. Therefore, due to the lack of such data concerning the indoor radon and thoron concentrations in the confined areas in IRAN, the first aim of this thesis is divided into 3 major parts: A) Measuring the indoor radon and thoron concentrations in the thermal spas in Dehloran, Iran by using passive method based on CR-39 detectors; B) Measuring the activity concentrations of three of the most important naturally occurring radionuclides (^{40}K, ^{226}Ra and ^{228}Ra)

in soil and also ^{226}Ra concentrations in water samples of Dehloran, Iran using a semi-conductor High Purity Germanium (HPGe) detector and RAD7 radon monitor device, respectively; C) Calculating the annual committed effective dose of Mashhad city in Iran caused by the inhalation of radon and thoron by measuring the indoor radon and thoron concentrations in the dwellings and also soil-gas radon measurement, as the most important source of indoor radon, by using RADUET and NRBP with CR-39 detector, respectively. Then, generating indoor radon maps of Mashhad city by ArcGIS software over a grid of 1×1 km by applying three different interpolation techniques, include Inverse Distance Weighting (IDW), Ordinary Kriging (OK), and Empirical Bayesian Kriging (EBK), in order to increase public awareness of environmental radioactivity and influence government policy with the purpose of reducing radon exposure in the general population.

By continuing the assessment of radiological hazards that the residents of buildings are exposed to, the second scope of this dissertation refers to the NORMs content measurement in the most common building materials in Iran. Since the information about the radionuclide activity concentrations of building materials in Iran is limited and the knowledge of activity concentrations of the building materials is needed to assess the possible radiological hazards that the residents of buildings are exposed to, in this thesis, I have also focused on the assessment of gamma-ray emitters in building materials and the estimated exposure to indoor gamma radiation from these materials in two cities of Iran (where the data is not available): A) HNBRA of Mahallat, and B) Semnan Province. Attempts have been made to evaluate the distribution of naturally occurring radionuclides in different building materials, therefore, measurements of the radioactivity of the most common building materials available on the local market were taken. The potential hazards which are associated with the studied materials were estimated by calculating the radium equivalent activity concentration, the absorbed dose, the annual effective dose and the external and the internal hazard indexes as well as the gamma and alpha indexes that can contribute to the radiological hazards affecting population health. The results also compared with the recommended worldwide values to estimate the radiological hazard to inhabitants from the used building materials;

Afterward, to estimate the contribution of corresponding building materials towards indoor external and internal doses received by inhabitants in Mahallat, the computer

code RESRAD-BUILD which is developed by Argonne National Laboratory (USA) in a standard model room was used. Three different case studies using different compositions of basic building materials in HNBR of Mahallat, taking into account the different densities and thicknesses of such materials, were applied in a simulation to determine how much of an influence each one has on the effective dose rate occupants are exposed to. The impact of indoor environmental parameters on the external and internal doses was also investigated. Finally, in order to determine the similarities and relationships between the various samples, the radiological data were processed by applying multivariate statistical methods including the Pearson correlation coefficient, principal component analysis (PCA) and cluster analysis (CA). To carry out the relevant statistical analysis of the obtained data's, IBM SPSS Statistics V21.0 software is used.

Lastly, as thoron gas has become increasingly recognized as a potential source for radiation exposure in dwellings, its long-term indoor exposure (passive measurement) and eventually calibration of solid-state nuclear track detectors (SSNTDs) for its measurement have been highly recommended by different organization to predict the exact thoron concentration distribution inside the calibration chamber and finding the *SSNTDs detector calibration factor*. Hence, the last aim of this dissertation stands on the simulation and prediction of the thoron distribution profile inside the Radiochemistry and Radioecology Institute (RRI) thoron calibration chamber, at the university of Pannonia for different configuration of inlet and outlet as well as flow rates by applying the computational fluid dynamics (CFD) technique. It is necessary to calibrate the detectors with a reference atmosphere to make sure the risks can be well evaluated. The RRI and its facilities were confirmed to be suitable for producing and sustaining required homogenous concentrations of thoron. RRI thoron exposure calibration chamber was designed and simulated in accordance with the CFD approach implemented in ANSYS FLUENT 2020 R1 code based on the finite volume method (FVM). Then, in order to validation, the simulation results are compared with analytical calculations as well as experimental measurement.

1.9 LITERATURE REVIEW

This section begins and reviews literature on the aforementioned goals and scopes of the work to cover all the concepts and performed investigations and findings of other

institutes which have been positively activated since last ten years in the field of radiochemistry and radioecology.

1.9.1 Indoor Radon/Thoron measurements and its Mapping

As describe before, the radon and thoron and their decay products contribute 52% of the total inhalation doses to human population (UNSCEAR, 2000). Thus, it is important to study the indoor radon and thoron levels and their decay products in the environment and radon soil-gas (to be the main source of radon in homes). The indoor radon and thoron levels depend upon various factors like geological setting of area, nature of soil, meteorological conditions, living style of the dwellers and type of building material used for the house construction. The major part of indoor radon and thoron comes from the soil and building materials, because the uranium and radium are uniformly distributed in these materials from the time of origination of earth (Adelikhah, 2021).

An indoor radon map is a powerful statistical tool with accuracy and high resolution which helps educating the public on environmental radioactivity. Indoor radon maps are based indoor radon measurements and are precise since the radon concentrations are measured at the point of exposure. Radon map is an important resource for any government seeking to reduce the exposure of its populace to radon gas. It influences government policies particularly on building infrastructures. Thus, it has an enormous value in both the economic and social aspect of the public. Measuring indoor radon/thoron concentrations and its mapping was consider for years and several papers were published around the world (Dubois, 2005; Faheem and Mati, 2007; Rahman et al., 2007; Chen et al., 2009; Dubois et al., 2010; Rafique et al., 2011; Kim et al., 2011; Szeiler et al., 2012; Kropat et al., 2014; Kumar and Chauhan, 2014; Sainz-Fernandez et al., 2014; Shahrokhi et al., 2015; Singh et al., 2015; Cinelli et al., 2015; Elío et al., 2017; Chen and Ford, 2017; Hoffmann et al., 2017; Özen et al., 2018; Park et al., 2018; Serge et al., 2019; Saputra et al., 2020; Shikha et al., 2021; Baptista et al., 2022; Chen, 2022), including in many Iranian cities (Sohrabi, 2005; Hadad et al., 2007, 2011, 2015; Bouzarjomehri et al., 2008; Mowlavi et al., 2012; Fahiminia et al., 2016; Yarahmadi et al., 2016; Shahbazi Sehrani et al., 2018; Mirbag and Shokati Poursani, 2019) to increase public awareness of environmental radioactivity and predict radon-prone areas which help authorities with regard to the development of an appropriate strategy

to reduce exposure to radon and thoron. Therefore, it increases the quality of life and improves public long-term health.

Many studies have carried out in India to measure indoor radon and thoron concentration in dwellings and also soil-gas radon concentration. For example, a survey conducted by Kumar and Chauhan in 2014 to measure indoor and thoron in North Indian dwellings. The radon and thoron concentration in their study varied from 17 to 51 Bq/m^3 and 9 to 73 Bq/m^3, while the radon soil gas varied from 2.80 kBq/m^3 to 6.46 kBq/m^3. Kumar also did the same measurement for Udhampur district, Jammu & Kashmir in India and the range of indoor radon/thoron concentrations is found to vary from 11 to 58 Bq/m^3 with an average value of 29 ± 9 Bq/m^3 and from 25 to 185 Bq/m^3 with an average value of 83 ± 32 Bq/m^3, respectively (Kumar et al., 2017). Moreover, other study of indoor radon, thoron and their progeny measurement in Tosham region Haryana, India was carried out by Singh et al. (2015). They used LR-115 dosimeters and the annual average of indoor radon were reported to be between 37 ± 18 Bq/m^3 to 80 ± 28 Bq/m^3. Shikha in 2022, also used the same detector as Singh and reported the annual average indoor radon and thoron concentration for dwellings of a Roopnagar district of Punjab in India, which fell within 41.40 ± 12.94 and 52.68 ± 18.37 Bq/m^3 (Shikha et al., 2022).

The EU recently revised and consolidated the Basic Safety Standards Directive (Council Directive 2013/59/EURATOM), which aims to reduce the number of radon-induced lung cancer cases and oblige EU Member States to establish a national action plan regarding the exposure to radon (EU BSS, Council Directive 2013/59/Euratom, 2014). At the same time, International Atomic Energy Agency started technical projects in order to assist countries to establish and implement national radon action. The Joint Research Centre (JRC) of the European Commission also decided to embark on a European Atlas of Natural Radiation (EANR) (De Cort et al., 2011), in line with its mission, based on the Euratom Treaty, which is to collect, validate and report information on radioactivity levels in the environment. Therefore, a huge effort has been taken to summarize data of indoor radon concentrations from different countries and to integrate them in a homogeneous way to produce a European map of indoor radon levels using a 10 km × 10 km grid cells (Dubois et al., 2010). Accordingly, the indoor radon measurements reported in Austria, Belgium and Croatia were between 5 to 8325 ,10 to 4100 and 249 to 508 Bq/m^3, respectively. Also, the corresponding values fell

between 20 to 25000, 2 to 590, 15 to 1044 and 16 to 6629 Bq/m^3 for Czech Republic, Denmark, Estonia and Finland, respectively. In case of France and Germany, it is also reported that indoor radon was estimated to be between 30 to 335 and 10 to more than 10000 Bq/m^3, respectively. In case of Hungary, the reported data was in the same range as Germany. As a results, the European indoor radon map over 10 km x 10 km grid cells of annual indoor radon concentration in ground-floor rooms are given in Figure 5.

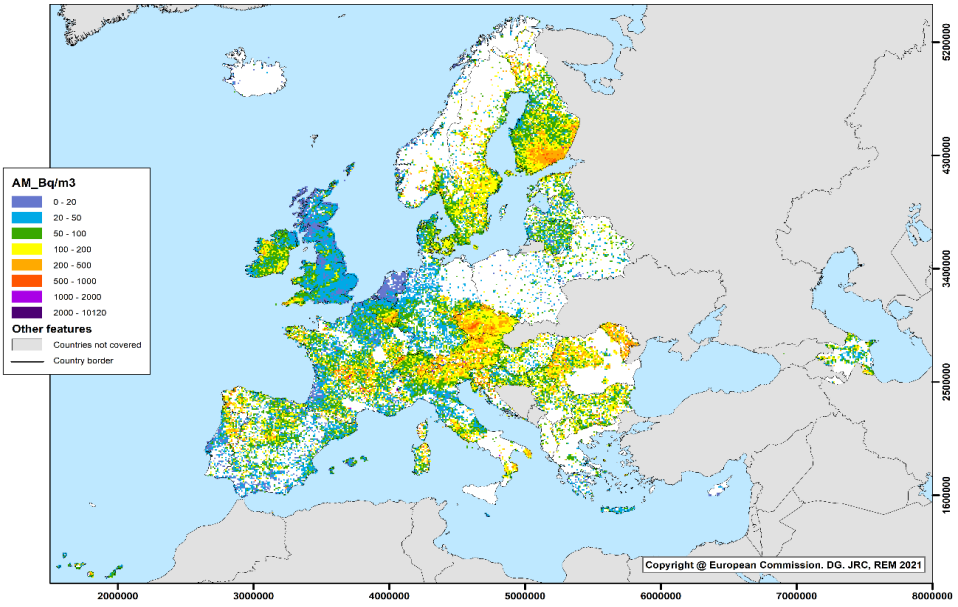

Figure 5. European indoor map reports the arithmetic means over 10 km×10 km grid cells (Dubois et al., 2010)

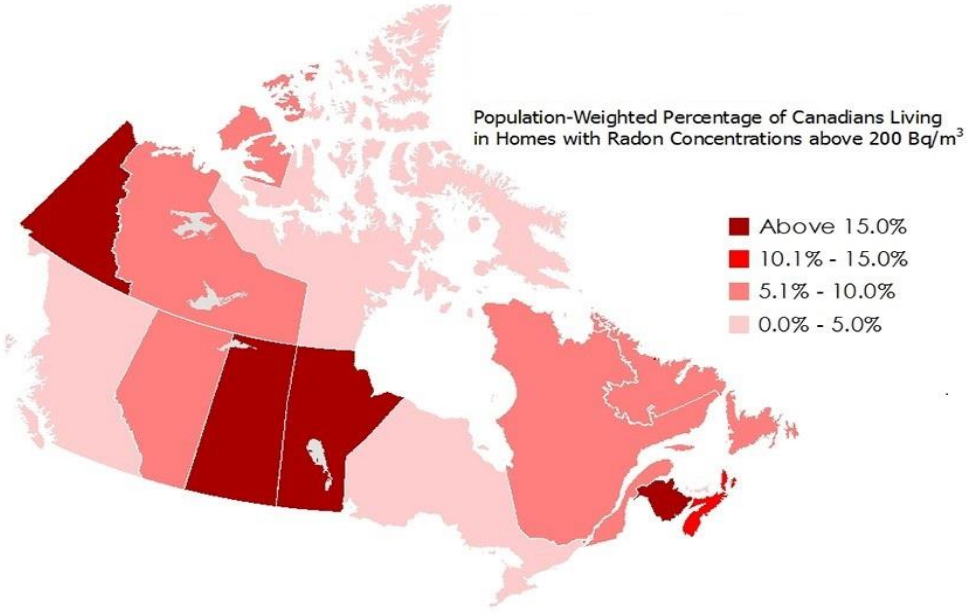

Figure 6. Radon risk map of Canada (Chen, 2022)

Radon and thoron measurements were conducted in a total of 3534 residential homes in 34 metropolitan areas of Canada from 2007 to 2013 by using RADUET detectors. Chen (2022) reported that radon and thoron concentrations were <3 to 2341 Bq/m^3 and Below the Lower Limit of Detection (LLD) to 1977 Bq/m^3, respectively (Chen, 2022). Also, an earlier survey was also conducted by Chen and Ford, (2017) to determine soil-gas radon in 14 Canadian cities which ranged between 11 to 36 kBq/m^3 (Chen and Ford, 2017). Figure 6 depicts the prevalence of radon in Canada, by province and territory, in terms of population-weighted percentages of Canadians living in homes with radon concentrations above 200 Bq/m^3 (Health Canada, 2016). EPA also developed the radon map to identify areas of the U.S. with the potential for elevated indoor radon levels (June 2019, EPA 402/F19/004, as shown in Figure 7.

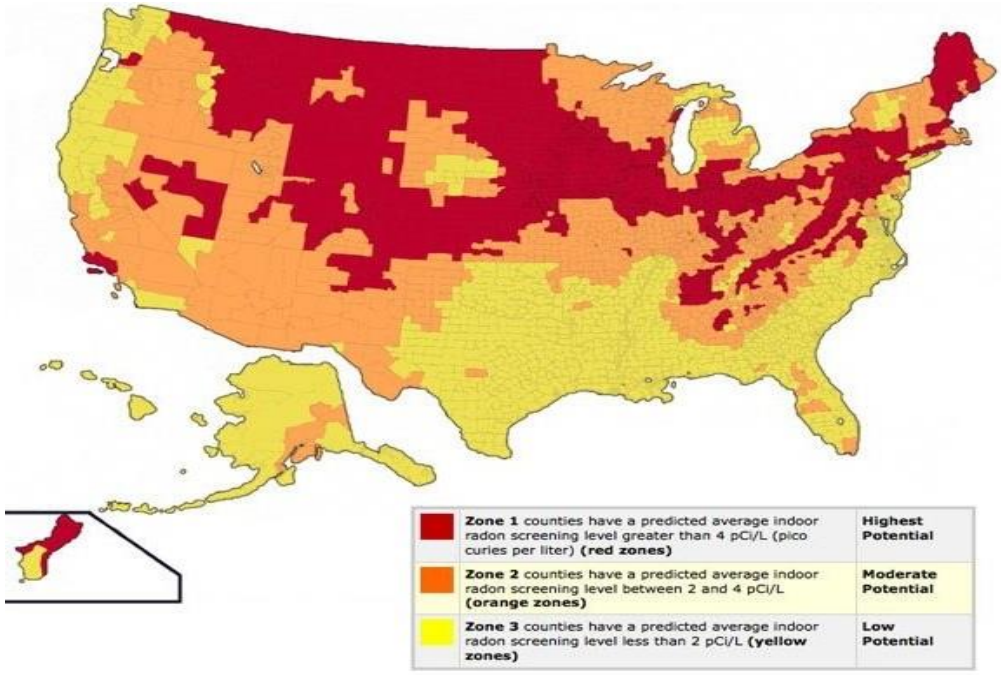

Figure 7. EPA map of radon zones in USA (EPA, 2003)

Furthermore, several studies of indoor radon and thoron in Iranian cities were performed by many scholars. In 2005, Sohrabi and Babapouran were conducted a study in 12 regions of Ramsar in 2 season to determine the effective doses of public from internal and external exposures indoors and outdoors (Sohrabi and Babapouran, 2005). Accordingly, the radon level ranged from 64 Bq/m^3 to 31080 Bq/m^3. The annual mean effective equivalent dose due to radon ranges from 2.48 to 71.74 mSv with maximum levels up to 640 mSv determined in some area in Talesh Mahalleh. In another survey conducted in 4 big cities in North and Northwest of Iran by Hadad et al. (2007) by

using passive and active measurements. The radon concentration recorded to be between 55 to 2386 Bq/m^3. The mean value of radon level during the year in Lahijan, Ardabil, Sar-Ein and Namin were 163, 240, 160 and 144 Bq/m^3, respectively. Haddad also measured the radon concentration inside dwellings in 10 cities of Yazd province in Central Iran (Hadad and Mokhtari, 2015). The corresponding annual arithmetic mean radon concentration were recorded to fell between 63 to 122 Bq/m^3. Bouzarjomehri et al. (2008), also measured radon levels in the basement of Yazd dwellings. Radon concentrations of the basements were between 5.55 to 747.4 Bq/m^3 with mean of 137.36 Bq/m^3 (Bouzarjomehri et al., 2008).

The radon level of residential dwellings in Shiraz were assessed using Solid State Nuclear Track Detectors, CR-39 polycarbonate films by Haddad et al. (2011). The annual average indoor radon concentration was 94 ± 52 Bq/m^3 (Hadad et al., 2011). The radon concentration in Tehran, Iran was also measured to be between 31 (Shahid Araqi in north) to 460.2 Bq/m^3 (Shahid Baqeri in west) with an average value of 104 Bq/m^3 (Shahbazi Sehrani et al., 2018). Besides that, Mirbag and Shokati Poursani, (2019) were done radon measurement in another big city of Iran, namely Isfahan. Their obtained data shown that the radon concentration in the residential and commercial buildings varied from 3 to 251 Bq/m^3, with a mean value of 28.57 Bq/m^3 (Mirbag and Shokati Poursani, 2019).

1.9.2 Radioecological study of thermal baths

The hot spring and its surrounding area are an example of an elevated source of natural radiation that includes increased concentrations of ^{222}Rn, ^{226}Ra and ^{232}Th. The water from the hot spring is used extensively for balneotherapy and in thermal baths. These leisure activities are extremely popular in Europe and Asia as natural treatments for various common ailments. A large number of studies have been conducted on indoor radon concentrations in thermal spas, e.g., in the Middle-Slovakian region, Lądek-Zdrój in south-western Poland, the thermal spas of Rudas and Hévíz in Hungary, Jáchymov in the Czech Republic, etc. (Szerbin et al., 1994; Jobbágy et al., 2010; Nowak et al., 2012; Nikolov et al., 2012; Zölzer, 2013; Walczak et al., 2016; Shahrokhi et al., 2016; Műllerová et al., 2016; Duran et al., 2019; Kasić and Kasumović, 2022; Bahtijari et al., 2022).

Nikolov et al. (2012) studied radon levels at the spa in Niška Banja, Serbia and measured activity concentrations indoors and in water in thermal pools and therapy rooms. The activity concentration of ^{222}Rn around indoor pool "Zelengora" was found to be more than two times higher than suggested level defined above for applying occupational protection (1000 Bq/m^3). Besides that, the measured activity concentration of radon in the air in the basement of the hotel "Radon" was (22.90±0.57) kBq/m^3. The corresponding dose estimate of occupational exposure to radon and radon daughter in treatment facilities, around thermal pools in Niska Banja spa were 18 mSv/year. Nikolov is also reported that the highest annual effective dose in case of ingestion in Niska Banja spa from public drinking fountains were estimated to be 0.50±0.07 mSv/year. The activity concentrations of NORMs in soil, rock and therapy mud were also recorded. The content of ^{226}Ra in the "bigar" rock is, for example, about 10 times higher than the maximal content of these isotope in agricultural soil samples from Vojvodina (northern province of Serbia), which is about 50 Bq/kg. This could be a reason for high amounts of radon in air, soil and water from natural springs in Niska spa (Nikolov et al., 2012).

In Hungary, bathing has been very popular for a long time because of its geological location. According to national statistics, there are more than a hundred thermal springs in Hungary. Some of these springs are used for medical purposes (e.g., radon therapy through drinking or bathing treatments (Somlai et al., 2007; Nagy et al., 2008), but some studies show that radon can be absorbed during radon therapy through the skin or by inhalation through the lungs into the bloodstream (Becker, 2003; Nagy et al., 2009). Hence, Shahrokhi et al. (2016) was measured the indoor radon concentrations of three randomly selected thermal baths in Hungary using CR-39 and an AlphaGUARD radon monitor with regard to the new updated standards of the European Basic Safety Standard (EU BSS, Council Directive 2013/59/Euratom, 2014). The annual average of indoor radon concentrations in Parad Medical Bath, Igal Health Spa and Eger Turkish Bath were estimated to be 159 ± 19, 176 ± 27 and 301 ± 30 Bq/m^3, respectively. In their study, the highest level of indoor radon concentration was observed in Eger Turkish Bath to be 403 ± 42 Bq/m^3 (Shahrokhi et al., 2016).

Moreover, radon activity concentrations at spas of the Visegrad Group, namely in Poland, Hungary, the Czech Republic and Slovakia, have also been investigated using three types of passive radon detectors (RAMARN, RADUET and NRPB) (Műllerová

et al., 2016). Their results showed that the average radon concentrations in spas are less than 400 Bq/m^3 in 86% of cases. However, radon concentration above 1000 Bq/m^3 was also found in spa of Czech Republic and Slovakia.

Guangdong is one of the provinces that have most hot springs in China, and many hotels have been set up near hot springs, with spring water introduced into the bath inside each hotel room for hot spring bathing to attract tourists. Song et al. (2005) was studied indoor and outdoor radon, as well as in hot spring waters, in four hot spring hotels in Guangdong (Song et al., 2005). Radon concentrations ranged 53.4–292.5 Bq/L in the hot spring water and 17.2–190.9 Bq/m^3 in outdoor air. In case of indoor radon, it was measured to be between 17-2144 Bq/m^3. Another survey was carried out in Beijing, China by Wang and his colleagues in 2017. They reported that the activities of ^{226}Ra and ^{222}Rn of geothermal water fell between 0.023–0.36 Bq/L and 0.47–29.70 Bq/L, respectively (Wang et al., 2017).

In Iran, there are some famous hot spas like as Ramsar and Mahallat. Ramsar includes about nine hot springs which are used by the public and vacationers as spas. The water has ^{226}Ra concentrations of up to 146 kBq/m^3 (Sohrabi et al., 1993). These springs are the origin of the elevated NORM in the areas around Ramsar. Radiological studies carried out in these areas include measurement of gamma exposure indoors and outdoors leading to an isodose map of the region, assessment of public personal doses, radon measurements indoors in houses in different regions around Ramsar during the four seasons as well as in the rooms of the Grand Hotels of Ramsar (Sohrabi et al., 1993), ^{226}Ra determination in water, in particular in that of the hot springs (Sohrabi et al., 1993, 1997). Ghiassi-nejad et al. (2002) reported that people in some areas of Ramsar were received an annual radiation absorbed dose from background radiation that is up to 260 mSv/year. While, hot springs of Abegarm-e-Mahallat are form travertine deposits, and of mixed-origin (Magmatic and Geothermal). These waters, used in local baths, have cooled down and deposited calcium carbonate as calcite (Beitollahi et al., 2007). Visitors and workers who use the baths served by the hot springs are exposed further to radiation through the inhalation of radon. According to the data reported by Beitollahi in 2017, the mean concentration of ^{226}Ra in Mahallat hot springs, measured by the emanation method, ranged from 0.48±0.05 to 1.35±0.13 Bq/l. ^{222}Rn concentrations measured in the hot springs using a liquid scintillation counter ranged from 145±37 to 2731±98 Bq/l. Mean radon concentrations in air were 487±160 and

15.4±2.7 Bq/m^3 for indoor and outdoor, respectively. Their results showed that the potential annual mean effective dose of the workers in the region is 5.60±1.61 mSv, while a tourist may receive an effective dose of 9.7±2.9 mSv per visit (Beitollahi et al., 2007).

1.9.3 NORMs content in soil and Building materials

Population it is exposed to the effects of external and internal radiation emanating from building materials. The inhalation of radon, thoron and their decay products contribute to the internal exposure, while the external exposure comes from the gamma emitting radionuclides. Radiologically the most important radionuclide is the ^{226}Ra (Sas et al. 2015; Kardos et al. 2015; Kuzmanović et al. 2020; Adelikhah et al. 2021). Due to this, the aim is to minimalize the radionuclide activity concentrations in the building materials, as much as is reasonably achievable, and to minimalize the radiation dose which the public is exposed to. For this purpose, knowing the dose limits for public exposure and measuring the levels of naturally-occurring background radiation emanated from the ground, air, water, food, the inside of buildings, etc. is essential for estimating the exposure of humans to natural sources of radiation (El-Taher, 2010). Consequently, the definition of the dose rates helps to make some preventive measures to be sure that the doses do not exceed the recommended limits. Moreover, the knowledge about gamma radiation is important in the construction industry to be capable to adopt preventative measures and decrease the unhealthy effects of the ionizing radiation.

Radiological hazard of building materials due to the presence of natural radioactivity has been highly investigated in various countries and areas of the world over the last years (Stoulos et al., 2003; El-Taher, 2010; Lu et al., 2012, 2014; Al-Sulaiti et al., 2011; Rafique et al., 2011; Turhan and Varinlioğlu, 2012; Muntean et al., 2014; Asaduzzaman et al., 2015; Kayakökü et al., 2016; Lee et al., 2019; Shahrokhi et al., 2020; Tuo et al., 2020; Imani et al., 2021; Amatullah et al., 2021; Kuzmanović et al., 2020; Kocsis et al., 2021). In the following, some of them will be reviewed:

A study carried out in Turkey, determining the natural radioactivity levels of granites used in constructions, have showed that the presence of a large amount orthoclase and radiogenic accessory minerals are the sources of high activity congregation levels in the country (Cetin et al., 2012). Özdiş et al. (2016) also assessed the natural radioactivity in 42 cements samples produced in Turkey and reported values were 18–143

Bq/kg for ^{226}Ra, 5–66 Bq/kg for ^{232}Thand 142–540 Bq/kg for ^{40}K (Özdiş et al., 2016). The natural radioactivity levels in 14 different building materials collected from building construction sites in Adana also reported by (Solak et al., 2012).

Many studies have performed in China to measure NORMs content in different building materials. For instance, Lu et al. (2012) have analyzed the corresponding NORMs activity for Xianyang, China. Thus, the average activity concentration of ^{226}Ra, ^{232}Th and ^{40}K in the studied building materials ranges from 13.4 to 69.9, 13.1 to 99.1 and 124.7 to 915.1 Bq/kg, respectively (Lu et al., 2012). In 2014, he also measured the same radionuclide for building materials used in Weinan, China. Their measurement results for building materials of Weinan showed that the specific activities of ^{226}Ra, ^{232}Th and ^{40}K range from 15.6 to 266.1, 11.8 to 64.2 and 180.8 to 835.1 Bq/kg, respectively, which are in the range of Chinese soil values (Lu et al., 2014).

In case of Korea, the geologic raw materials and frequently used building materials such as granite rocks, sands, gravels and concretes were collected by Lee et al. (2019). Based on their survey, activity concentration of ^{226}Ra was measured 21 (in Concrete samples) to 268 (in Gravel samples) Bq/kg while the activity concentrations of ^{232}Th and ^{40}K were also fell between 32 to 267 Bq/kg and 280 to 1730 Bq/kg, respectively (Lee et al., 2019). Consequently, gravel samples showed the highest concentration of ^{232}Th and ^{40}K as well. In another study which performed in Korean raw materials used in building industry, the radionuclide concentrations ranged from 0.06 to 4.13 ± 0.21 Bq/g for ^{226}Ra, 0.08 to 33.6 Bq/g for ^{232}Th, and from minimum detectable activity to 4.06 Bq/g for ^{40}K, respectively (Hassan and Chae, 2019).

A major study also carried out for common building materials (brick, cement and sand) used in Bangladeshi dwellings by Asaduzzaman et al. (2015). Correspondingly, the mean concentrations in the analyzed building material samples ranged from 49.4 to 60.5 Bq/kg for ^{226}Ra, from 64.7 to 82.0 Bq/kg for ^{232}Th and from 927.2 to 1080.3 Bq/kg for ^{40}K. The highest mean values of radionuclide concentration in their study were found in the cement and red sand samples.

In case of Iranian building materials, Ashrafi and Jahanbakhsh in 2019, measured the concentrations of natural radionuclide of 48 granite stones samples which are commonly used as building materials in Azerbaijan province (in the northwest region of Iran) by using a gamma–beta-radiation spectrometer (Ashrafi and Jahanbakhsh, 2019).

The average activity concentrations of ^{238}U, ^{232}Th, and ^{40}K were estimated as 66 Bq/kg, 57 Bq/kg and 996 Bq/kg, respectively. Furthermore, a total of 29 widely used granite samples from both local and foreign suppliers which are used as a decorative inner cover on walls and floors in Iran were collected by Abbasi in 2013, to determine the natural radioactivity concentrations (Abbasi, 2013). Hence, the average concentrations of ^{226}Ra, ^{232}Th and ^{40}K were in the ranges of 3.8 to 94.2, 6.5 to 172.2, and 556.9 to 1539.2 Bq/kg, respectively. The radon exhalation rates have also been studied and values were in the range of 0.32 to 7.86 Bq/m^2. h. Their results showed that the most of the studied granite samples that incorporated in constructions appear to be safe as building material but some samples have hazard indices more than the maximal permitted values for building materials (1 mSv/year) and are not quite safe to be used indoors.

Amini Birami et al. (2019), determined the concentrations of natural radionuclides in different types of rock and soil samples from a high-level natural radiation area, Northern Iran. As reported, the activity concentrations of radionuclides in rock samples ranged 23 to 93 Bq/kg for ^{226}Ra, 24 to 118 Bq/kg for ^{232}Th, and 462 to 1190 Bq/kg for ^{40}K. The activity concentrations of radionuclides in the soil samples were ranged from 4 to 24, 284 Bq/kg for ^{226}Ra, ND to 107 Bq/kg for ^{232}Th, and 7 to 853 Bq/kg for ^{40}K (Amini Birami et al., 2019). Based on their data, the highest activity concentrations and radiological hazard indices were related to Arud granitic body and Ramsar's soil. Different building materials available in the market in the Ramsar HNBRA were also analyzed for both radon exhalation rate and natural radionuclide content by Bavarnegin and et al. (2013). Accordingly, radon exhalation rates from the samples varied from below the LLD up to 384 Bq/m^2 h. The activity concentration of ^{226}Ra, ^{232}Th and ^{40}K varied from below the minimum detection limit up to 86,400, 187 and 1350 Bq/kg, respectively. As a result of their study, radon exhalation rate and radium content in some local stones used as basements were extremely high and these samples are the main sources of indoor radon emanation as well as external gamma radiation from uranium series (Bavarnegin and et al., 2013).

Different production plants of ceramic tiles and glazes have been investigated by Fathabadi et al. (2011) to find the presence of radioactive elements with focus on natural radioactivity. Therefore, the ^{226}Ra concentration in zircon were ranged from 3300 to 4600 Bq/kg and mean-specific activity in ceramic glaze were reported to be between

347 to 920, 42 to 250 and 433 to 1850 Bq/kg for ^{226}Ra, ^{232}Th and ^{40}K, respectively (Fathabadi et al., 2011). Fathivand and Amidi, (2007) were also collected total of 42 cement samples from various manufacturers and suppliers in Iran to determine natural radioactivity and associated hazards on them. The specific activities of ^{232}Th, ^{226}Ra and ^{40}K were measured in samples and results ranged from minimum values of 8, 16, 101 Bq/kg to maximum values of 17, 43 and 141 Bq/kg, respectively (Fathivand and Amidi, 2007).

1.9.4. Thoron calibration chamber and detector calibration

UNSCEAR reports are provided the limited information on thoron exposure and also indoor thoron researches have never been systematically conducted. Therefore, considerable attention has been drawn to measurement of the activity concentration of the thoron gas in air and indicate that the precise estimation of indoor thoron concentration is principal because, firstly, it could not be neglected due to the issue of concern from the radiological point of view and dose assessment purpose and secondly, could distort radon measurements (Tokonami et al., 2001; Eappen et al., 2007; Sorimachi et al., 2012; Zhang et al., 2010; Csordás et al., 2015; Tokonami, 2020).

The only way to know whether a radon/thoron level is elevated is to test of it. However, as mentioned earlier, many radon/thoron surveys have been initiated, but they have used many different measurement passive monitors (etch track detectors, activated charcoal and electret) and active instruments (ionization chambers, scintillation cells and solid-state detectors). Although the working principles are similar, it is difficult in practice to maintain a reasonable and accurate standard of measurement and quality. In addition, new laboratories and companies continually enter the field of radon and radon isotopes measurements and new measurement techniques and devices are still being developed. Consequently, it is necessary to improve and standardize technical methods of measurements and to ensure that radon and thoron testing devices and laboratories provide accurate and reliable data on radon and thoron levels.

It is clear that all thoron measuring instruments need a uniform standard with which they can be calibrated so that all the measurements are comparable and the uncertainty of each individual measuring instrument. Therefore, long-term indoor exposure of thoron concentration (passive measurement) and subsequently solid-state nuclear track detectors (SSNTDs) calibration methods for its measurement have been developed and

becomes an important topic to be determined. On the one hand, predict the exact concentration distribution inside the calibration chamber and resulting the SSNTDs detector calibration are the vital key in order to obtain a better assessment of the measurement data, but on the other hand, the technical difficulties concerning measurement due to short half-life of thoron and etc., makes the development of an appropriate thoron calibration chamber and its validation complicated (compared with radon calibration chamber).

Several calibration monitors have been developed and many methods used to measure thoron concentration (Gaware et al., 2011; Irlinger, 2015). Researchers kept developing the monitors and methods to estimate the radiological hazard accurately. Thoron monitors need to be calibrated and tested against a reference atmosphere, in other words, a standard activity concentration. Researchers in Germany created a reference atmosphere of thoron based on a certified activity standard of Th-232 (Röttger et al., 2010). They have developed a procedure for precise emanation measurements with a relative standard uncertainty <0.4% which can also be performed within the scope of the characterization of open sources for different applications in radon metrology.

The National Henri Becquerel Laboratory (LNHB) in France developed a thoron activity standard to be used in calibrating monitors (Sabot et al., 2015). Their measurement system was based on a reference volume using an alpha detector, which is able to measure thoron and its decay products to define the thoron concentration of a thoron reference atmosphere. The authors defined an appropriate geometry to measure a thoron atmosphere under specific conditions using Monte Carlo and Comsol simulations. As a result, Sabot et al. have obtained useful spectra for the measurement of a thoron atmosphere, since they can directly measure the gas and also the decay products.

Kotrappa and Steck in 2010, developed the electret ionization chamber to measure thoron gas by improving its sensitivity to thoron by increasing the entry area of the gas by making extra holes in the side of the S-chambers (Kotrappa and Steck, 2010). Other privileges are rapid readout without the need to process the sensor chemically or microscopically analyze it. The electret ionization chamber method has been displayed to work at low/high humidity and low/high temperatures. This new development will benefit to radon measurement companies that can now use electret ionization chamber system to measure thoron as well as radon.

Zhang et al. (2010) used a locally built and good-maintained thoron chamber which is located at Peking University, China to measure thoron gas accurate by using the Lucas scintillation cell and AB-5 (Zhang et al., 2010). Compared with the experimental results in pure thoron or a mixed $^{222}Rn/^{220}Rn$ environment, the deviations with RAD7 were less than ±10%. This method using a LSC has the advantages of simple, swift and easy operation, suitable for a reference standard for ^{220}Rn concentration measurement in pure ^{220}Rn environment. This method does not have the uncertainty of spectroscopic analysis and can also be used in environments with a high thoron concentration. Also, a thoron chamber with a total volume 300 L was established at Fudan University, China. The main purpose of this chamber was the calibration and intercomparison of thoron measurements. The chamber provided a thoron source made from lantern mantle which was saturated with Th-232. Thoron sources were prepared and designed so as to be in the lattice shapes and the geometry was taken into account. The environmental parameters such as temperature and humidity are well controlled and programmed (Zhao et al., 2010).

Eappen, Sapra and Mayya in 2007 also applied a technique to estimate thoron gas using a scintillation cell as well. They applied an on-line Lucas cell sampling and counting technique which estimates the thoron concentration, corrected for the contribution of ^{212}Pb, which leads to temporally increasing background counts in the cell. A simple mathematical formulation has been derived to arrive at the true counts due to thoron alone. Validation of the methodology was also done using a standard thoron source with varying thoron concentrations passing through the LSC.

In 2011, Ismail and Jaafar were performed a study to find the proper size of a thoron detector chamber, in case of a CR-39 passive Nuclear Track Detector. Moreover, Sorimachi et al. (2012) conducted a study using the National Institute of Radiological Sciences (NIRS) chamber in Japan, to check passive detectors and influence of the humidity, wind and ambient aerosol in the air on their measurements (Sorimachi et al., 2012). NIRS has the facilities to calibrate thoron monitors using a 150 L volume chamber. These facilities are available to calibrate thoron monitors as well. However, the thoron chamber is bigger compared with the thoron chamber and is about 24400 L, big enough to walk inside it. These two chambers are used for conducting regular international intercomparison measurements checking and calibrating thoron and radon detectors of the different laboratories from different countries (Janik et al., 2014).

Recently, the CFD method has drawn attention to the prediction and visualization of the distribution pattern of radon and thoron concentrations in confined areas. Agarwal et al. (2014) have employed the CFD technique to assess the thoron distribution in confined volumes in the presence of a forced flow as in the case of delay volume used as a mitigation device. Accordingly, thoron distribution inside a chamber followed a complex behavior and varied with respect to air exchange rate (and air flow profile) of the chamber. This study showed that changes in flow rate and inlet-outlet configuration of delay chamber affect the thoron distribution profile inside it (Agarwal et al., 2014). In other study, Agarwal et al. (2019) have also applied the CFD technique for studying the effect of variations in the ventilation rate on the distribution pattern of the thorn concentration in a thoron test house (Agarwal et al., 2019). They have changed the ventilation rate from 0.1 h^{-1} to 9.0 h^{-1}. The simulated results of velocity and thoron gas concentration profile for the entire test domain showed that the increase of ventilation rate leads to the flow induced turbulence enhancing the mixing of thoron gas in indoor air.

Zhou et al. (2001) applied the finite difference method to derive discrete equations before linking them to the commercial FUJITSU/a-FLOW code to study the concentrations and their distributions of radon and thoron as well as their progenies in a model room (Zhou et al., 2001). Rabi et al. (2017) implemented a ^{222}Rn distribution inside a typical Moroccan room using Fortran software (Rabi et al., 2017). Chauhan et al. (2014) and Agarwal et al. (2019) in this regard also used the software Fluidyn MP based on the Finite Volume Method (Chauhan et al., 2014; Agarwal et al., 2019). As an important result, all of the surveys have clearly demonstrated that CFD modelling is a capable tool to predict the distribution of radon and thoron gas as well as their progeny.

MATERIALS AND METHODS

2.1 DESCRIPTION OF THE STUDY AREAS

The first studied area in this thesis is Mashhad city in Iran. Mashhad is the second largest metropolis in Iran and is the capital of Razavi Khorasan Province in northeastern Iran. It has an area of 351 km^2 and its population is more than 3 million people according to the last census (Statistical Centre of Iran, 2016). It has witnessed rapid growth over the last two decades, mostly as a result of its economic, social and religious attraction. The city is 985 m above sea level with the geographic coordinates of 36º 17′ 45″ N, 59º 36′ 43″ E. Geologically, the Kalaj mountains, which consist of granitic hills covered by silty deposits, are situated to the south of Mashhad, towards the northwest is Kale Ghaemabad that is comprised of more sandy soil, and in all other directions is a plateau with a mix of clay loam and soft sandy soils. Figure 8 shows the location of Mashhad in Iran.

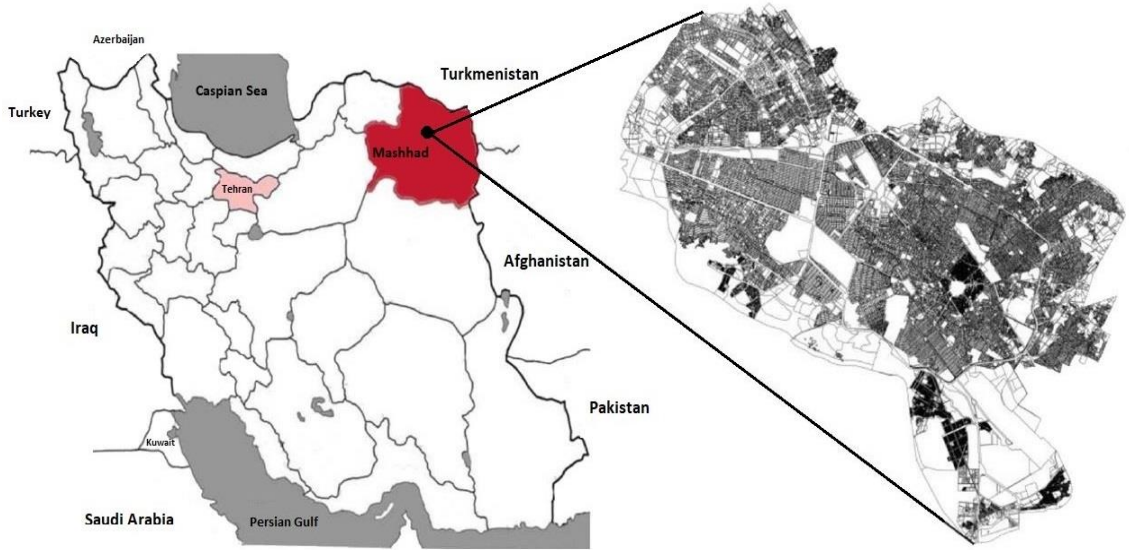

Figure 8. Location of the city of Mashhad in Razavi Khorasan Province, Iran

Other cities which considered to measure the activity concentration of naturally occurring radionuclides in the commonly used structural building materials, are HNBR of Mahallat and Semnan Province as well which are shown in Figure 9. Mahallat, with a population of approximately 53 thousand and surface area of 37 km^2, is one of the oldest towns in Iran. It is located in Markazi Province in north-western Iran (N 32° 54′, E 50° 27′) and is surrounded by mountains. Mahallat is recognized as a HNBRA. It contains several sources of spring water with high levels of radioactivity known as Abegarm-e-Mahallat, a region to the north-east of Mahallat.

Moreover, Semnan province with the 5.6% of the whole area of Iran is the sixth big province in the country. The center of this province is located at 228 km away from Tehran and its distance from the international waters of the Persian Gulf and the Caspian Sea, in turn, is 1600 and 200 km. The province is divided into two parts: a mountainous region, and the plains at the foot of the mountains. It is built from the north towards southern part in a vast field with heavy slope and includes the city of Semnan. It is situated in southern flank of the Alborz range and north of the great desert of Central Iran. Therefore, geologically it belongs to the Alborz and central Iran structural zones where one of the most completed Quaternary successions in Iran is exposed. In the East of Semnan City, Quaternary deposits occupy about 98% of the surface area, of which the Alluvial represents one of the most important geomorphological features in the area. The study of Quaternary deposits in the East of Semnan has attracted the interest of many earth scientists.

Figure 9. Location of the city of Mahallat and Semnan Province, Iran

The last area of studied in this thesis is Dehloran hot spa in Iran. Dehloran is a city in Ilam Province located in Western Iran (see Figure 10) and surrounded by mountains with a population of 66,000 inhabitants. The specific ecological environment of this area and its geology (rich in natural resources) are of particular importance to this city as they provide the opportunity for industrial development and tourism activities to stimulate and accelerate economic growth. Unique natural phenomena, e.g., natural tar spring, hot water springs and caves, deem this area ideal for research. Water from hot springs is used for medical treatments and irrigation. This particular spring is located

3 km from the center of Dehloran. The maximum temperature of the water in the spring is 50 ºC. The study area is on the western part of the Zagros folded area. The age of the geological formations that outcropped in the region is related to the Cretaceous lower to the recent. From the old to the new, Sarvak, Pabdeh, Gurpi, Asmari, Gachsaran, Aghajari, and Bakhtiari formations occur in the study area (Mirzaee, 2019).

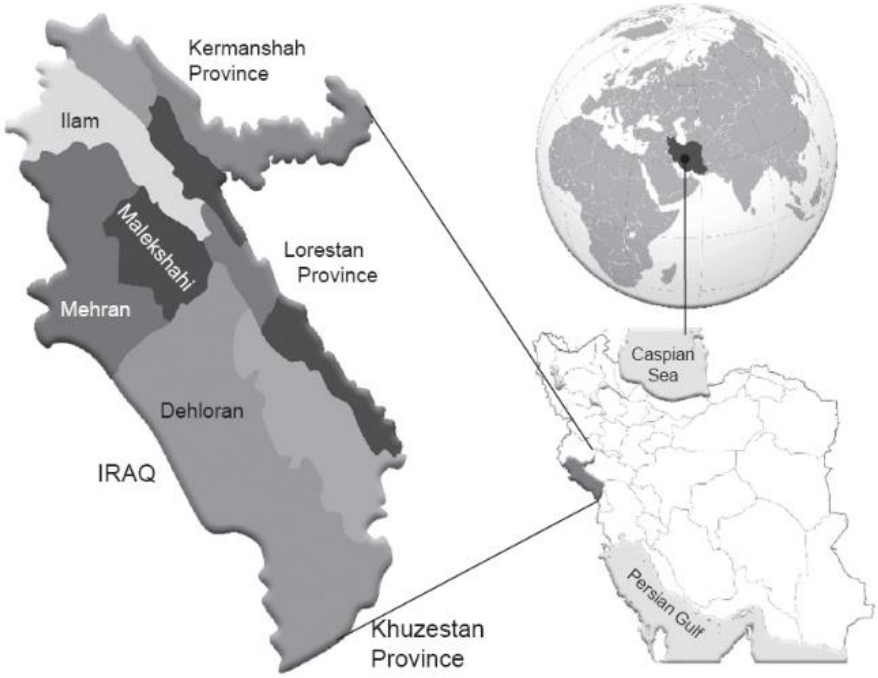

Figure 10. Location of the city of Dehloran in Ilam Province, Iran

2.2. SAMPLE COLLECTION AND PREPARATION

Indoor radon and thoron concentrations are measured in the living rooms of houses in Mashhad city. To determine the indoor concentrations of radon and thoron, a RADUET selective radon and thoron chambers type with solid-state nuclear track detector CR-39 detector was used. All detectors were hung at a height of 1-2 m above the ground using hard wire and positioned at least 20 cm away from any of the wall surfaces in the living rooms of the houses. The majority of the houses examined were built 15 to 45 years ago using bricks composed of sand and cement along with cemented floors. The indoor radon and thoron measurements were conducted over a period of 90 days in total during the summer (July–September 2019) and winter (December 2019–February 2020). Regarding the participants recruited, the priority was given to older houses by selecting of 3 to 5 dwellings from each district randomly depending on size of residential area; likewise, regarding the ethical concern, all the collected participant information considered privately and just shared research team and after

finishing the study all data were destroyed to confidentially protection for participants. Additionally, the participant was informed about the results. Prior to this study, no such an experience regarding radon mapping were conducted in this area; The participant was asked verbally to join voluntarily maybe compromised because of benefits this study provides to them, and we aware them the used detectors does not have any hazard health or recording any kind of data. Participant was informed that they can opt out from the survey at any time but necessary to inform research team 10 days in advance to return the detectors (while no such a case happened). In addition, in order to measure soil-gas radon concentrations of Mashhad city, a hole was dug in the soil of about 11 cm in diameter and 50-60 cm in depth. Then, a long PVC tube was fixed into the hole with the covered top end of the tube protruding from the ground by about 5 cm. At the bottom of each tube, a NRBP radon dosimeter was placed for a period of 45 days between July and September 2019. To reduce the risk from possible rainfall and prevent any flow through the PVC tube into the atmosphere, the tube was filled with paper and the top end covered. After exposure, all detectors were wrapped in protective aluminum foil and returned for processing at the Institute of Radiochemistry and Radioecology at the University of Pannonia.

On the other hand, commonly used structural building materials, namely sand and gravel, brick, cement, gypsum, tiles, ceramic, granite, marble and mosaics, were collected randomly from different markets and suppliers of construction materials in Semnan Province and HNBRA of Mahallat to measure the ^{226}Ra, ^{232}Th and ^{40}K activity concentration. All of the samples were properly cataloged, labelled, and named according to each sample's origin and sample location. Till several days all of the samples were dried at room temperature before being pulverised, homogenised, sieved (grain size <3 mm) and finally dried in an oven at approximately 105 °C for 24 hours to constant weight. 500 grams of each prepared and homogenized sample was sealed in leak-proof Marinelli beakers for more than 28 days to ensure ^{222}Rn and its short-lived daughter products reached equilibrium with ^{226}Ra (Adelikhah et al. 2020; Shahrokhi et al. 2020; Imani et al., 2021).

Regarding the sample collection from the hot spa, different locations inside the thermal bath were chosen for the measurements of indoor radon and thoron levels as well as the concentration of dissolved ^{226}Ra in thermal water. The majority of these locations are where patients undergo treatments (baths as well as swimming pool areas). To

determine the concentrations of radon and thoron, RADUET detectors were also used. The detectors were placed at least 40 cm away from doors and windows, 100 to 180 cm above the floor and about 8 to 15 cm away from any other objects for a period of 45 days. In case of water samples, they were preserved immediately after collection by 1N HNO_3 to decrease the pH to 2 in order to avoid the absorption of radium into the walls of the bottles. The soil samples from farms were also collected to determine the impact of thermal water used for irrigation on the distribution of naturally occurring radionuclides in the soil. All samples were randomly collected due to expected changes in the concentration of radionuclides with the distance from the source of water.

2.3 RADON/THORON MONITOR DEVICES

Radon measurements are divided into categories based on the propose of technique: (A) Passive measurement; (B) Active measurement; The sampling and duration measurement depends on the device used and method may vary over a wide range of grab sampling, time-integrated sampling (short-term and long-term) and continuums sampling known as real-time radon monitoring, as sample-taken measurement occurs and shows results. However, radon measure devices are also classified differently based on their used method of radon monitoring in addition to other classification, i.e., electrostatic collection of decay products (RAD7, Tesla TSR2, EQF3220), ionizing chamber device (AlphaGUARD), photomultiplier counter and scintillation (Liquid scintillation or scintillation cell), radon absorption (active charcoal), etched track detectors (CR-39, LR115).

Active measurement:

AlphaGUARD is a battery or net-operated portable instantaneous or continuous radon monitor based on an ionization chamber with high recording storage capacity. In addition to the radon concentration measurement, it also records simultaneously relative humidity, ambient temperature and atmospheric pressure using its integrated sensors. AlphaGUARD due to its high sensibility 0.62 L ionization chamber with the sensitivity of 1 cpm at 20 Bq/m^3, very low uncertainty (instrument calibrator error: 3%) and the ability of operating in almost any environment conditions in mines, laboratories and also for complementary investigations in buildings (-15 °C to +60 °C, 800 mbar to

1050 mbar and 0% to 99% air humidity), usually use a reference instrument and calibration equipment in order to perform air, water, soil and exhalation measurements. The range of measuring starts from as low as 2 up to 2,000,000 Bq/m^3 (Saphymo, 2016).

On the other hands, the DURRIDGE RAD7 is a truly versatile radon and thoron detector which is also used by researchers worldwide. The equipment is portable and battery operated, and the measurement is fast. It comes complete with a built-in air pump, rechargeable batteries, and a detachable wireless printer. It also a good device to measure radon in water over a concentration range of from less than 10 pCi/L to greater than 400,000 pCi/L. To determine the dissolve radon concentration in the water samples, the emanometry measurement method based on water degassing was conducted using RAD7. The setup of the RAD7 detector with the RAD-H_2O accessories used for the measurements is shown in Figure 11 (DURRIDGE, 2018).

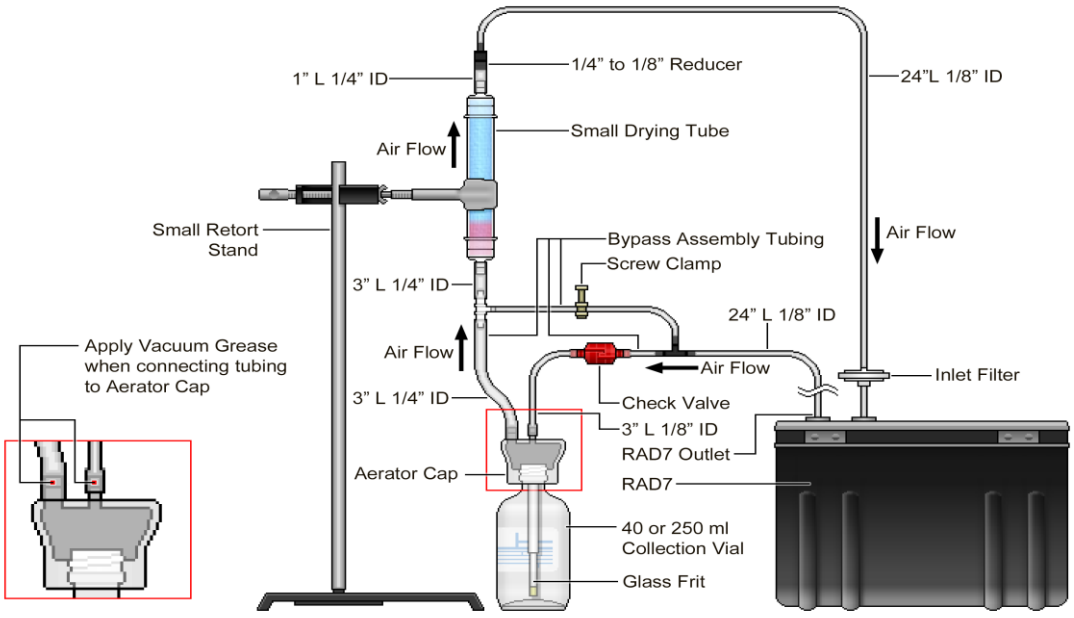

Figure 11. RAD7 radon monitor device to measure radon concentration in water

The RAD7 setup utilizes a closed loop aeration arrangement where the air and water volumes are constant and independent of the rate of flow. The operation of the device consists of ejection of radon from the water sample using a bubbling kit, the ejected radon then enters a hemisphere chamber through air circulation and polonium nuclei are produced through the decay of radon. These are collected onto the silicon solid-state detector in a high electric field, which are then counted and estimated as concentration of radon in water sample through the in-built software.

Passive measurement:

Passive radon measurement devices are generally less expensive and are used in most for integrated monitoring of real estate transactions and the output is an average of radon concentration for the whole measurement period, while, active devices are more expensive but are more precise and can give a historical view of radon changed concentration during measurements (WHO, 2009). Some of the examples of commercially available passive radon dosimeters are RADUET and NRPB which is used in this dissertation.

For instance, RADUET detectors consist of two diffusion chambers with different ventilation rates, and each chamber contains a CR-39 chip with the dimensions of 10 × 10 mm^2 (RADUET, Radosys Ltd., Budapest, Hungary) for detecting the alpha particles emitted from radon and thoron as well as their progenies (Tokonami et al., 2005; Adelikhah et al., 2020). A CR-39 is used as the detecting material and placed at the bottom of the chamber with sticky clays. The low diffusion rate chamber is comprised of an electrically conductive plastic with an inner volume of 30 cm^3. Six holes in the wall of the high diffusion rate chamber, composed of the same material, are covered with a sponge material to prevent decay products of radon and thoron as well as aerosols from infiltrating into the chamber. Radon in air can penetrate into the chamber through an invisible air gap between its lid and bottom through diffusion. Since this air gap functions as the high diffusion barrier, thoron can scarcely go into the chamber with such a small pathway due to its very short half-life, compared with that of radon. While one chamber only measures radon, the other detects both radon and thoron levels. The concentration of thoron is then determined by subtracting the track densities.

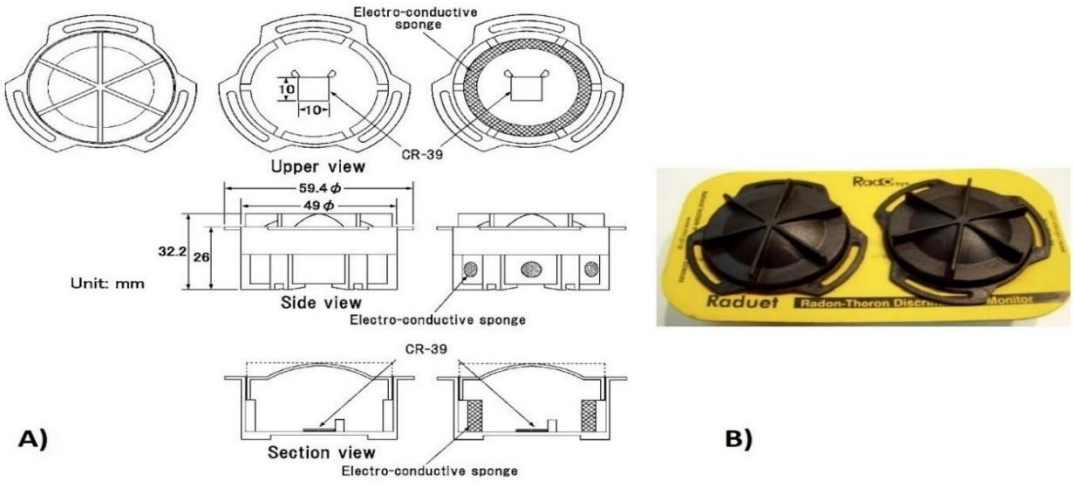

Figure 12. RADUET detector, A) layout drawing and B) panoramic view

2.4 EXPOSURE TO RADON AND THORON

As it was explained on introduction section, because radon and thoron diffuse into the air from the ground, building materials, etc., people inhale radon and thoron in their lives on a daily basis. Inhaled radon reaches the lungs and emits α-particles, causing internal exposure of the lungs. Radon inhaled into the body further decays into progeny nuclides, which then migrate from the lungs and the esophagus to the digestive organs together with sputum, causing further internal exposure. The concentration of radon/thoron in air by using the CR-39 detectors is calculated using Equation 1 based on the density of tracks on etched detectors:

$$C_{Rn/Tn} = \frac{(N_t - N_b) \times E}{(T \times A)} \quad (1)$$

where $C_{Rn/Tn}$ denotes the average indoor radon/thoron concentration (Bq/m^3), N_t stands for the total number of tracks, N_b represents the number of background tracks, E is the calibration factor (Bq m^{-3} h tracks^{-1} mm^2), T denotes the exposure period (hours), and A stands for the reading area of the tracks (mm^2). The track densities were counted using a high-resolution image scanner and image analysis software which was developed in the RRI institute by (Bátor et al., 2015).

2.4.1 Calibration of CR-39 detectors

The author calibrated the detectors using a certified leak-free metal radon chamber (Genitron EV 03209, Volume: 210.5 L) and a certified radon source (Pylon RN2000A, a passive radon gas source) supplying a known concentration of radon to the chamber, as shown in Figure 13. The Pylon RN2000A source (calibrated in DURRIDGE Company Inc.) was supplied with a removable cap which is used to seal the container or radon gas to completely disperse when the cap is removed. The solid radium, covered by the aluminium container, continues to emanate radon gas at a constant rate following the standard growth rate (DURRIDGE Company Inc., n.d.). Table 2 is summarized the given official data related to the source used in this study by producer.

Table 2- The specifications of the radon source (Pylon 2000A) used in this study

2000A Specifications	
Parent nuclide	Ra-226
Date of manufacture	1998. August.11
Nominal activity	105.7 kBq
Activity Tolerance	0.4% (0.4 kBq)
Daily Emanate Radon	110310.7 Bq

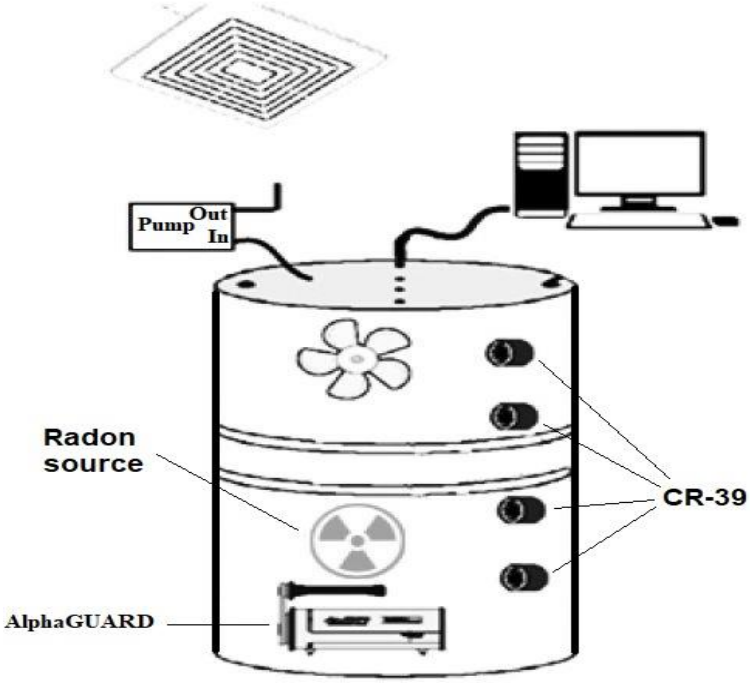

Figure 13. CR-39 calibration chamber

Radon concentration inside the chamber monitored during calibration using a calibrated ionizing chamber device (AlphaGUARD PQ2000 PRO), a device that usually use as a reference device in calibration producer. AlphaGUARD set up in diffusion mode to conduct measurements over a period of each 30 minutes. The concentration of radon inside of the chamber calculated based on the radon mass transfer as:

$$R_s = \left(\frac{f\, A_{Ra}\, e^{-\lambda_{Ra} t_{Ra}}}{V_{stp}}\right)(1 - e^{-\lambda_{Rn} t_{Rn}}) \quad (2)$$

Where R_s is radon concentration in the calibration chamber, f stands for radon emanation fraction from the source, A_{Ra} refers to activity concentration of source (Ra-226 Activity kBq), λ_{Ra} is the decay constant for radium, λ_{Rn} represents the decay constant for radon, t_{Ra} is the time interval from the source creation date to the starting measurement date, t_{Rn} is the time interval for the total duration of radon accumulation and V_{stp} is the corrected air volume inside the calibration barrel at standard pressure and temperature (1 bar; 0 °C). Therefore, the calibration factor "E" (Bq h mm^2/m^3 tracks) is given by the following Equation:

$$E = \frac{R_s\, T}{N_{net}} \quad (3)$$

Where T is exposure time, N_{net} stands for the net tracks after etching. During the CR-39 calibration, the air temperature and the humidity monitored (17±2 °C to 25±2 °C

and 50%±3% to 60%±3% relative humidity) to keep the condition as close as possible to the field measurement.

Regarding the thoron calibration factor, the author followed the same method as radon. On the other hand, technical difficulties concerning measurements due to the short half-life of thoron (56 sec), etc. make the development of a suitable thoron calibration chamber and its validation complicated when compared with a radon calibration chamber. Therefore, a thoron calibration chamber was recently developed at the Institute of Radiochemistry and Radioecology (RRI) at the University of Pannonia. The author is employed the technique of computational fluid dynamics (CFD) to predict accurately the concentration distribution of thoron inside the chamber and its spatial distribution at different flow rates. It is explained in details in section 2.8.

2.4.2 Estimation of annual effective dose, ELCR and LCC associated with radon/thoron exposure

The exposure of human beings to ionizing radiation from natural sources is a continuing and inescapable feature of life on earth. International organizations such as ICRP, UNSCEAR and NCRP have proposed a methodology for estimating radiation dose for radon and thoron. ICRP and UNSCEAR have proposed the radiation dose assessment methodology (Epidemiological dosimetrist models) for radon and each country has established the radiation dose assessment methodology accordingly (UNSCEAR, 2000; ICRP, 1994 2007). UNSCEAR proposed a method for evaluating effective dose by applying the major exposure factors and dose coefficients to the radioactive concentration of radon in the air. This is similar to the method proposed by the ICRP, but there are some differences in approaches to dose coefficients. As a result, doses depend mainly on the concentration of radon progeny, the duration of exposure, the breathing rate, and the aerosol properties, including the activity size distribution of the radon progeny aerosol and the unattached fraction.

Therefore, the annual committed effective doses originating from the inhalation of radon or thoron inside the dwellings were calculated using the following equation provided by (UNSCEAR, 2000):

$$E_{Rn/Tn} = C_{Rn/Tn} \times F_{Rn/Tn} \times t \times K_{Rn/Tn} \quad (4)$$

where $E_{Rn/Tn}$ denotes the annual committed effective dose from exposure to radon or thoron (mSv/year); $C_{Rn/Tn}$ stands for the annual average radon or thoron concentrations in houses (Bq/m^3); and $F_{Rn/Tn}$ represents the indoor equilibrium factors for radon or thoron and their respective progenies. The following values were provided by UNSCEAR (2000), F=0.40 and F=0.02 for radon and thoron, respectively; t is the number of hours spent inside annually (7000 h); and $K_{Rn/Tn}$ denotes the following dose conversion factors recommended by UNSCEAR (2000): K_{Rn}= 9 nSv and K_{Tn}= 40 nSv per unit of integrated radon & thoron concentrations (Bq h/m^3), respectively.

In addition, the ICRP has re-evaluated its estimates of lung cancer risk from inhalation of radon progeny and approximately doubled its risk estimate (ICRP, 2010). In Publication 137, Occupational Intakes of Radionuclides: Part 3 (ICRP, 2018), ICRP has published new dose coefficients for radon progeny. For the calculation of doses following inhalation of radon and radon progeny in mines and most buildings, the ICRP recommends a dose coefficient of 3 mSv per mJ h m^{-3} (approximately 10 mSv per working level month (WLM)). The ICRP considers this dose coefficient to be applicable to the majority of circumstances with no adjustment for aerosol characteristics.

The term "Excess Lifetime Cancer Risk" (ELCR) implies the risk of death of cancer in excess of the "natural" background risk, resulting from a lifetime exposure to carcinogens. The Excess Lifetime Cancer Risk (ELCR) per 100,000 people was calculated using Equation 5 (Vaeth and Pierce, 1990):

$$ELCR = E_{Rn/Tn} \times D_L \times R_F \quad (5)$$

where $E_{Rn/Tn}$ denotes the annual committed effective dose (mSv/year); D_L represents the life expectancy, estimated to be 70 years; and R_F stands for the risk of fatal cancer per Sievert of 5.5×10^{-2} Sv^{-1} as recommended by ICRP Publication 103.

Finally, the Lung Cancer Cases per year per million people (LCC) was estimated by using the risk factor lung cancer induction 18×10^{-6} mSv^{-1} and calculated by Equation 6 (Ismail and Jaafar, 2010):

$$\text{LCC} = E_{Rn/Tn}\times18\times10^{-6} \quad (6)$$

2.5 RADON MAPPING AND CROSS-VALIDATION

Radon mapping has profound economic and social implications, moreover, a high-resolution, accurate and statistically robust radon map is crucial to increase public awareness of environmental radioactivity and influence government policy with the purpose of reducing radon exposure in the general population. Depending on the datasets applied, two types of maps can be used: 1. Indoor Radon Maps which are based on indoor radon measurements (as applied in this study), and 2. Geogenic Radon Maps which are based on geological information (Bossew et al., 2013); i.e., geogenic reasons elevated indoor radon levels or an elevated probability of their occurrence must be expected. Geogenic factors are high radium concentrations in rock and soil, high permeability due to the coarse texture of the ground or due to fracturing of rocks, hydrological peculiarities and others. Therefore, the measurement of "what earth delivers in terms of radon" is the principal advantage of Geogenic Radon Maps (Bossew et al., 2013). On the other hand, the main advantage of Indoor Radon Maps is that radon levels are directly measured at the point of exposure. Many factors are affecting on indoor radon concentrations briefly as follows (Also shown in Figure 14):

1. *Geogenic factors:* source of indoor radon, and factors controlling radon transport into dwellings

- Geology (bedrock, surface and near-surface deposits, topsoil geochemistry, ...)
- Soil texture, permeability, etc.

2. *Meteorological factors:* enhance radon transport into dwellings, and influence life styles and building characteristics

- Barometric pressure (difference indoors -outdoors)
- Precipitation, height of the building (heating), etc.

3. *Anthropogenic factors:* enhance radon transport and accumulation into dwellings

- Height of the building (stack effect)
- Type of foundation, ventilation, etc.

Radon maps should be adapted to the objectives of the Radon Plan. This requires a multidisciplinary approach, with different criteria (no mutually exclusive) depending on the aims of the program which are:

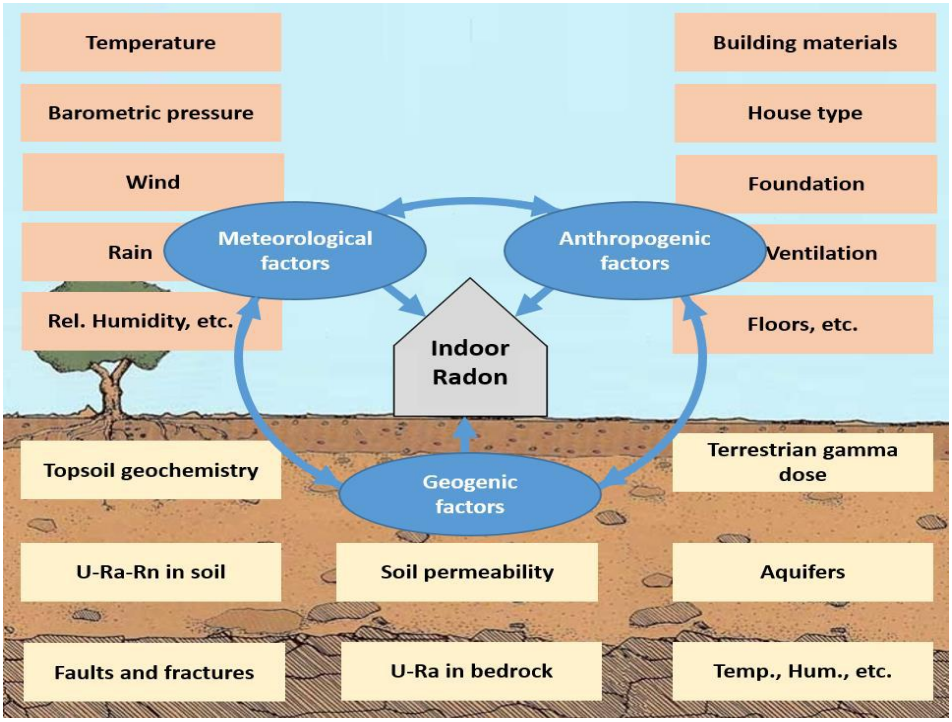

Figure 14. Factors affecting indoor radon concentrations

a) *Protection of individuals*: detect dwellings with high radon concentration (so remediation activities can start), and/or prevent the radon accumulation indoors (building regulations). In these cases, probability maps play an important role in the radon action plan. b) *Protection of collective*: reduce radon exposure to inhabitants. Reduction policy should be spatially focused where the majority of the collective dose occurs. Such areas are where the highest radon-related lung cancer incidence is expected, even if indoor radon concentrations are relatively low. Maps which link radon and population density are essential.

In this thesis, an indoor radon map for Mashhad dwellings was generated by using ArcGIS software version 10.7 over a grid with the dimensions of 1 km × 1 km, moreover, three interpolation methods were tested: inverse distance weighting (IDW), ordinary kriging (OK), and Empirical Bayesian kriging (EBK). Indeed, the IDW interpolation technique estimates a weighted average at an unsampled point ($\acute{Z}_0$) according to its distance (d_i) to the sampled points (Z_i):

$$\acute{Z}_0 = \frac{\sum_{i=1}^{n} \frac{1}{d_i^p} Z_i}{\sum_{i=1}^{n} \frac{1}{d_i^p}} \quad \text{if} \quad d_i > 0; \text{ otherwise } (d_i = 0): \ \acute{Z}_0 = Z_i \qquad (7)$$

where "p" is the inverse distance weighting power (idp), which represents "the degree to which the nearer points are preferred over more distant points" (Bivand et al., 2008).

IDW assumes that, on average, nearby points are more similar to each other than more distant points, and therefore the weights for the closer ones are higher than the weights for distant points. Regarding the ordinary kriging, it is the most widely used kriging method. It serves to estimate a value at a point of a region for which a variogram is known, using data in the neighborhood of the estimation location. While, EBK is a geostatistical interpolation method that automates the most difficult aspects of building a valid kriging model. EBK also differs from other kriging methods by accounting for the error introduced by estimating the underlying semivariogram. Other kriging methods calculate the semivariogram from known data locations and use this single semivariogram to make predictions at unknown locations; this process implicitly assumes that the estimated semivariogram is the true semivariogram for the interpolation region. By not taking the uncertainty of semivariogram estimation into account, other kriging methods underestimate the standard errors of prediction.

In this thesis, the arithmetic mean (AM) was used over grid cells with the dimensions of 1 km × 1 km to predict the mean indoor radon concentration on the ground floor of buildings in the grid cells where no data was available. It is important to keep in mind that radon maps are only a probabilistic tool to make policy decisions such as prioritization; they cannot be used to derive radon concentrations for an individual dwelling. The accuracy of the different techniques was also assessed by using six indicators, namely the mean absolute error (MAE), root mean square error (RMSE), root mean squared logarithmic error (RMSLE), index of agreement (IA), percentage bias (PB) and coefficient of determination (R^2) as presented in Equations 8–12:

$$\text{MAE} = \frac{1}{n}\sum_{i=1}^{n}|Z_i - X_i| \tag{8}$$

$$\text{RMSE} = \sqrt{\frac{1}{n}\sum_{i=1}^{n}(Z_i - X_i)^2} \tag{9}$$

$$\text{RMSLE} = \frac{1}{n}\sum_{i=1}^{n}\big(log(Z_i + 1) - log(X_i + 1)\big)^2 \tag{10}$$

$$\text{IA} = 1 - \frac{\sum_{i=1}^{n}(Z_i - X_i)^2}{\sum_{i=1}^{n}(|X_i - \bar{X}| - |Z_i - \bar{X}|)^2} \tag{11}$$

$$\text{PB} = 100\frac{\sum_{i=1}^{n}(Z_i - X_i)}{\sum_{i=1}^{n}X_i} \tag{12}$$

$$\text{R}^2 = 1 - \frac{\sum_{i=1}^{n}(Z_i - X_i)^2}{\sum_{i=1}^{n}(|X_i - \bar{X}|)^2} \tag{13}$$

where Z_i and X_i denote the predicted and measured values in the validation location (S_i), n stands for the number of points in the validation group, and X represents the

mean of X_i. *MAE* and *RMSE* are commonly used to assess model performance. These parameters are positive values and the closer they are to 0, the better the model fit is. *IA* is a standardized measure of the degree of model prediction error; it varies from 0 (no agreement at all) to 1 (perfect match). *PB* (%) measures the average tendency of having larger/smaller predicted values than those observed, the optimal value is 0 and positive/negative values indicate overestimation/underestimation bias (Janik et al., 2018). R^2 is the fit line explaining how well the model fits a dataset; R^2=1 for a perfect model (Alexander et al., 2015).

2.6 GAMMA SPECTROMETRY

A high-resolution gamma ray spectrometer, equipped with an ORTEC GMX 40-76 HPGe semiconductor radiation detector by relative efficiency of 40%, used to evaluate all gamma emitting components, both by quality and quantity through the detection of the amplitude and energy level of the emitted gamma photons from isotopes, and hence determining the specific activities of the radionuclides (^{232}Th, ^{226}Ra and ^{40}K) in the samples. The detector was covered with a 20-centimeter thickness of lead shield and a layer of nickel all around to decrease the natural background rate. Data and detected gamma rays analyzed by Aptec MCA Multichannel Analyzer software.

To measure spectra of gamma rays emitted from samples, 500 to 600 g of each sample was pulverized to less than 3 mm before being dried at 105 °C for 6 h to remove moisture. The samples were then placed into Marinelli beakers and sealed for approximately 29 days in order to reach secular equilibrium between ^{226}Ra and ^{222}Rn prior to counting (Schötzig and Debertin, 1983). The ^{226}Ra activity concentration was determined by using the energy peaks of its decay products ^{214}Pb and ^{214}Bi at 352 (35%) and 609 keV (45%), respectively. The ^{232}Th activity concentration was determined by the own gamma lines of its decay products ^{228}Ac and ^{208}Tl at 911 (28%) and 2614.51 keV (36%), respectively. The ^{40}K activity concentration was calculated using its own gamma line at the energy of 1460.8 keV (11%) (Bé et al. 2007). The system was calibrated with an IAEA-375 soil reference material with known activity concentration of radionuclides. The energy calibration was carried out by three sealed sources: ^{137}Cs with a gamma line of 661.6 keV, ^{60}Co with two gamma lines of 1173.2 and 1332.5 keV and ^{241}Am with an X-ray line of 59.5 keV (Bé et al. 2007).

The activity concentration of radionuclides (Bq/kg) calculated using following equation (Adelikhah et al., 2020; Shahrokhi et al. 2020; Imani et al., 2021):

$$A_i = \frac{1000N}{T_c P_\gamma \varepsilon M e^{-\lambda t}} \quad (14)$$

where A_i is activity concentration of specific radionuclide in time of sampling (Bq/kg), N denotes the net count rate of photopeak, T_c represents the live counting time (second), P_γ stands for probability of gamma ray transition via the specific energy, $\mathcal{E}$ is the counting efficiency at specific photopeak energy, M is the sample mas (kg), t represents time interval between sampling and measuring (day), and λ is decay constants (expressed as $\frac{Ln\,2}{t_{1/2}}$ which $t_{1/2}$ is half-life of radionuclide calculated). The background was measured for an empty Marinelli container with the same geometry of standard and sample container for 200,000 s. The typical measurement time for each sample was also 80,000 s.

The Minimum Detectable Limit (MDL) and uncertainty and of the measurement in accordance with given data by Aptec analyzer software are calculated by Equation (15) and (16) as follow:

$$MDL = \frac{(\sigma^2 + 2\sigma(\sqrt{2B}))}{t} \quad (15)$$

where MDL is minimum detectable for photo-peak energy, σ is uncertainty, B is background rate under photo-peak ROI and t live counting time.

Respective uncertainties were determined according to the statistical uncertainties of the peak areas provided by the Aptec analyzer software as follow:

$$\sigma = \frac{2\sqrt{C+B}}{C} \quad (16)$$

where σ is uncertainty, C is net sample count rate under photo-peak ROI (cps) and B is net background rate under photo-peak ROI (cps).

2.7 ASSESSMENT OF RADIOLOGICAL HAZARD EFFECTS

Indoor exposure to gamma rays, mainly determined by the materials of construction, is inherently greater than outdoor exposure if earth materials have been used; the source geometry changes from half-space to a more surrounding configuration indoors. When the duration of occupancy is taken into account, indoor exposure becomes even more significant (UNSCEAR, 2000). Several radiological parameters, such as

radium equivalent activity, external and internal hazard index, absorbed dose rate, external gamma radiation and internal alpha radiation was calculated to evaluate the potential radiological hazards and assess the radiation risk to human.

2.7.1 Radium equivalent activity (Ra_{eq})

Since NORMs are composed of different amounts of ^{226}Ra, ^{232}Th and ^{40}K, the radium equivalent activity index (Ra_{eq}) was used. It is calculated according to the assumption that 370 Bq/kg for ^{226}Ra, 259 Bq/kg for ^{232}Th and 4810 Bq/kg for ^{40}K produce the same gamma radiation dose and can be calculated using Equation 17 (Beretka and Mathew, 1985):

$$Ra_{(Eq)} = A_{(Ra\text{-}226)} + (A_{(Th\text{-}232)} \times 1.430) + (A_{(K\text{-}40)} \times 0.077) \quad (17)$$

where A_{Ra}, A_{Th} and A_K are the activity concentrations of ^{226}Ra, ^{232}Th and ^{40}K, respectively in Bq/kg. The recommended maximum value of the radium equivalent activity index (Ra_{eq}) for the given building material should not exceed 370 Bq/kg, corresponding to the annual effective dose of 1.5 mSv/year (NEA-OECD, 1979).

2.7.2. Absorbed gamma dose rate (D) and the annual effective dose rate (AED)

To estimate annual effective doses, account must be taken of (a) the conversion coefficient from absorbed dose in air to effective dose and (b) the indoor occupancy factor. The average numerical values of those parameters vary with the age of the population and the climate at the location considered. The absorbed gamma dose rate, caused by NORMs in building materials, and the corresponding annual effective dose rate were calculated using Equations 18 and 19, respectively (European Commission, 1999):

$$D = (0.92 \times A_{(Ra\text{-}226)}) + (1.1 \times A_{(Th\text{-}232)}) + (0.080 \times A_{(K\text{-}40)}) \quad (18)$$

$$AED_{(indoor)} = D \times T \times 0.8 \times 0.7 \times 10^{-3} \quad (19)$$

where D represents the absorbed gamma dose rate from NORMs (nGy/h), AED stands for the annual effective dose rate (μSv/year), 0.7 is the conversion factor (Sv/Gy), 0.8 is the indoor occupancy factor, and T denotes the number of hours in a year (8760 h/year).

2.7.3. Hazard indices for external gamma radiation (H_{ex}, I_γ)

In this thesis, the following hazard index for the external gamma radiation doses emitted from building materials to ensure their safe use was applied (Beretka and Mathew, 1985):

$$H_{ex} = \left(\frac{A_{Ra-226}}{370} + \frac{A_{Th-232}}{259} + \frac{A_{K-40}}{4810} \right) \leq 1 \quad (20)$$

where *A* denotes the activity concentrations of specific radionuclides (Bq/kg). $H_{ex} = 1$ corresponds to a radium equivalent activity of 370 Bq/kg. If the limit is exceeded ($H_{ex} > 1$), it means the potential external dose to exposed individual would be higher than the acceptable level meaning a potential health risk to the public. The European Commission (EC) also proposed an index called the gamma index (I_γ) to verify whether the guidelines issued by the EC concerning the usage of building materials are met. I_γ is calculated using the following formula (European Commission, 1999):

$$I_\gamma = \left(\frac{A_{Ra-226}}{300} + \frac{A_{Th-232}}{200} + \frac{A_{K-40}}{3000} \right) \leq 1 \quad (21)$$

2.7.4. Hazard indices for internal alpha radiation (H_{in}, I_α)

In order to measure the excess internal alpha radiation exposure caused by inhalation of ^{222}Rn and its short-lived decay products originating from building materials, the internal hazard index (H_{in}) can be used, which has been defined as (Beretka and Mathew, 1985; El-Taher, 2010):

$$H_{in} = \left(\frac{A_{Ra-226}}{185} + \frac{A_{Th-232}}{259} + \frac{A_{K-40}}{4810} \right) \leq 1 \quad (22)$$

H_{in} should be less than 1 for the use of building materials in the construction of dwellings to be regarded as safe (Krieger, 1981). Alpha index (I_α) was also suggested by Krieger and Stoulos as given below (Krieger, 198; Stoulos et al., 2003):

$$I_\alpha = \frac{A_{Ra-226}}{200} \quad (23)$$

2.8 CFD MODELLING APPROACH, BOUNDARY CONDITIONS AND PARAMETERS FOR THORON CALIBRATION CHAMBR

The geometric model considered in this study was based on a calibration chamber in a laboratory at the Institute of Radiochemistry and Radioecology at the University of Pannonia, as is shown in Figure 15. The calibration chamber is made of stainless steel with a volume of 210.5 liters with a lid that can be opened to insert instruments that need to be calibrated. The temperature and humidity are measured as well as controlled inside the chamber. These values were nearly constant and found to be 20-22 ˚C and approximately 50%, respectively. The chamber contains ports to insert thoron gas from an external source. Furthermore, unstructured triangular meshes were used for ANSYS

meshing due to their high degree of accuracy, adaptive meshing capabilities and parallel processing with a minimum volume of 3.92×10^{-11} m^3 using 3,422,491 cells.

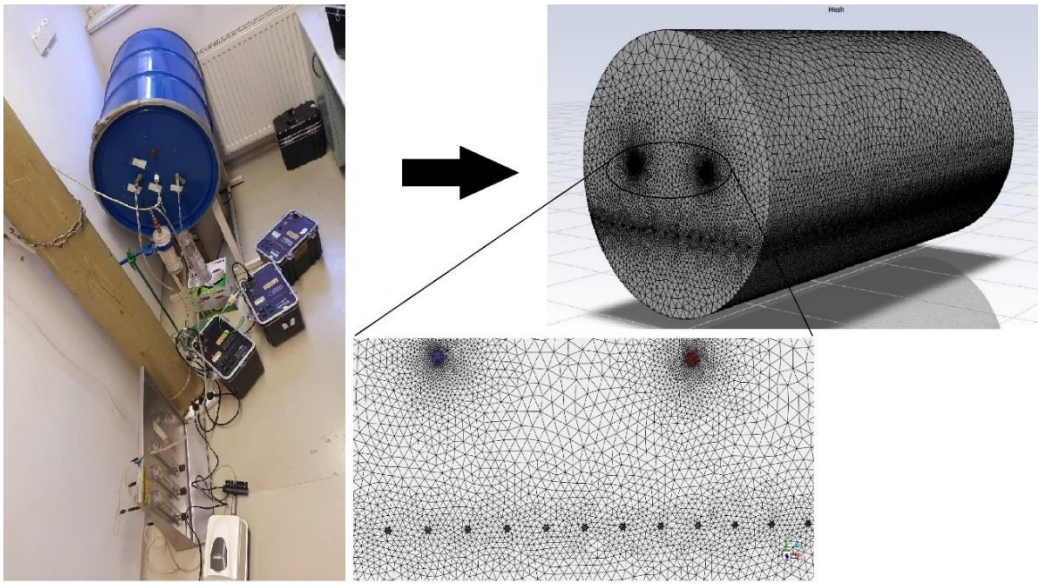

Figure 15. Schematic diagram of the thoron calibration chamber with its meshing

2.8.1 CFD simulation approach

The CFD software based on the finite volume method (FVM) has been used to predict and visualize the spatial distribution of thoron inside the calibration chamber. CFD involves solving a set of nonlinear partial differential equations using numerical methods. Fundamental physical laws are represented by these equations that govern fluid flow and related phenomena, namely the conservation of mass, momentum and energy. CFD analysis tools solve the system of mass, energy, and momentum conservation equations known as the Navier-Stokes equations to determine the air velocity, temperature and contaminant concentration at each of these nodes in space and time. Since each of the equations for the conservation of mass, energy, momentum, and chemical or biological species involve the pressure, temperature, velocity, and concentration of an element and its neighbors, the equations for all of the elements must be solved simultaneously. Nowadays CFD is used most often than the experimental approach to study the indoor air quality (IAQ) problems. This involves the solving the flow behavior numerically by using a computer. Due to the limitations of the experimental approach and the increase in the performance and affordability of computers, CFD provides a practical option for computing the airflow and pollutant distributions in confined areas.

In this thesis, modeling and simulation is carried out by CFD code, ANSYS FLUENT package because of its abilities to solve species model conflation with energy (heat), air flow in two and three dimensions. Ansys Fluent is the industry-leading fluid simulation software known for its advanced physics modeling capabilities and unmatched accuracy. By discretizing and linearizing equations as well as under the relevant boundary conditions (e.g., inlet, outlet, solid surfaces, etc.), the computational domain is enclosed. Some important assumptions are made: A) continuous incompressible airflow and B) homogeneous as well as uniform temperature distribution inside the chamber. Accordingly, the steady-state inside flow field could be expressed by continuity and conservation of momentum equations as follows.

2.8.2 Governing the equations

All variants of CFD methods are based on the governing equations for fluid flow, which are called transport equations and derived from the laws of conservation of mass, momentum and energy as well as the conservation of species (contaminants) and the turbulence scales of k and Ɛ (Etheridge and Sandberg, 1996). All transport equations have the same general form and comprise 4 terms called transient, convection, diffusion and source term which are written, respectively. In steady state model, the transient section is equal to zero and all sources are also equal to zero. Hence, mass transport is governed by two processes as:

-Molecular diffusion, which is stated by Fick's law

-Turbulent diffusion, which is the transportation of contaminants by turbulent (eddy) diffusion. Generally turbulent diffusion coefficient is greater than molecular diffusion coefficient.

ANSYS FLUENT can model the mixing and transport of chemical species by solving conservation equations describing convection, diffusion, and reaction sources for each component species. For all flows, ANSYS FLUENT solves conservation equations for mass and momentum (Fluent, 2006). For flows involving heat transfer or compressibility, an additional equation for energy conservation is solved. For flows involving species mixing or reactions, a species conservation equation is also solved. Additional transport equations are also solved when the flow is turbulent.

2.8.2.1 Conservation of mass

The equation for conservation of mass, or continuity equation, can be written as follows:

$$\frac{\partial \rho}{\partial t} + \frac{\partial}{\partial x}(\rho u) + \frac{\partial}{\partial y}(\rho v) + \frac{\partial}{\partial z}(\rho w) = 0 \quad (24)$$

where ρ, density and u, v and w are the velocity components in the x, y, z directions, respectively. This Equation is the general form of the mass conservation equation and is valid for incompressible as well as compressible flows for laminar flow.

2.8.2.2 Conservation of momentum

The momentum equations, which are also called the Navier- Stocks equations, for the turbulent air flow (with turbulence viscosity and diffusion coefficient), with some simplifying, are expressed in x, y and z directions as:

U-momentum in x direction:

$$\frac{\partial}{\partial t}(\rho u) + \frac{\partial}{\partial x}(\rho u u) + \frac{\partial}{\partial y}(\rho u v) + \frac{\partial}{\partial z}(\rho u w) = -\frac{\partial P}{\partial x} + \frac{\partial}{\partial x}\left(\mu_e \frac{\partial u}{\partial x}\right) + \frac{\partial}{\partial y}\left(\mu_e \frac{\partial u}{\partial y}\right) + \frac{\partial}{\partial z}\left(\mu_e \frac{\partial u}{\partial z}\right) + \frac{\partial}{\partial x}\left(\mu_e \frac{\partial u}{\partial x}\right) + \frac{\partial}{\partial y}\left(\mu_e \frac{\partial v}{\partial x}\right) + \frac{\partial}{\partial z}\left(\mu_e \frac{\partial w}{\partial x}\right) \quad (25)$$

V-momentum in y direction:

$$\frac{\partial}{\partial t}(\rho v) + \frac{\partial}{\partial x}(\rho u v) + \frac{\partial}{\partial y}(\rho v v) + \frac{\partial}{\partial z}(\rho v w) = -\frac{\partial P}{\partial y} + \frac{\partial}{\partial x}\left(\mu_e \frac{\partial v}{\partial x}\right) + \frac{\partial}{\partial y}\left(\mu_e \frac{\partial v}{\partial y}\right) + \frac{\partial}{\partial z}\left(\mu_e \frac{\partial v}{\partial z}\right) + \frac{\partial}{\partial x}\left(\mu_e \frac{\partial u}{\partial y}\right) + \frac{\partial}{\partial y}\left(\mu_e \frac{\partial v}{\partial y}\right) + \frac{\partial}{\partial z}\left(\mu_e \frac{\partial w}{\partial y}\right) - g(\rho - \rho_0) \quad (26)$$

W-momentum in z direction:

$$\frac{\partial}{\partial t}(\rho w) + \frac{\partial}{\partial x}(\rho u w) + \frac{\partial}{\partial y}(\rho w v) + \frac{\partial}{\partial z}(\rho w w) = -\frac{\partial P}{\partial z} + \frac{\partial}{\partial x}\left(\mu_e \frac{\partial w}{\partial x}\right) + \frac{\partial}{\partial y}\left(\mu_e \frac{\partial w}{\partial y}\right) + \frac{\partial}{\partial z}\left(\mu_e \frac{\partial w}{\partial z}\right) + \frac{\partial}{\partial x}\left(\mu_e \frac{\partial u}{\partial z}\right) + \frac{\partial}{\partial y}\left(\mu_e \frac{\partial v}{\partial z}\right) + \frac{\partial}{\partial z}\left(\mu_e \frac{\partial w}{\partial z}\right) \quad (27)$$

where, P is the static pressure, $\mu e=(\mu + \mu_t)$ is the air effective (laminar and turbulent) viscosity coefficient, where μ and μ_t refer to dynamic and turbulent viscosity, respectively. The standard k-ε model was used to incorporate the effect of turbulence on the flow field given that it is capable of describing the investigated phenomenon and has been used by many scholars (Zhou et al., 2001; Akbari et al., 2013; Chauhan et al., 2014; Adelikhah et al., 2022), while ρ is the air density, ρ_0 is the air density at a reference temperature and g is the gravity acceleration in the y direction (Awbi, 2002).

Two-equation models are the simplest available means of calculating turbulent stresses in the recirculation flow where the length scale distribution cannot be calculated algebraically. The Standard k- ε model as a two-equation model is a semi empirical model based on model transport equations for the kinetic energy k and its dissipation rate ε. For using this model, it is assumed that the flow is fully turbulent and that the effects of molecular viscosity are negligible (Awbi, 2002). Launder and Spalding (1974) also proposed a modified version of the k- ε model (Launder and Spalding, 1974).

2.8.2.3 Conservation of thermal energy

The thermal energy equation per unit volume in closed area is as:

$$\frac{\partial}{\partial t}(\rho T) + \frac{\partial}{\partial x}(\rho u T) + \frac{\partial}{\partial y}(\rho u T) + \frac{\partial}{\partial z}(\rho u T) = \frac{\partial}{\partial x}\left(\Gamma_e \frac{\partial T}{\partial x}\right) + \frac{\partial}{\partial y}\left(\Gamma_e \frac{\partial T}{\partial y}\right) + \frac{\partial}{\partial z}\left(\Gamma_e \frac{\partial T}{\partial z}\right) + S_T \quad (28)$$

In this equation:

$\Gamma_e = \Gamma + \Gamma_T$ refers to the effective (laminar and turbulent) diffusion coefficient Where, Pr=σ=μ/T represents the Prandlt number of fluid, and S_T is a thermal source term (W/m^3).

2.8.2.4 The concentration of species equation

When the species transport model is selected and the individual species are defined in the model then the conservation equation including the convection and diffusion is solved for each species, *C*, through the solution of a convection-diffusion equation for each species. Then mass fraction of the species is predicted by FLUENT and the conservation equation for species transport model is as the following general form:

$$\frac{\partial C}{\partial t} = S + \nabla \cdot (D \nabla C) - \nabla \cdot (UC) - \lambda C \quad (29)$$

where *C* represents the thoron concentration in the domain volume (Bq/m^3), *S* refers to the thoron source (Bq/m^{3}s), *D* denotes the thoron diffusion coefficient (m^2/s), *U* stands for the mean airflow velocity (m/s) and λ is the thoron decay constant (0.01246 s^{-1}). During the simulation, the walls of the calibration chamber were isolated and the Neumann boundary condition applied. The main airflow was along the z-axis of the coordinate system chosen for the simulation.

In order to determine the optimum positions of the inlet and outlet as well as the spatial distribution of thoron inside the calibration chamber, simulations were initially carried

out using different chamber configurations and flow rates (5 to 100 l/min), as given in Table 3. Simulations were conducted until the convergent results were obtained in each case.

Table 3. Different positions of the inlet and outlet in the thoron calibration chamber for CFD simulations

Chamber configuration	**Position coordinates (x, y, z) along the axis (m)**	
	Inlet port	**Outlet port**
I	0, 5, 0	0, -5, 0
II	0, 10, 0	0, -10, 0
III	-10, -10, 0	10, -10, 0
IV	10, 10, 0	-10, 10, 0
V	0, 15, 0	0, -15, 0

2.8.3 Analytical prediction

In order to predict the transmission factor of thoron, the thoron concentration at the outlet (C_{out}) was also estimated analytically using a chamber of a specified volume, at a given flow rate and subjected to a particular thoron concentration at the inlet (C_{in}). Therefore, by applying the uniform mixing model, which is based on the assumption that the gas mixes uniformly inside the closed volume, the thoron concentration at the outlet (C_{out}) was calculated according to the following equation:

$$\frac{C_{out}}{C_{in}} = \frac{1}{1+\frac{\lambda V}{Q}} \tag{30}$$

where C_{out} and C_{in} denote the thoron concentration at the outlet and inlet (Bq m^{-3}), respectively; λ stands for the decay constant of thoron (0.01246 s^{-1}), V refers to the volume of the closed chamber (m^3) and Q represents the volumetric flow rate (m^3/s) which is measured by the rotameter in the inlet and applied to calculate the transmission factor of thoron (C_{out}/C_{in}). Consequently, by assuming the uniform mixing model, the variation in the transmission factor of thoron with the flow rate (Q) is illustrated in Figure 16. As is shown in the following figure, at very high flow rates, the transmission factor approaches saturation.

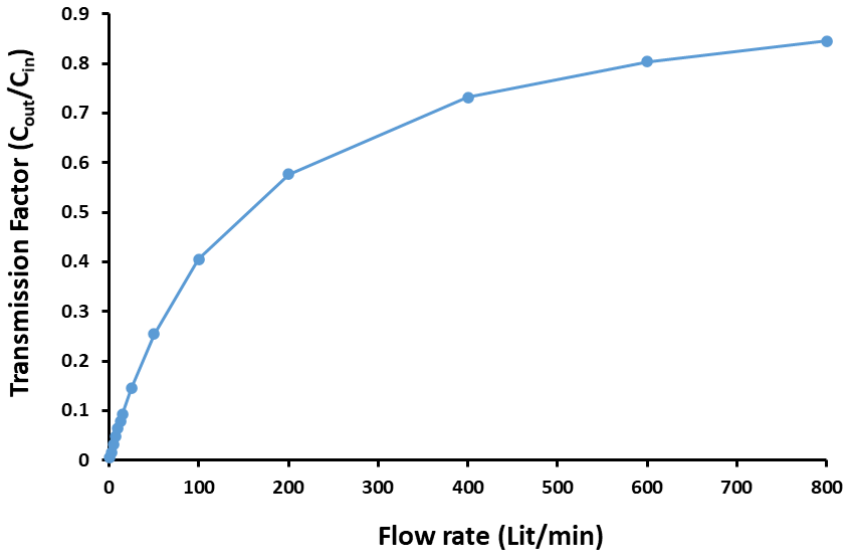

Figure 16. Variation in the transmission factor of thoron with the flow rate according to the analytical model

2.8.4 Experimental set up and CFD validation

Currently, three different sources of ceramic with different thorium contents are available at RRI (Jobbágy and Bety-Denissa, 2010) and previously performed experiments have shown that the sources are suitable for the purposes of research. Therefore, the investigations were continued along these lines (Csordás et al., 2015; Fábián et al., 2017) and concentrations of up to 19 kBq/m^3 can be produced inside the chamber by different sources. The sources of ceramic were produced by Sibelco. The IDs of the ceramics, which were used in the paper (FSZ, WB, GR), are from the product numbers (FSZ/WG-SK, WB30PM-T, GR-T) of this company. Afterwards, the source was placed outside the chamber to obtain optimized configuration from the simulation step. Having passed through a drying column and filter, the air was pumped through the source before entering the chamber and mixed inside it by a fan. The air exiting via the outlet was recirculated through the source creating a closed loop. A schematic diagram of the experimental setup is shown in Figure 17.

The activity concentration of thoron gas was continuously measured at the inlet (C_{in}) and outlet (C_{out}) by using RAD7 radon/thoron detectors manufactured by DURRIDGE, USA. The measurements were done using the "thoron protocol" over a 5 minute-long repeating cycle. The detectors were placed outside the chamber and connected to it by plastic pipes. As the half-life of thoron is less than 1 min, measurements of the activity

concentration of thoron gas must commence immediately after sampling. For the optimized chamber configuration and at different flow rates, five sets of experiment were carried out, the steady state C_{in} and C_{out} observed as well as the consequent transmission factor of thoron calculated.

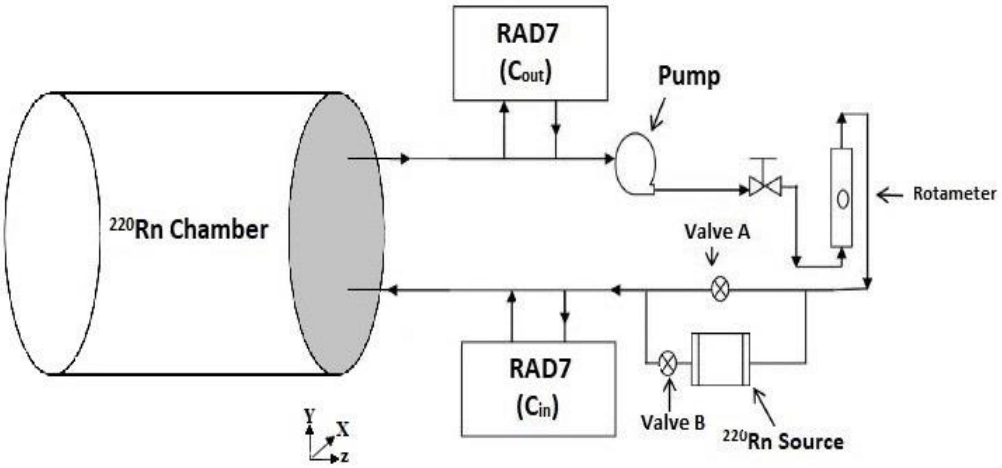

Figure 17. Experimental setup for measuring thoron activity concentrations in the thoron calibration chamber at RRI

The transmission factors of thoron (C_{out}/C_{in}) obtained from experiments, simulations and analytical models in the thoron calibration chamber at RRI at various flow rates between 2 and 25 l/min based on the optimized Configuration and the results are reported in the next chapter.

RESULTS AND DISCUSSIONS

3.1 First case of study: Mashhad, Iran

3.1.1 Indoor radon and thoron measurements in Mashhad dwellings

To estimate the impact of indoor radon and thoron on residentials as well as develop and implement the most economical method to reduce radon exposure using a radon map, within this study, the radon and thoron concentrations in 78 houses were surveyed over a total exposure time of 90 days (45 days in both the summer and winter) by using a RADUET detector as well as soil-gas radon concentrations in different districts of Mashhad, Iran by using NRPB detectors based on the CR-39. Indoor radon and thoron concentrations are measured in the living rooms of houses at ground level. Regarding the recruited of participants, the priority was given to the older houses by selecting of 3 to 5 dwellings from each district randomly de-pending on size of residential area. The majority of the houses examined were built 15 to 45 years ago using bricks composed of sand and cement along with cemented floors. The frequency distribution of the indoor radon and thoron for the 78 houses assessed in Mashhad over the two seasons are shown in Figure 18. In addition, a comparison among normal distribution and log-normal distribution of data is also illustrated in Figure 19 (Adelikhah et al., 2021).

The indoor ^{222}Rn and ^{220}Rn concentrations in the winter ranged from 75±11 to 376±24 Bq/m^3 with a mean value of 150±19 Bq.m^3 and from below the Lower Limit of Detection (LLD) to 166±10 Bq/m^3 with a mean value of 66±8 Bq/m^3, respectively. In the case of the summer, the indoor ^{222}Rn and ^{220}Rn concentrations ranged from 50±11 to 305±24 Bq/m^3 with a mean value of 114±18 Bq/m^3 and from below the LLD to 122±10 Bq/m^3 with a mean value of 48±6 Bq/m^3, respectively. In addition, the annual average indoor ^{222}Rn and ^{220}Rn concentrations in the studied areas were 132±19 Bq/m^3 and 58±7 Bq/m^3, respectively (Adelikhah et al., 2021). The main source of indoor ^{222}Rn originates from soil gas infiltration, building materials and ventilation (WHO, 2009). Meanwhile, during cold winters, residents use natural gas and close all vents causing the radon accumulation in the houses.

On the other hand, world organizations such as ICRP, WHO and U.S. EPA have recommended various guidelines for radon exposure (UNSCEAR, 2000; EPA, 2003; WHO, 2009; ICRP, 2010). The annual average indoor radon concentration is below the recommendation values (300 Bq/m^3) by the ICRP in 2010. The results concerning

the annual average radon concentration exceed the action level (100 Bq/m^3) recommended by the WHO in 2009. When compared to the worldwide geometric mean (GM) of 37 Bq/m^3 (GSD=2.2) reported by UNSCEAR in 2000, the indoor radon in the city of Mashhad is almost 4 times (139.68 Bq/m^3) and approximately 3 times (105.8 Bq/m^3) higher than the world average in the winter and summer, respectively. It was also found that during the winter and summer, the indoor radon concentrations in 31% and 20% of the dwellings were higher than the reference level of 148 Bq/m^3 recommended by the U.S. EPA in 2003.

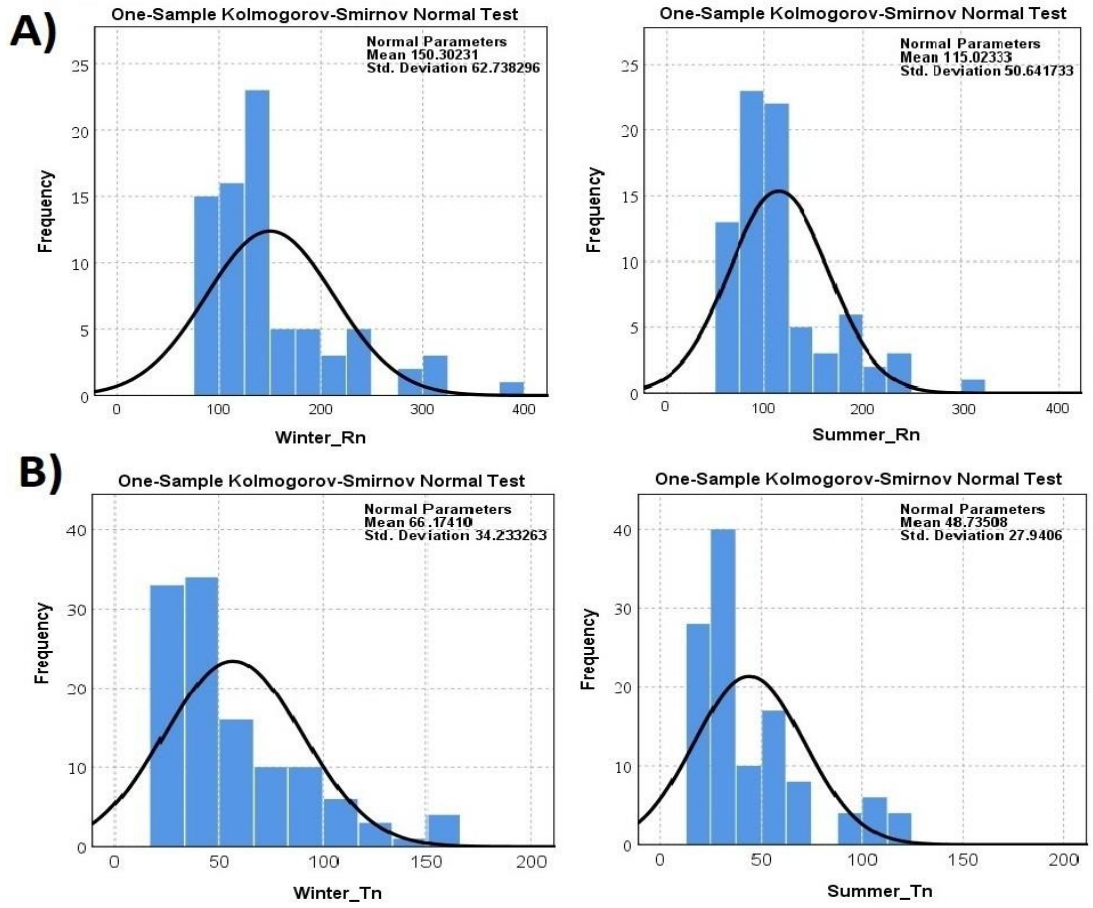

Figure 18. Normal Distribution of indoor A) radon and B) thoron concentrations (Bq/m^3) over the two seasons at ground level of dwellings examined in Mashhad

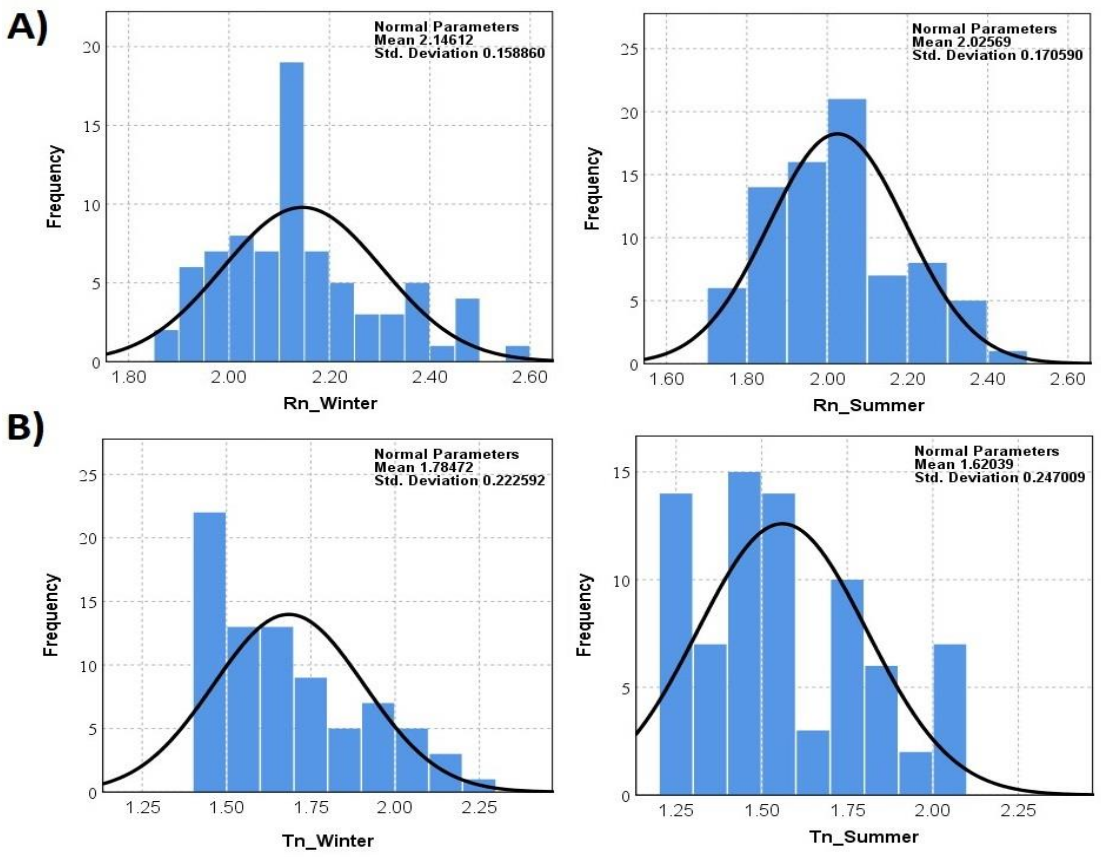

Figure 19. Log-Normal Distribution of indoor A) radon and B) thoron concentrations (Bq/m^3) over the two seasons at ground level of dwellings examined in Mashhad

The graph in Figure 20 shows the correlation between indoor ^{222}Rn and ^{220}Rn concentrations for the dwellings examined in Mashhad. Regarding the relationship between radon and thoron concentrations, no clear and strong correlation between was observed and thoron concentrations could not be predicted from widely available in-formation concerning radon. However, indoor radon and thoron concentration might directly depend on the activity of ^{226}Ra and ^{232}Th (^{228}Th) in building materials, ground is the main entry path of radon at dwellings; therefore, it could say that the content of both ^{222}Rn and ^{220}Rn depends on the building materials and soil composition (Adelikhah et al., 2021).

As previously discussed, the main source of indoor radon originates from soil-gas infiltration, ^{222}Rn concentrations in the soil gas of different districts in Mashhad were also measured by using a passive method based on CR-39 detectors in the summer when soil moisture and precipitation are low. In order to determine soil-gas radon concentrations, only 36 NRPB dosimeters were retrieved from where they were set up, while the remaining 6 dosimeters were considered lost.

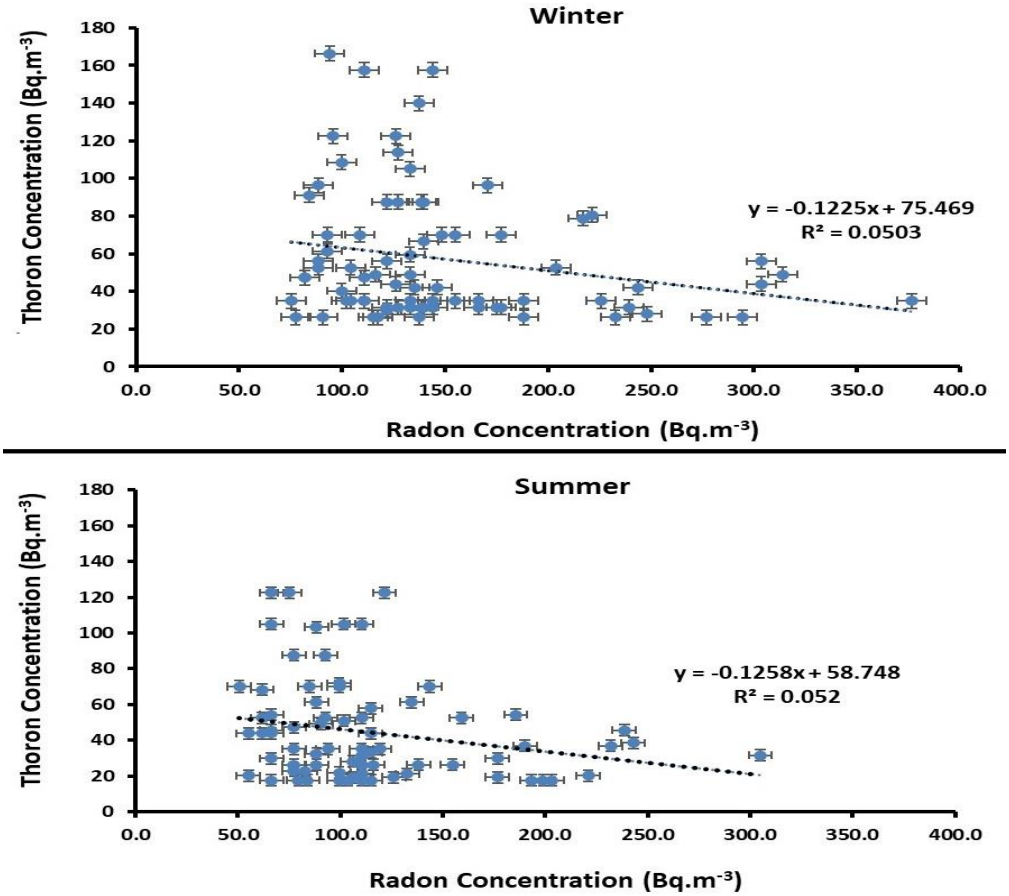

Figure 20. Correlation between the indoor radon and thoron concentrations of the 78 houses examined in Mashhad over two seasons

Figure 21 shows a histogram of soil-gas radon concentrations in Mashhad during the summer. The soil-gas radon concentrations recorded in the studied area fell within the range of 1.07±0.28 to 8.02±0.65 kBq/m^3 with a mean value of 3.07±1.09 kBq/m^3. As is shown in Figure 20, the activity concentrations of radon vary from location to location, possibly because of the physic geological properties of the types of soil studied, topographic differences, as well as geomorphology and meteorological conditions of the region. The average radon concentrations in both soil-gas and indoor environments are approximately the minimum and maximum values in the same region, respectively. Moreover, the correlation between indoor radon and soil-gas radon concentrations for the districts studied is shown in Figure 22. The correlation analysis yielded a positive correlation (R^2=0.361) between average indoor radon and soil-gas radon concentrations.

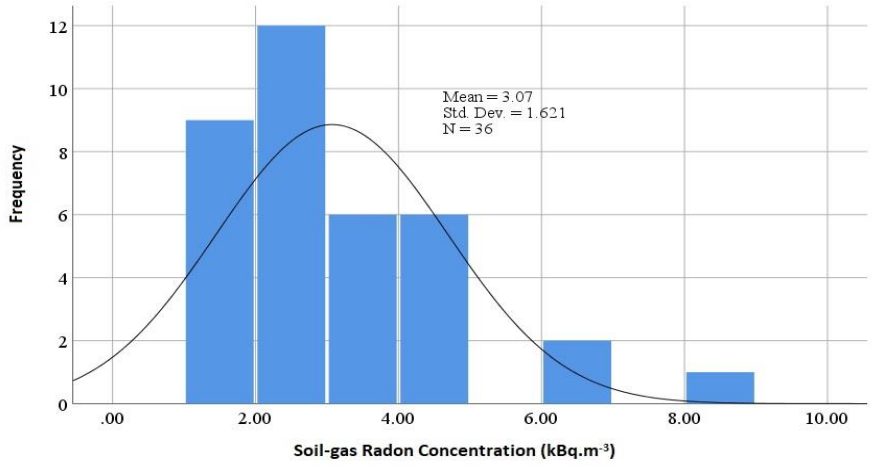

Figure 21. The soil-gas radon concentrations (kBq/m^3) in the studied area

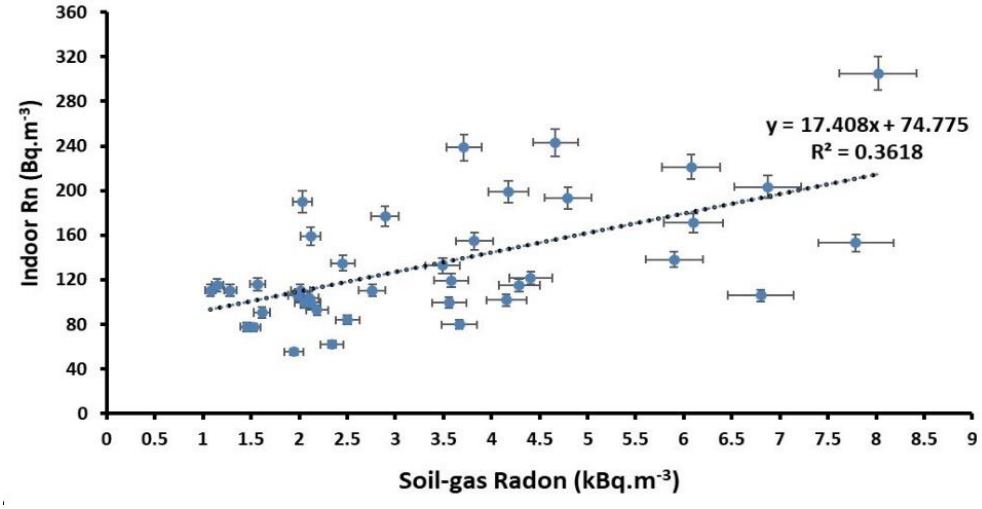

Figure 22. The correlation between indoor radon and soil-gas radon concentrations

The statistical analysis was performed using IBM SPSS Statistics 21. The Kolmogorov-Smirnov test was applied to test the null hypothesis for the homogeneous distribution of the datasets. The Kruskal–Wallis non-parametric test with the Dunn's post-hoc analysis was also used to test whether the samples originated from the same distribution based on the comparison of medians.

The normality distribution of data was checked using the Kolmogorov–Smirnov test. Considering the normality assumption in the null hypothesis of the Kolmogorov–Smirnov test, the probability value (p-value) in all tests was less than 1%; therefore, the normality distribution of radon and thoron concentrations in any of the following sub-factors was rejected. In this study, by applying the Kruskal–Wallis nonparametric test with Dunn's post hoc analysis, the null hypothesis, due to the absence of a statistically significant difference in the average gas concentration, was rejected; therefore,

the season and type of gas affect the gas concentration (P-value < 0.05). The difference in radon concentrations between well-ventilated and poorly ventilated dwellings was statistically significant ($p < 0.05$). It was assumed the house with natural ventilation as a poor ventilated and house with mechanical ventilation system as a well-ventilated house. This finding indicates that the radon concentration is lower for well-ventilated dwellings compared to poorly ventilated ones. The results of this study are consistent with others that have been conducted concerning this topic (Mehra et al., 2011; Dey and Das, 2012; Kapdan and Altinsoy, 2012). Because the level of indoor radon concentration depends on the degree of indoor ventilation, moreover, in well-ventilated dwellings, radon can easily escape and does not accumulate inside, indoor radon concentrations are less in well-ventilated dwellings compared to poorly ventilated ones (Mehra et al., 2011).

Table 4 shows descriptive statistics resulted from the measurement of the indoor radon and thoron concentrations in the 78 houses studied in Mashhad during the two seasons considered. Furthermore, the results reveal a seasonal variation in indoor radon and thoron concentrations, which are higher in the winter than in the summer. This is because doors and windows of dwellings remain closed most of the time in the winter compared to the summer, hence ventilation is poorer in the winter. The ratio of winter to summer concerning indoor radon and thoron concentrations was also established for all 78 dwellings studied. This ratio of indoor radon concentrations ranged from 1.23 to 1.48 with an average value of 1.31. With regard to the indoor thoron concentration, the average of this ratio was similar, namely 1.36. The reason of heterogeneous behavior of seasonal variations in ^{222}Rn and ^{220}Rn concentrations might be that the source of ^{220}Rn mainly limited to the concentration of ^{232}Th (^{228}Th) in building materials, while in case of radon, ground is in addition. Therefore, in summer due to high air exchange rate, e.g., using ventilator, opening windows, the concentration of both ^{220}Rn and ^{222}Rn goes down, while in winter as the air exchange rate is lower than summer, the concentration of ^{220}Rn and ^{222}Rn build up but as the source of indoor ^{222}Rn is both ground and building material rather than the only source of ^{220}Rn as building materials, the seasonal change of indoor thoron concentration is less than that of indoor radon.

Table 4. Basic Statistics of indoor and soil gas ^{222}Rn and ^{220}Rn concentrations in samples from Mashhad

Season	Parameter	A.M[1]	G.M[2]	S.D[3]	Min	Max	Winter/summer ratio (mean)	
							^{222}Rn	^{220}Rn
Summer	Indoor radon (Bq/m^3)	115.02	105.8	50.64	50.8	305.2	1.31	1.36
	Indoor thoron (Bq/m^3)	48.73	37.4	27.95	<LLD	122.5		
	Soil-gas radon (kBq/m^3)	3.07	2.71	1.621	1.078	8.021		
Winter	Indoor radon (Bq/m^3)	150.3	139.68	62.74	75.3	376.6		
	Indoor thoron (Bq/m^3)	66.17	49.41	34.24	<LLD	166.3		

[1] A.M= Arithmetical mean, [2] G.M= Geometrical mean, [3] S.D = Standard deviation.

A comparison of radon concentration in the soil-gas under investigation with those reported in other countries is also given in Table 5. It can clearly be seen that the radon concentration in soil samples from Sri Ganganagar district and the northern state of Rajasthan in India, the city of Najaf in Iraq, and Yemen are in close agreement with the present work. It can be concluded that the soil in Mashhad is suitable for construction without posing any health hazards.

Table 5. Comparison of soil-gas radon concentrations under investigation with those in other countries using different methods and sampling depths

Region	Radon in soil-gas (KBq/m^3)	Measuring method	Sampling depth (cm)	Reference
Băita-Stei, Romania	5.5-512	Lucas Cell	40-80	Cosma et al., 2013
Bolsena, Italy	7-176	RAD 7	60-70	Cinelli et al., 2015
Bulgaria	3-97	AlphaGuard	100	Kunovska et al., 2013
Hungary	1-47.1	RAD 7	80	Szabó et al., 2014
Najaf, Iraq	0.009-9.29	RAD 7	5-60	Hasan et la., 2011
Rajasthan, India	0.94-10.05	RAD 7	100	Mittal et al., 2016
Sharr-Korabi, kosovo	0.295-32	SSNTDs	80	Kikaj et al., 2016
Slovenia	0.9-32.9	AlphaGuard	100	Vaupotič et al., 2010
Sri Ganganagar, India	0.9-10.10	RAD 7	10-100	Duggal et al., 2014
Yemen	0.15-13.56	SSNTDs	0-150	Al Mugahed et al., 2019
Mashhad, Iran	**1.07-8.02**	**SSNTDs**	**50-60**	**Present study**

3.1.2 Radiation dose and risk assessment of dwellings in Mashhad

In this thesis, the average of the radon concentrations in the summer and winter is assumed to be the annual average radon concentration in Mashhad dwellings. The corresponding annual effective dose from the inhalation of radon and thoron was calculated as 3.7±0.5 mSv/year. The committed effective dose from indoor radon and thoron was found to vary from 2.11 to 9.73 mSv/year with a mean value of 4.22 mSv/year for

the winter, and 1.51 to 7.92 mSv/year with a mean value of 3.14 mSv/year for the summer. It can be seen that the committed effective doses were higher in the winter compared to the summer. The excess lifetime cancer risk and lung cancer cases per year per million people are also calculated to be 14.1 and 65.4, respectively.

According to the WHO in 2009, the risk of lung cancer increases by 16% per 100 Bq/m^3 increase in radon concentration (long-time average) (WHO, 2009). Therefore, the dose-response relation is linear, i.e., the risk of lung cancer is proportional to radon exposure (WHO, 2009). Nevertheless, based on a report produced by the Ministry of Health's Center for Disease Management in Iran, cancer is the third most significant cause of death after road traffic accidents and cardiovascular mortality. In 2019, Roshandel et al. reported that the age-standardized rates (ASR) of lung cancer were 127 and 52.1 per 100,000 Iranian males and females, respectively (Roshandel et al., 2019). In the case of Razavi Khorasan Province, the ASR was 121.2 and 54.0 per 100,000 Iranian males and females, respectively. Therefore, based on the annual average excess risk due to radon inhalation in Mashhad which is 14/100,000, i.e., less than the age-standardized death rate from cancer in Mashhad. Hence, indoor radon exposure is responsible for approximately 12% of lung cancer deaths in this city which is close to the estimates by WHO in 2009 of the worldwide proportion of lung cancer due to radon (3-14%).

Given the annual average excess risk values by comparing local radiological risks with national cancer incidence data, it can be concluded that the local risks are raised but not necessarily representative of the city as a whole. This radiation risk assessment should be considered with caution as the radon measurements are not sufficiently representative of the investigated area, moreover, calculations made using ICRP data only provide a broad overview of the risk and comparison with the national cancer incidence rate. Therefore, extensive measurements are needed for a reliable comparison. It is also essential to measure the amount of natural radiation in each area as this can determine the suitability of the environment for a healthy lifestyle. The indoor and outdoor gamma exposure rates in the air 1 m above the ground from terrestrial radionuclides and cosmic rays in Mashhad are 155.73±13.92 nGy/h and 126.15±15.66 nGy/h, respectively (Sohrabi et al., 2015). Using a determined conversion factor as 0.7 Sv/Gy, converting the absorbed dose to effective (UNSCEAR, 2000), the annual indoor and outdoor effective dose rates of the public from gamma exposure are

0.95±0.08 and 0.77±0.09 mSv/year. Therefore, by comparing these values with the corresponding annual effective doses from the inhalation of radon and thoron (3.7±0.5 mSv/year), it can be concluded that most of the doses received indoors in the dwellings studied in Mashhad city are from the inhalation of radon and thoron (about 79 % of the total dose). A comparison of the indoor radon concentration and radiation risk assessment under investigation with those reported in other Iranian cities is also provided in Table 6.

3.1.3 Spatial distribution map of indoor radon concentrations

An indoor radon map is a powerful statistical tool with accuracy and high resolution which helps educating the public on environmental radioactivity. Indoor radon maps are constructed with indoor measurements and are precise since the radon levels are measured at the point of exposure. Radon map is an important resource for any government seeking to reduce the exposure of its populace to radon gas. It influences government policies particularly on building infrastructures. Thus, it has an enormous value in both the economic and social aspect of the public.

The spatial map of the indoor radon levels for the study area was generated with the following interpolation techniques: Inverse Distance Weighting (IDW), Ordinary Kriging (OK) and Empirical Bayesian Kriging (EBK). The IDW and OK techniques, known as Kriging techniques, depend on the distance between two points, namely those of observation and estimation in the interpolation, IDW weighted the contribution of the observed points on the estimated interpolation with regard to this distance alone. On the other hand, OK also considers the correlation between the points and forms an initial function, i.e., covariance or variogram, which can iteratively be updated. The OK calculates the semivariogram from identified data points and uses this single semivariogram to make estimates at unidentified points, but in the case of EBK it takes into account the uncertainty as well.

The spatial distribution map of indoor radon concentrations in Mashhad dwellings were plotted in Figures 23-25 by various interpolation techniques, e.g., IDW, OK and EBK over a grid with the dimensions of 1 km×1 km using ArcGIS software version 10.7. The arithmetic mean was used over the grid cells to predict a mean indoor radon concentration on the ground-floor level of buildings in the grid cells where no data was

available. Accordingly, radon concentrations were lower than standard values in eastern residential areas and were higher in central as well as southern districts. Nevertheless, when the spatial autocorrelation between cells was considered, predictions about radon concentrations using different methods range from 65 to 260 Bq/m^3. These values may be more realistic and similar to average values found in some dwellings in the region.

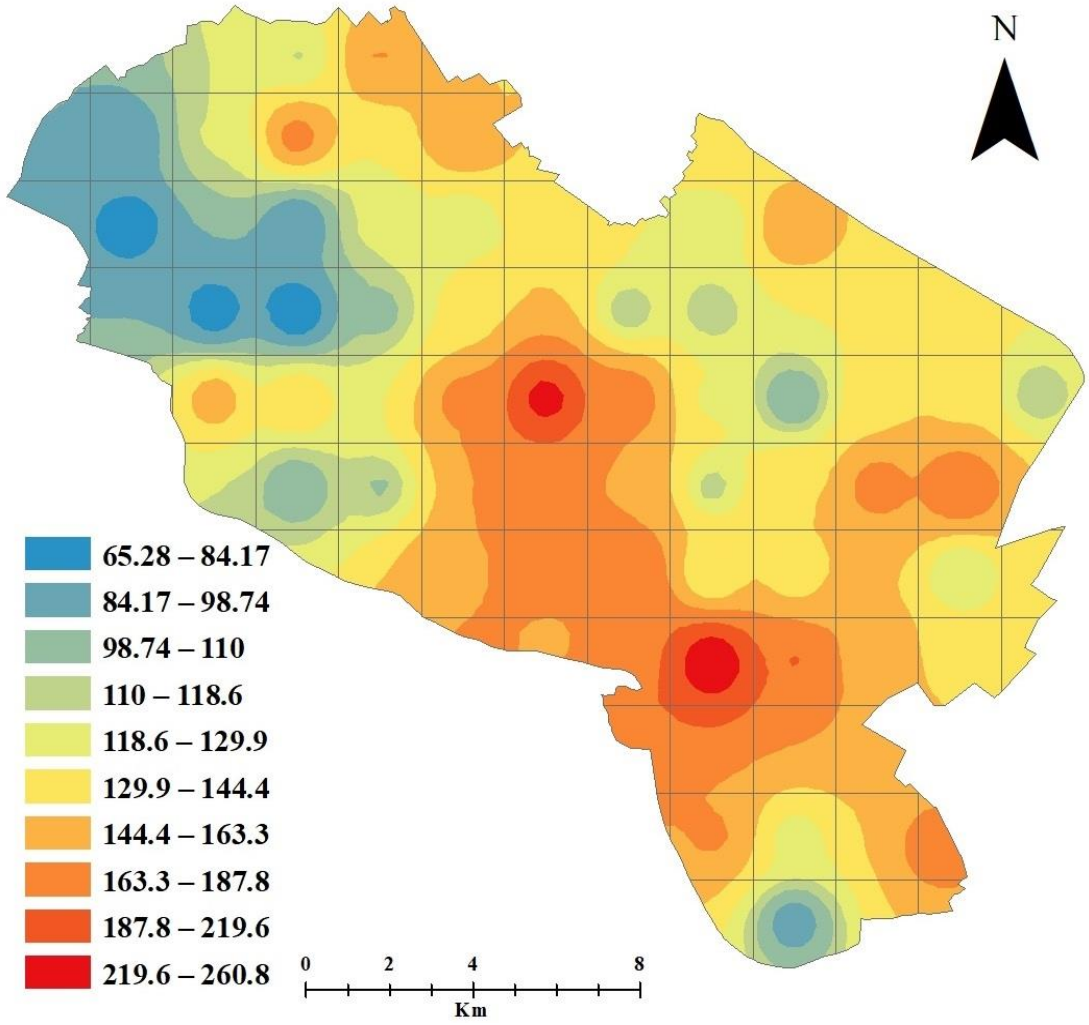

Figure 23. Predicted indoor radon map of Mashhad dwellings over a grid with the dimensions of 1 km×1 km using the IDW interpolation technique

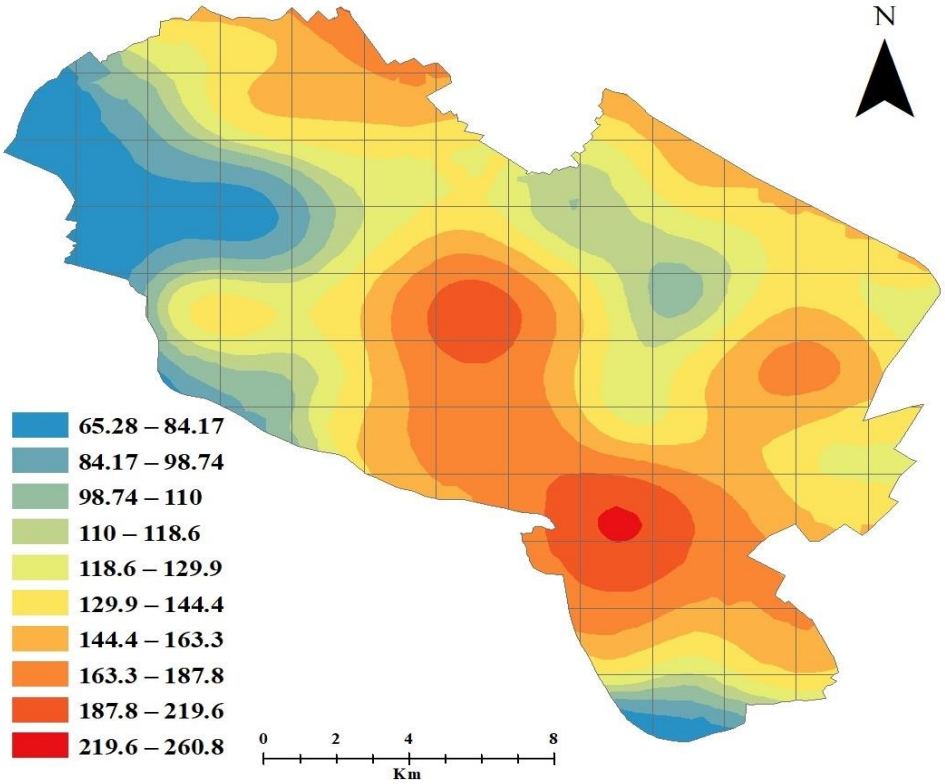

Figure 24. Predicted indoor radon map of Mashhad dwellings over a grid with the dimensions of 1 km×1 km using the OK interpolation technique

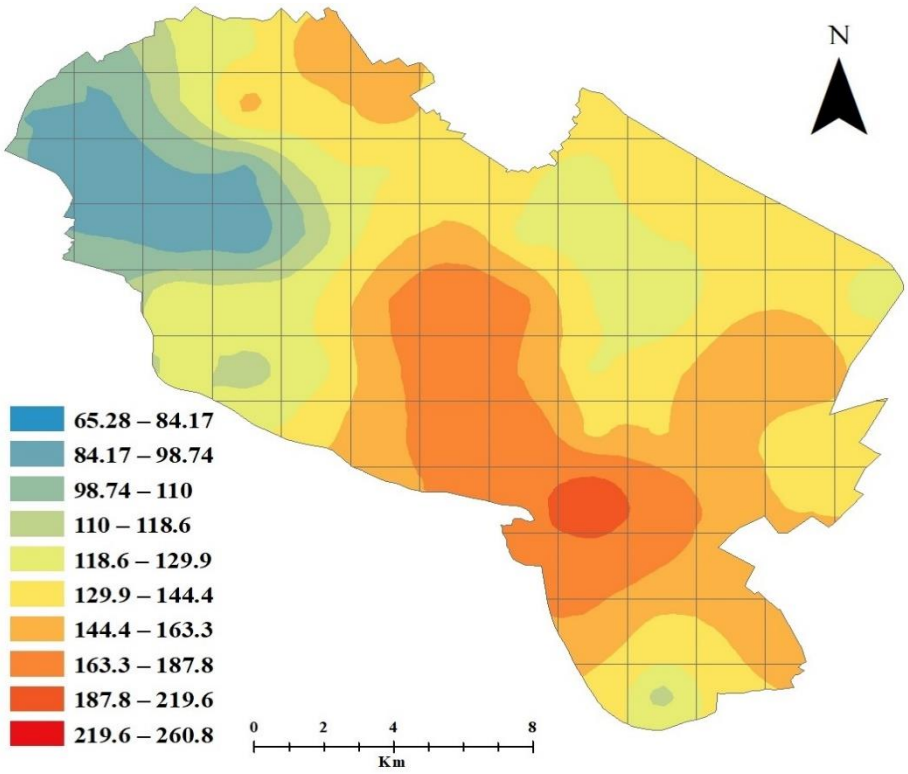

Figure 25. Predicted indoor radon map of Mashhad dwellings over a grid with the dimensions of 1 km×1 km using the EBK interpolation technique

Table 6. Studies on indoor radon concentration (Bq/m^3) and radiation health risk in various Iranian cities

Region	**Dwellings number**	**Mean Radon concentration (SD)**	**Mean effective dose (mSv/year)**	**ELCR**	**LCC× 10^{-6}**	**Excessive rate (%)**	**Reference**
Isfahan	51	28.57 (39.38)	0.72	2.7×10^{-1}	12.96	4%>100 $Bq.m^{-3}$	Mirbag and Shokati Poursani, 2019
Lahijan	400	163 (57)	3.43	1.3×10^{-2}	61.74	In most dwellings>100 $Bq.m^{-3}$	Hadad et al., 2007
Mashhad	148	31.9	(0.25-3.78)	---	---	5.3% of apartments >100 $Bq.m^{-3}$	Mowlavi et al., 2012
Qom	123	95.83	2.41	9.2×10^{-3}	43.38	24.3%> 100 $Bq.m^{-3}$	Fahiminia et al., 2016
Ramsar	500	Autumn:355 Winter:476	Autumn: 8.95 Winter: 12	3.44×10^{-2} 4.6×10^{-2}	161.11 216	--	Sohrabi, 2005
Shiraz	185	57.6 (33.06)	1.45	5.6×10^{-3}	26.1	5.4%>100 $Bq.m^{-3}$	Yarahmadi et al., 2015
Tehran	30	104	2.62	1×10^{-2}	47.16	38%>100 $Bq.m^{-3}$	Shahbazi Sehrani et al., 2019
Yazd	84	137.4 (149.5)	3.46	1.3×10^{-2}	62.28	30% of basements> 148 $Bq.m^{-3}$	Bouzarjomehri and Ehrampoosh, 2008
Mashhad	**78**	**Summer:115(51) Winter:150 (62)**	**Summer: 3.1 Winter: 4.2**	**(12.3×10^{-3}) (15.9×10^{-3})**	**(56.7) (74.1)**	**Summer: 20%>148 $Bq.m^{-3}$ Winter: 31%> 148 $Bq.m^{-3}$**	**Current study**

Table 7. Summary of the cross-validation results

Method	**MAE**	**RMSE**	**RMSLE**	**PB**	**R^2**
IDW	28.159	34.931	0.01210	20.069	0.234
EBK	28.235	35.148	0.01218	20.123	0.224
OK	28.424	36.364	0.01346	20.268	0.169

Moreover, the accuracies of the various techniques applied according to five indicators are given in Table 7. IDW, which predicts unknown values using known values concerning their distance, was proven to be more suitable for predicting mean indoor radon concentrations over grids with the dimensions of 1 km×1 km (i.e., arithmetic mean, ground floor), due to the lower MAE and RMSLE values of 28.159 and 0.01210, respectively, in addition to a lower bias, 20.069 to be exact. However, all mentioned models have a tendency to overestimate bias (PB> 0). In addition, the model with the higher R^2 is IDW which indicate that this model fits more the data well.

3.2 Second case of studies: Semnan Province and HNBR of Mahallat, Iran

The radiological survey has conducted to monitor radioactivity of most common building materials in Semnan Province, Iran and HNBR of Mahallat and assess the corresponding radiation risk. Several radiological parameters, such as radium equivalent activity, external and internal hazard index, absorbed dose rate, external gamma radiation and internal alpha radiation was calculated to evaluate the potential radiological hazards and assess the radiation risk to human.

3.2.1 Specific radioactivity in Semnan building materials

Table 8 presents the NORMs activity concentrations of the studied building materials. ^{226}Ra activity concentration was found to vary from 7±1 to 44±9 with mean value of 27±5 Bq/kg. The concentration of ^{226}Ra was the highest in tile and the lowest in marble sample. The activity concentrations of ^{232}Th in the measured samples ranged from 6±1 (in marble sample) to 60±11 Bq/kg with mean value of 23±4 Bq/kg. Granite had the highest concentration of ^{232}Th. The activity concentration of ^{40}K also were measured to be between 28±3 (in marble sample) and 1085±113 Bq/kg (in granite sample). The average activity concentration of ^{40}K was 322±41 Bq/kg. Higher activities of ^{226}Ra, ^{232}Th and ^{40}K were recorded in various building materials such as tiles, ceramic, bricks and granite but, with the exception of the granite samples, did not remarkably exceed the worldwide average values (Imani et al., 2021).

According to the results of Table 8, the average activity concentrations of NORMs for the mentioned building materials analyzed were, with the exception of ^{40}K in granite samples, lower than the worldwide average values for these building materials of 50, 50 and 500 Bq/kg, respectively (UNSCEAR, 1993). Moreover, in only one granite

sample, out of the 29 building materials analyzed, the activity concentration of ^{232}Th exceed the recommended value of 50 Bq/kg (UNSCEAR, 1993).

Table 8. Ranged and mean values of ^{226}Ra, ^{232}Th and ^{40}K activity concentrations of studied building materials

Building Material	**No.**	**Activity concentration (Bq/kg)**			
			^{226}Ra	**^{232}Th**	**^{40}K**
Sand and Gravel	3	Range	18-31	17-25	243-454
		Average±SD	24±5	22±5	362±45
Bricks	5	Range	20-39	19-34	167-536
		Average±SD	301±7	28±4	338±54
Gypsum	3	Range	10-13	11-17	66-172
		Average±SD	12±2	14±2.0	116±14
Cement	5	Range	24-38	11-18	145-312
		Average±SD	31±6	15±4	231±31
Ceramic	3	Range	29-35	22-32	208-411
		Average±SD	32±6	27±7	292±40
Tile	3	Range	31-44	28-30	279-481
		Average±SD	36±9	29.0±7	361±41
Granite	3	Range	28-43	38-60	714-1085
		Average±SD	38±7	47±8	917±101
Marble	2	Range	7-8	6-8	28-39
		Average±SD	7±1	7±1	34±3
Mosaic	2	Range	11-19	10-11	104-187
		Average±SD	15±2	10±1	145±16
Total	29	Range	**7-44**	**6-60**	**28-1085**
		Average±SD	**27±5**	**23±4**	**322±41**
Worldwide average			50[a]	50[a]	500[a]

SD=standard deviation

[a] Worldwide average given in UNSCEAR, 1993

The basic statistics of the studied building materials with regard to the NORMs activities are shown in Table 9 (Imani et al., 2021). The histograms are also given in Figures 26 (A-C). By analyzing the frequency distribution of all corresponded radionuclides, the histogram of ^{226}Ra and ^{232}Th indicates a normal distribution (bell-shaped). While ^{40}K revealed in some level of multi-modality. This multimodal feature of ^{40}K demonstrates the complexity of minerals in building materials.

Table 9. Descriptive statistics of studied building materials

Variables	**^{226}Ra**	**^{232}Th**	**^{40}K**
Median (Bq/kg)	30	22	279
Std. deviation (Bq/kg)	11	12	247
Skewness	0	1	2
Kurtosis	-1	2	3
Geometric Mean (Bq/kg)	24	20	242

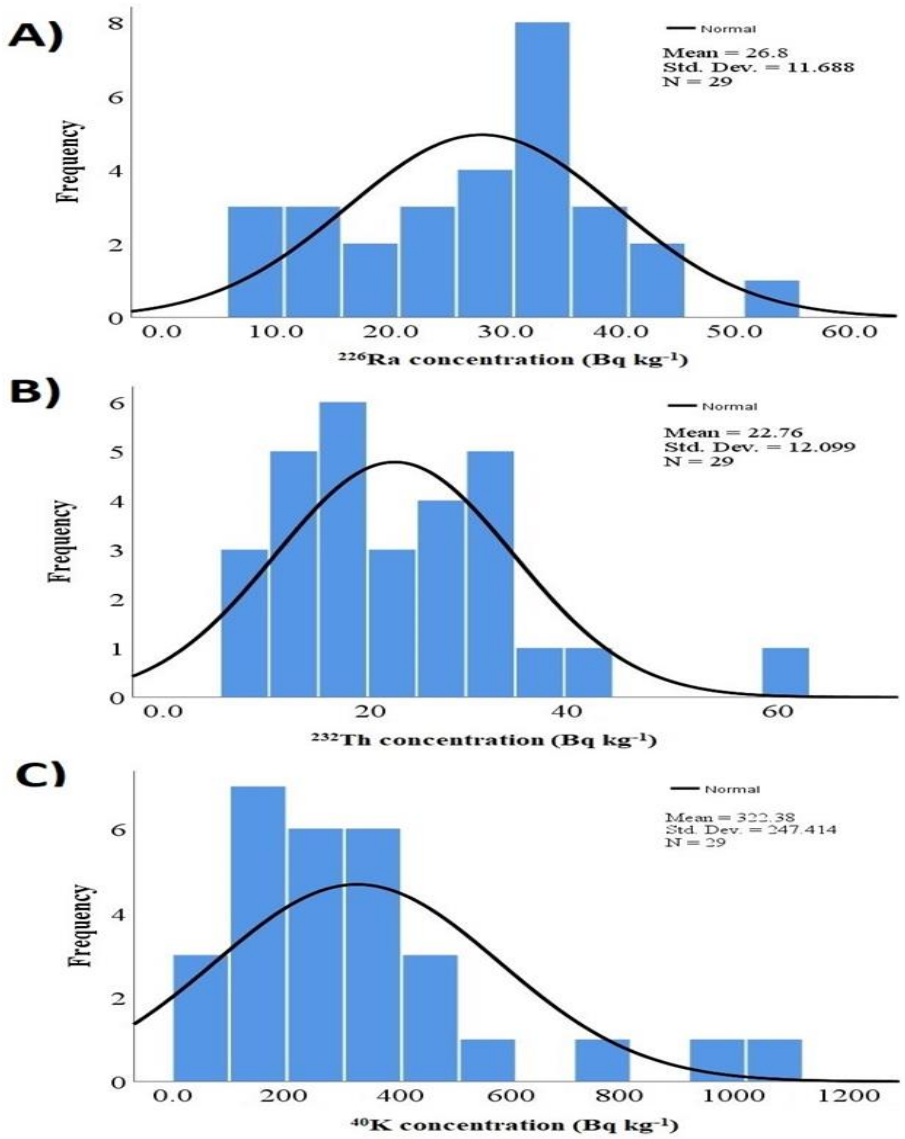

Figure 26. Frequency distribution of A) ^{226}Ra, B) ^{232}Th and C) ^{40}K

Table 10 contains the range and mean values of the radium equivalent activities of each studied building material. Accordingly, Ra_{eq} in all samples varied from 18 to 184 Bq kg^{-1} with a mean value of 84 Bq/kg. The highest value of Ra_{eq} is estimated in samples of granite (184 Bq/kg), which is significantly lower than 370 Bq/kg. The estimated absorbed gamma dose rate in air (D) and annual effective dose rate (AED) of different types of structural building materials are also presented in the fifth and sixth columns of Table 10. From the data in Table 10, the estimated maximum absorbed gamma dose rate of 168 nGy/h was in samples of granite, while the minimum value of approximately 16 nGy/h was recorded in samples of marble. The estimated mean value of D in the studied samples is 75.58 nGy/h, which is slightly higher than the worldwide average provided by the European Commission in 1999. The values of AED vary from

77 for marble to 826 μSv/year for granite. The estimated mean value of AED for all samples is 371 μSv/year, which is less than the average value for all the building materials. In addition, the highest values of H_{ex} and I_{γ}, which were both recorded in granite, are 0.50 and 0.70, respectively (see Table 10). Moreover, the obtained corresponding mean values were both below the recommended level of 1 (Beretka and Mathew, 1985; UNSCEAR, 2000). Therefore, we can conclude that the external gamma radiation does not pose any radiological hazards when these building materials are used for construction in Semnan Province, Iran. Finally, the highest values of H_{in} and I_{α} are 0.61 (in granite) and 0.22 (in tile and granite), respectively, revealing that the internal hazard is below the critical value (Imani et al., 2021).

3.2.2 Multivariate statistical analysis

Multivariate statistical analysis includes the Pearson correlation coefficient as well as cluster and principal component analyses (PCA). These methods were used to clarify correlations and link between the used variables, more exactly the impact of the measured radiological parameters of measures samples and the natural radionuclides' distribution. To evaluate the intensity of the relationship between the examined variables, the Pearson correlation coefficient was calculated. An applicable statistical method which visually presents the degree of correlations between variables is cluster analysis. PCA is used as a usual tool to summarize the set of patterns between analyzed variables in set of data. Varimax normalized method was used to process data for PCA evaluation. The main reason why PCA is that commonly used, is that once correlations were identified, data can be compressed reducing the number of dimensions and without any substantial information loss. To carry out the relevant statistical analysis of the obtained data's we used a software named IBM SPSS Statistics V21.0.

3.2.2.1 Analysis of Pearson's correlation coefficient

In order to determine the relation and strength of association between several radiological parameters and radionuclides, Pearson correlation analysis has been done. The data from Table 11 (The Pearson coefficient analyses) indicates a strong positive and statistically significant correlation between ^{226}Ra and ^{232}Th because the decay series of radium and thorium appear together in nature (Tanaskovi et al., 2012).

Table 10. Results of different hazard indices associated with the radioactivity of the studied building materials in Semnan Province

Building Material	No.		Ra_{eq} (Bq/kg)	D (nGy/h)	AED (μSv/y)	I_γ	I_α	H_{ex}	H_{in}
Sand and Gravel	3	Range	76-89	71-80	348-393	0.29-0.33	0.09-0.15	0.21-0.24	0.25-0.31
		Average±SD	83±16	75±7	366±37	0.31±0.06	0.12±0.03	0.22±0.04	0.29±0.06
Bricks	5	Range	67-108	59-96	287-469	0.24-0.39	0.10-0.20	0.18-0.29	0.25-0.40
		Average±SD	96±17	86±8	421±38	0.35±0.06	0.15±0.03	0.26±0.05	0.34±0.06
Gypsum	3	Range	38-42	34-36	169-179	0.14-0.15	0.05-0.07	0.10-0.11	0.13-0.15
		Average±SD	41±6	35±3	174±13	0.15±0.02	0.06±0.01	0.11±0.02	0.14±0.02
Cement	5	Range	64-76	57-68	281-333	0.23-0.27	0.12-0.19	0.17-0.20	0.24-0.31
		Average±SD	70±14	63±6	309±32	0.25±0.05	0.15±0.03	0.19±0.04	0.27±0.05
Ceramic	3	Range	82-107	73-95	356-466	0.29-0.33	0.15-0.17	0.22-0.29	0.32-0.37
		Average±SD	93±20	83±9	406±44	0.34±0.07	0.16±0.03	0.25±0.05	0.34±0.07
Tile	3	Range	100-108	88-97	434-478	0.36-0.40	0.15-0.22	0.27-0.29	0.36-0.41
		Average±SD	105±22	94±10	460±50	0.39±0.08	0.18±0.04	0.28±0.06	0.38±0.08
Granite	3	Range	163-184	150-168	735-826	0.63-0.70	0.14-0.22	0.44-0.50	0.52-0.61
		Average±SD	176±26	160±12	786±60	0.67±0.1	0.19±0.03	0.48±0.07	0.58±0.09
Marble	2	Range	18-21	16-18	77-89	0.06-0.07	0.03-0.04	0.05-0.06	0.07-0.08
		Average±SD	20±3	17±1	83±7	0.07±0.01	0.04±0.01	0.05±0.01	0.07±0.01
Mosaic	2	Range	37-42	36-37	177-182	0.14-0.15	0.06-009	0.10-0.11	0.14-0.16
		Average±SD	41±6	33±3	180±13	0.15±0.02	0.07±0.01	0.11±0.02	0.15±0.02
Total	29	Range	**18-184**	**16-168**	**77-826**	**0.06-0.70**	**0.03-0.22**	**0.05-0.50**	**0.07-0.61**
		Average±SD	**84±15**	**76±7**	**371±35**	**0.31±0.1**	**0.13±0.03**	**0.23±0.04**	**0.30±0.06**
Recommended value or worldwide average			370[a]	50[b]	1000[c]	≤1[d]	≤1[e]	≤1[f]	≤1[g]

[a] Any Radium equivalent activity concentration over this value may raise radiation hazard according to NEA-OECD (1979)

[b] Worldwide average background gamma radiation reported by UNSCEAR (2008)

[c] The worldwide average value of AED reported by UNSCEAR (2008)

[d] The reference level radioactivity index in building material according to UNSCEAR (2000)

[e] The recommended value reported in ICRP (1994)

[f] The recommended value reported in Beretka and Mathew (1985)

[g] The recommended value reported in Krieger (1981)

Moreover, there is a direct correlation among ^{226}Ra and ^{232}Th with all of the calculated radiological parameters possibly because the building materials are rich in ^{226}Ra and ^{232}Th, which plays a significant role in assessing the hazardous nature of such materials. Furthermore, a weaker correlation, albeit still statistically significant, was observed between these two radionuclides and ^{40}K (Imani et al., 2021).

Table 11. Pearson's correlation matrix for variables

Parameters	**^{226}Ra**	**^{232}Th**	**^{40}K**	**I_γ**	**Ra_{eq}**	**D**	**AED**	**H_{ex}**	**H_{in}**	**I_α**
^{226}Ra	1									
^{232}Th	0.813	1								
^{40}K	0.467	0.689	1							
I_γ	0.838	0.946	0.792	1						
Ra_{eq}	0.852	0.952	0.776	0.998	1					
D	0.844	0.944	0.788	1.00	0.999	1				
AED	0.844	0.944	0.788	1.00	0.999	1.00	1			
H_{ex}	0.852	0.952	0.776	0.999	1.00	0.999	0.999	1		
H_{in}	0.899	0.942	0.733	0.984	0.991	0.988	0.988	0.990	1	
I_α	0.999	0.774	0.484	0.787	0.812	0.799	0.799	0.809	0.881	1

3.2.2.2 Principal Component Analysis (PCA)

The principal component analysis (also known as factor analysis) is multivariate statistical technique used to identify important components that explain most of the variances of the original system. It is designed to reduce a set of original variables to a small number of indices for analyzing similarities and differences present among the observed variables that are not readily evident from simple correlation analysis. In this study, the varimax rotation was applied with Kaiser normalization procedure to process the PCA among the radiological parameters (Kaiser, 1958). From the correlation matrix, to describe the number of notable factors the eigenvalues and eigenvectors are extracted (Only factors with eigenvalues greater than 1) and explained the percent of variance. The values of rotated factors 1 and 2 are reported in Table 12. Factor Analysis (FA) yielded two factors with eigenvalues < 1, explaining 95.58% of the total variance. From the rotated spaces of components 1 and 2 (Figure 27), Factor 1 accounts for 59.83% of the total variance, identified mostly by high positive loading of ^{232}Th and ^{226}Ra activity concentrations. Factor 2 accounts for 35.75% of the total variance and related to significant positive loading of ^{40}K. From the overall FA, it can be concluded that by and large ^{226}Ra and ^{232}Th enhance the radioactivity of all the building materials (Imani et al., 2021).

Table 12. Rotated factor loadings of variables

Variables	Component	
	1	2
^{226}Ra	0.88	0.26
^{232}Th	0.78	0.54
^{40}K	0.29	0.96
I_{γ}	0.77	0.64
Ra(eq)	0.78	0.62
D	0.77	0.64
AED	0.77	0.64
H(ex)	0.78	0.62
H(in)	0.82	0.57
I_{α}	0.86	0.29
% of variance explained	59.83	35.75

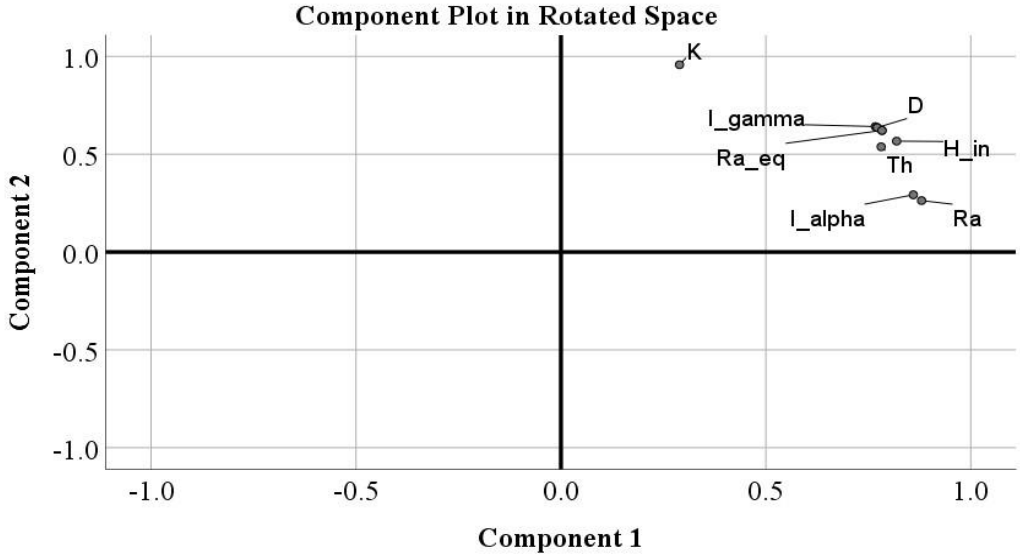

Figure 27. Graphical representation of Factors 1 and 2

3.2.2.3 Cluster Analysis (CA)

CA is a data classification technique that is comprised of a series of multivariate methods, which are used to identify true groups of data. The degree of similarity between the radioactivity and calculated radiological hazard parameters was determined by CA using IBM SPSS Statistics version 21 software. In CA, the linkage method was used to find out the correlation coefficient distance between radiological parameters, the outcome dendrogram shows in Figure 28. In this dendrogram, all 10 parameters can be classified into three major clusters. Cluster-I consists of ^{226}Ra, ^{232}Th, AED, H_{ex}, H_{in}, I-alpha and I-gamma. The results from this cluster reveal that the main radiological health hazard parameters exist due to the ^{226}Ra and ^{232}Th activity concentrations; while Cluster-II is associated with Ra_{eq} and D; and Cluster-III includes ^{40}K, which indicates

that the activity concentration of ^{40}K does not contribute significantly to the natural radioactivity. The results according to the derived dendrogram are in good agreement with correlation and factor analyses. Therefore, the data belongs to studied parameters primarily relies on the natural radioisotope's activity concentrations (Imani et al., 2021).

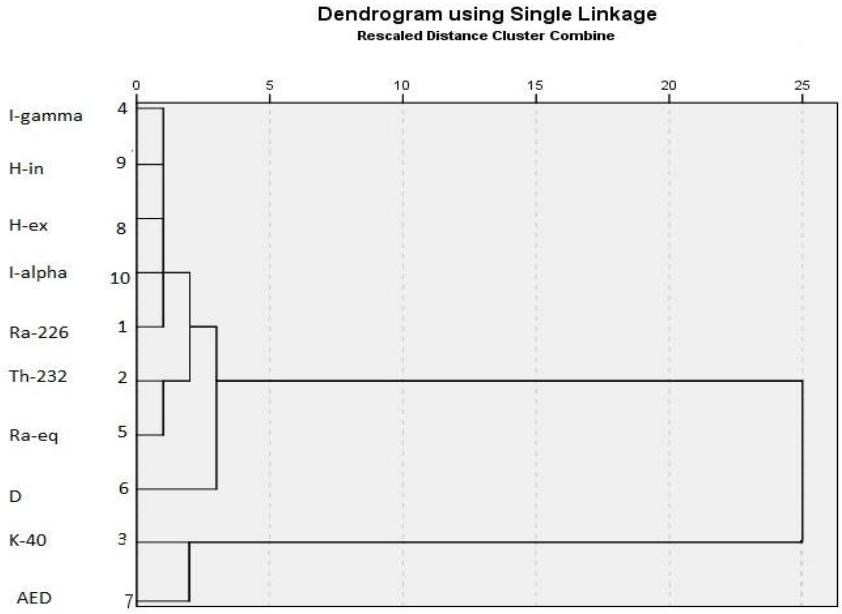

Figure 28. Dendrogram showing the clustering of variables

3.2.3 Specific radioactivity in building materials of Mahallat

As explained in first chapter, a survey has been designed firstly, to measure the radioactivity content of the most common building materials available on the local market of Mahallat (an area exposed to a high level of natural background radiation); and secondly, to estimate the contribution of building materials towards indoor external and internal doses received by inhabitants in Mahallat using the computer code RESRAD-BUILD in a standard model room developed by Argonne National Laboratory. Accordingly, Table 13 shows the concentrations of naturally occurring radionuclides recorded in the dry samples of building materials. The average activity concentration of ^{226}Ra, ^{232}Th and ^{40}K in the samples measured were 34±6, 27±6 and 276±58 Bq/kg, respectively. It can be seen that concentrations measured were, in most cases, below worldwide average values (UNSCEAR, 2000). Due to the statistical analysis, it was found that the concentrations of ^{40}K and ^{226}Ra were higher than the worldwide average value in 17% and about 26% of the samples, respectively. The highest activity of ^{226}Ra, ^{232}Th and ^{40}K were found in various building materials (tiles, sand, gravel

and bricks), but did not significantly exceed the worldwide average values. The activity indexes for all of the samples were calculated and found to be less than 1.0, the value recommended by EU BSS, likewise the statistical analysis of the obtained data with regard to the mass activity of ^{40}K, ^{226}Ra and ^{232}Th in the samples of building materials is presented in as shown in Table 13.

Table 13. Measured mass activities and statistical analysis of naturally occurring radionuclides in building materials of HNBR of Mahallat (Bq/kg)

Building Material	**^{226}Ra**	**^{232}Th**	**^{40}K**	**I***	**$Ra_{(eq)}$**	**D**	**AED**
Sand and Gravel	38±8	44±10	204±46	0.4	117.4	100.3	492
Sand and Gravel	29±4	25±4	238±38	0.3	82.9	73.1	358
Sand and Gravel	33±6	34±6	337±60	0.4	107.7	94.9	466
Sand and Gravel	28±5	27±5	378±71	0.4	95.3	85.4	419
Bricks	35±5	23±4	410±78	0.4	100.2	90.9	446
Bricks	38±7	32±6	357±66	0.4	111.9	99.2	487
Bricks	31±8	28±5	428±79	0.4	103.6	93.3	458
Bricks	34±6	27±5	413±80	0.4	104.9	94.4	463
Gypsum	29±4	20±4	82±17	0.2	62.8	54.3	266
Gypsum	22±5	18±3	94±16	0.2	55.2	47.8	234
Gypsum	25±4	23±5	85±19	0.2	63.7	54.5	267
Gypsum	31±4	24±5	107±22	0.3	74.2	64	314
Cement	31±4	23±5	224±48	0.3	82.1	72.5	356
Cement	42±8	28±6	239±52	0.4	100.0	88.3	433
Cement	34±5	23±5	257±56	0.3	86.4	76.9	377
Cement	27±4	25±5	198±40	0.3	77.8	68.1	334
Ceramic	35±5	23±5	308±67	0.3	91.5	82	402
Ceramic	33±5	28±8	258±73	0.3	93.2	82	402
Ceramic	33±4	33±7	381±81	0.4	109.8	97.4	478
Tile	43±10	29±6	314±71	0.4	108.1	96.1	471
Tile	53±14	31±8	292±75	0.4	120.3	106.6	523
Tile	41±9	30±8	348±92	0.4	110.6	98.4	483
Tile	46±10	33±9	401±82	0.5	124.8	111.3	546
Minimum	22±5	18±3	82±18	0.2	55.2	47.8	234
Maximum	53±14	44±10	428±79	0.5	124.8	111.3	546
Average	34±6	27±6	276±58	0.3	95.0	84	412
Median	33	27	292	-	-	-	-
Skewness	0.8	1.0	-0.5	-	-	-	-
Kurtosis	0.9	2.2	-0.9	-	-	-	-
Geometric Mean	34	27	250	-	-	-	-

***I**: the radiation index of the material

Accordingly, in most samples, the mass activity of ^{40}K fell within the range of ~200 to ~380 Bq/kg, while the corresponding values for ^{226}Ra and ^{232}Th were from ~30 to ~ 40 and ~25 to ~30 Bq/kg, respectively. The radium equivalent activities, gamma-ray absorbed dose rates and annual effective doses were estimated for the analysed samples based on the mass activity of the naturally occurring radionuclides. The results of the calculations can be also seen in Table 13.

The calculated values of radium equivalent activities were between 55 and 125 Bq/kg with a cumulative average of 95 Bq/kg. Meanwhile, the gamma-ray absorbed dose rates were measured to be between 48±9 and 111±26 nGy/h with a cumulative average of 84±17 nGy/h, which is higher than the worldwide average value of 55 nGy/h (UNSCEAR, 2000). Based on the values of estimated gamma-ray absorbed dose rates, the annual effective doses were calculated to be within the range of 234±45 to 546±125 μSv/yr with a cumulative average of 412±82 μSv/yr. Finally, since ^{226}Ra series and ^{232}Th series are usually found together in nature, and good correlation between them is indicative of common sources, which, in general, are associated with a mineralogical component. In most of the studied building materials in Mahallat, there is also a positive correlation between ^{226}Ra and ^{232}Th. The strongest linear relationship is observed between ^{226}Ra and ^{232}Th in Sand and Gravel, and Ceramic with R^2= 0.98 and R^2= 0.56, respectively; However, the corresponding correlation coefficient is slightly lower for other building materials.

A comparison between the measured activity concentrations of ^{226}Ra, ^{232}Th and ^{40}K for the analyzed building materials and the results of similar studies reported in different countries are given in Table 14. For instance, in case of Semnan province, the ranges of activity concentrations of ^{226}Ra, ^{232}Th and ^{40}K for samples of brick and sand recorded are comparable to the values obtained in Egypt and India (Medhat, 2009; Ravisankar et al., 2014), while results obtained for cement are comparable to those measured in Nigeria (Agbalagba et al., 2014). The concentrations of these radionuclides measured in the samples of gypsum and granite are also comparable with results from other Iranian studies (Mehdizadeh et al., 2011; Ashrafi and Jahanbakhsh, 2019), while the results obtained for ceramic are comparable to Serbian (Kuzmanović et al., 2020) but dramatically lower than those from China and Saudi Arabia (Tuo et al., 2020; Al-Sewaidan, 2019). The activity concentrations of these radionuclides for the samples of tile and marble were higher compared to results from Italy (Righi and Bruzzi, 2006). It is noteworthy that the mean values of NORMs are changing from one location to another.

Table 14. A comparison between the activity concentration of radionuclides presented in studied building materials and other areas

Country	Material	No.	Activity concentration (Bq/kg) (Mean)			References
			^{226}Ra	^{232}Th	^{40}K	
China	Brick	4	14	39	678	Tuo et al., 2020
	Ceramic	6	172	135	351	
	Granite	14	356	318	1636	
	Concrete	4	16	51	605	
Serbia	Brick	12	45	49	646	Kuzmanović et al., 2020
	Ceramic tile	5	67	61	828	
	Concrete tile	2	30	18	255	
	Granite	2	200	77	1280	
	Concrete	10	17	21	253	
Iran	Granite	29	77	45	1017	Abbasi, 2013
	Gravel	32	20	6	451	Mehdizadeh et al., 2011
	Brick	77	37	12	851	
	Gypsum	30	8	2	116	
	Cement	17	40	29	291	
Egypt	Sand	15	33	27	385	Medhat, 2009
	Gravel	18	10	5	159	
	Brick	30	30	21	289	
	Gypsum	21	39	25	226	
	Ceramics	29	52	33	450	
	Tile	30	35	23	377	
	Granite	16	65	60	920	
	Marble	25	32	25	466	
Iran	Bricks	7	35	28	402	Shahrokhi et al., 2020
	Gypsum	2	27	21	92	
	Cement	3	34	25	229	
	Ceramic	6	33	28	315	
	Tile	2	46	31	339	
Saudi Arabia	ceramic	20	89	105	773	Al-Sewaidan, 2019
	cement	4	22	10	102	
Qatar	sand	4	13	3	225	Al-Sulaiti et al., 2011
	cement	6	23	10	120	
	White cement	3	19	5	63	
Nigeria	cement	5	30	25	251	Agbalagba et al., 2014
	White cement	6	42	30	340	
India	Sand	7	11	130	297	Ravisankar et al., 2014
	Brick	8	5	23	374	
	Cement	3	37	34	188	
Iran	Sand	3	24	22	362	Imani at al., 2021
	Brick	5	31	28	338	
	Gypsum	3	12	14	116	
	Cement	5	31	15	231	
	Ceramic	3	32	27	292	
	Tile	3	36	29	361	
	Granite	3	38	47	917	
	Marble	2	7	7	34	
	Mosaic	2	15	10	146	

3.2.3.1 Radiological dose assessment using RESRAD-BUILD computer code

Regarding the modelling of indoor external and internal exposure due to different building materials containing NORMs in Mahallat by RESRAD-BUILD computer code, the exposure pathways were including inhalation, radon gas, external exposure, deposition and immersion. RESRAD-BUILD is a model designed to estimate the possible radiation dose received by an individual, who works or lives in a building containing radioactive material, by taking into account different pathways for human exposure including external exposure directly from the source, external exposure due to air submersion and internal exposure due to indoor ^{222}Rn, ^{220}Rn, their progenies, etc. This code allows users to calculate the time-integrated dose over the period of exposure at time intervals specified by the user (Yu et al., 2003). Three different case studies using different compositions of basic building materials, taking into account the different densities and thicknesses of such materials, were applied in a simulation to determine how much of an influence each one has on the effective dose rate occupants are exposed to. In this regard, the parameters of a standard model room, with the dimensions of 4.0×5.0×2.8 m outlined in the document entitled Radiation Protection 112, were applied in the simulation (European Commission, 1999). Since all buildings are constructed from a combination of basic building materials, variations in the proportions of such materials used to compose walls, floors and ceilings were applied in the simulation by taking into consideration their different densities and thicknesses to evaluate the influence of such parameters on the variation in the external and radon doses an individual in the simulated room is exposed to using the computer code RESRAD-BUILD.

Ceilings and walls were built from the same basic materials - namely brick, cement and sand - in equal proportions. Three different forms of floor that is, cement, tiled and ceramic - were also assumed (The mean activity concentrations of naturally occurring radionuclides used in the simulation are already given in Table 13). The location of the exposed person for the purpose of the external dose assessment was chosen to be at the center of the room and 1 m above the floor (Yu et al., 2003), moreover, an indoor occupancy rate of 80% was assumed (UNSCEAR, 2000). The density of the building materials was also assumed to be 2000 kg/m^3 for brick, 2960 for gypsum, 2400 for tiles and 2350 for cement. Other main input parameters used as input data regarding dose assessments are also listed in Table 15.

Table 15. The main parameters applied for effective dose calculations

Parameters	Unit	Value
Breathing rate	m^3 /d	22
Deposition velocity	m/s	1×10^{-2}
Ventilation rate	1/h	0.1-2
Radon emanation rate	--	0.2
Porosity	--	0.1
Radon diffusion rate	m^2/s	2×10^{-5}
Resuspension rate	--	5×10^{-7} s^{-1}
Release air fraction	--	0.1
Type of the source	--	Volume (x-, y and z-direction)
Source geometry	--	Rectangular
Shielding thickness	cm	No shielding

In the first round of simulations the variation in the composition of building materials making up walls, floor and ceiling was considered. Then the effect of variation in the room parameters, namely wall thickness and ventilation rate were assessed. The simulation of indoor doses including indoor external and internal exposure doses, as well as the effective dose was carried out over 76 years, the average lifetime of Iranians. Therefore, the measured activity concentrations of ^{226}Ra, ^{232}Th and ^{40}K were individually inputted into the RESRAD-BUILD computer code (Adelikhah et al., 2022). Variations in effective dose from both the walls and floor of the room that occupants are exposed to are shown in Figure 29 (A-C) for a standard room with a wall thickness of 20 cm and air exchange rate (ACH) of 0.5 h^{-1}. As reported by Yoshino et al., 2004, it should be mentioned that the ACH was assumed to be 0.5 h^{-1} in line with the minimum ACH legislated in most European countries and in accordance with Japanese regulations for ACH (Yoshino et al., 2004).

Figure 29 (A-B) shows a long-term variation in the indoor external and radon doses inhabitants are exposed to over an average lifetime of 76 years for the 3 different case studies. Accordingly, a considerable rise in the indoor doses was observed over the first 30 years, however, beyond this period, the indoor doses became relatively constant. Based on Figure 29C, the maximum effective dose rate was exhibited by the *case study two*, namely a tiled cement floor, that ranged from 504 to 1433 μSv/year, which is below the recommended maximum limit set by the International Commission on Radiological Protection (ICRP) of 3-10 mSv/year (ICRP, 1994). The highest external and radon doses - calculated to be 369 and 1064 μSv, respectively - were also exhibited in case study two because of the higher concentrations of ^{226}Ra and ^{232}Th in

these materials. Therefore, the choice in building materials has a noticeable contribution towards the indoor doses inhabitants are exposed to (Adelikhah et al., 2022).

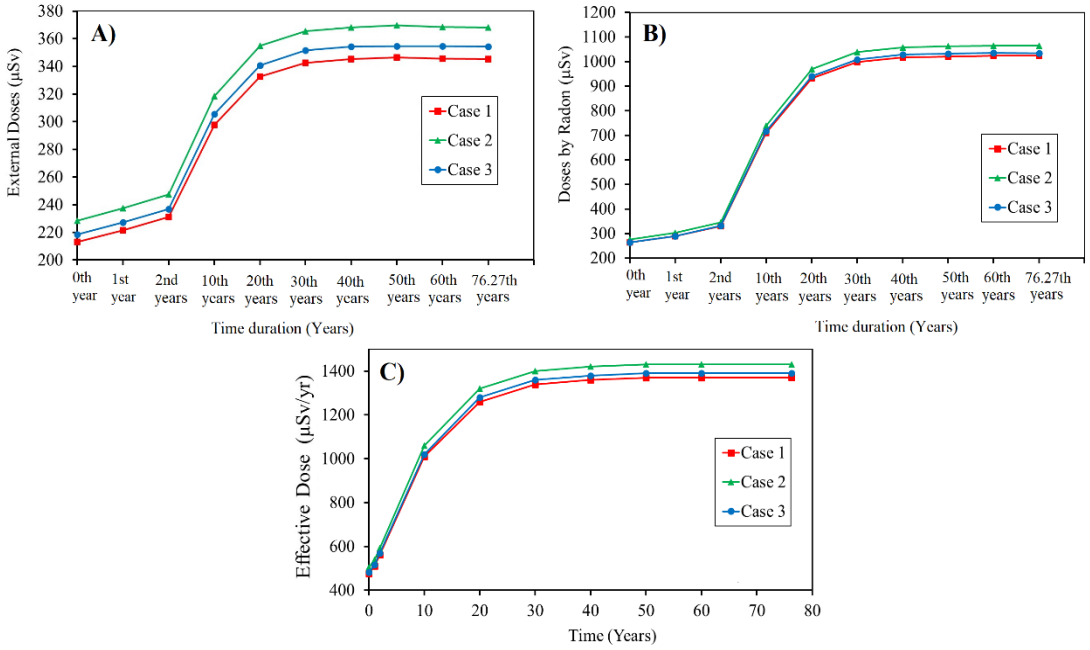

Figure 29. Long-term variation in A) external radiation dose, B) radon dose and C) Effective dose that inhabitants are exposed to in a standard room in which the wall thickness is 20 cm and ACH is 0.5 1/h in three different case studies

3.2.3.2 Sensitivity analysis

Sensitivity analysis is a technique used to study and identify the parameters that have a significant effect on the results of dose assessments and to explore potential reductions in the uncertainties associated with such parameters. In order to more realistically estimate radiological risks, variations in essential parameters of the room, e.g., wall thickness and air exchange rate, used in the RESRAD-BUILD computer code were taken into account. In this regard, the wall thickness and air exchange rate were varied from 10 to 60 cm and 0.05 to 2.0 1/h, respectively. These parameters were applied to the materials used in case study two, as the maximum effective dose rate was regarded as a worst-case scenario as is shown and described in Figure 29.

Alterations made to the indoor doses regarding the wall thickness and air exchange rate are illustrated in Figures 30A and B, respectively. Accordingly, it can be seen that the wall thickness and air exchange rate both play a large role in terms of the indoor dose occupants are exposed to. Increasing the thickness of any part of the room means increasing the amount of the building material and NORM concentrations which will

lead to a further increase in the indoor dose rate. Based on Figure 30A, as the wall thickness increases, the indoor doses also increase, moreover, for wall thicknesses of 30 cm or more, dose remains relatively constant, which is in good agreement with results presented in previous studies (Majid et al., 2013; Risica et al., 2001) and is contradictory to earlier expectation that the increase in concrete thickness would increase the dose rates in dwelling. Indeed, the dose increases with the wall thickness to a point because of the external gamma dose rate, which is mitigated by self-absorption, and the greater wall thickness also increases the potential amount of radon isotopes exhaled into the room, mitigated by the distance radon is able to travel in the building material. Consequently, when the thickness is bigger than 30 cm, it will start to serve as a shield to its own radiation and showed in Fig 30A and any addition of wall thickness over 30 cm would not increase further the indoor dose rates and could be ignored.

However, a continuous increase in doses as a result of wall thicknesses in excess of 40 cm and exposure to ^{226}Ra found in building materials has been reported (Abdullahi et al., 2020). On the other hand, radon, one of the biggest contributors to the total dose, can easily escape from the wall matrix if the wall is narrower. If the wall is thicker, the relative amount of radon that escapes from the building decreases. According to Figure 30B, by increasing the air exchange rate, the effective dose is dramatically reduced with values ranging from 3590 μSv/year for ACHs of 0.05 1/h to 296 for ACHs of 2.00 1/h. Consequently, in terms of the indoor environment - an extremely important subject from the perspective of human health - that is, indoor air quality and energy efficiency, the ventilation rate significantly affects the inhalation dose, which is inversely correlated with radon and the airborne concentrations of its decay products.

Finally, the results indicate that the computer code RESRAD-BUILD is a useful tool to evaluate radiological human health risk for buildings contaminated with radionuclides and to monitor and control the radioactivity of building materials. The data in this study could also contribute towards the database of natural radionuclides found in building materials, improve current technical regulations and laws concerning the radioactive content of building materials, lead to the proposal of a radiological reduction method as well as raise public awareness of radiological risk. Consequently, the legislation of a national standard into the Iranian legal system describing the requirements for the radiological examination of the building materials, is necessary before their introduction on the market.

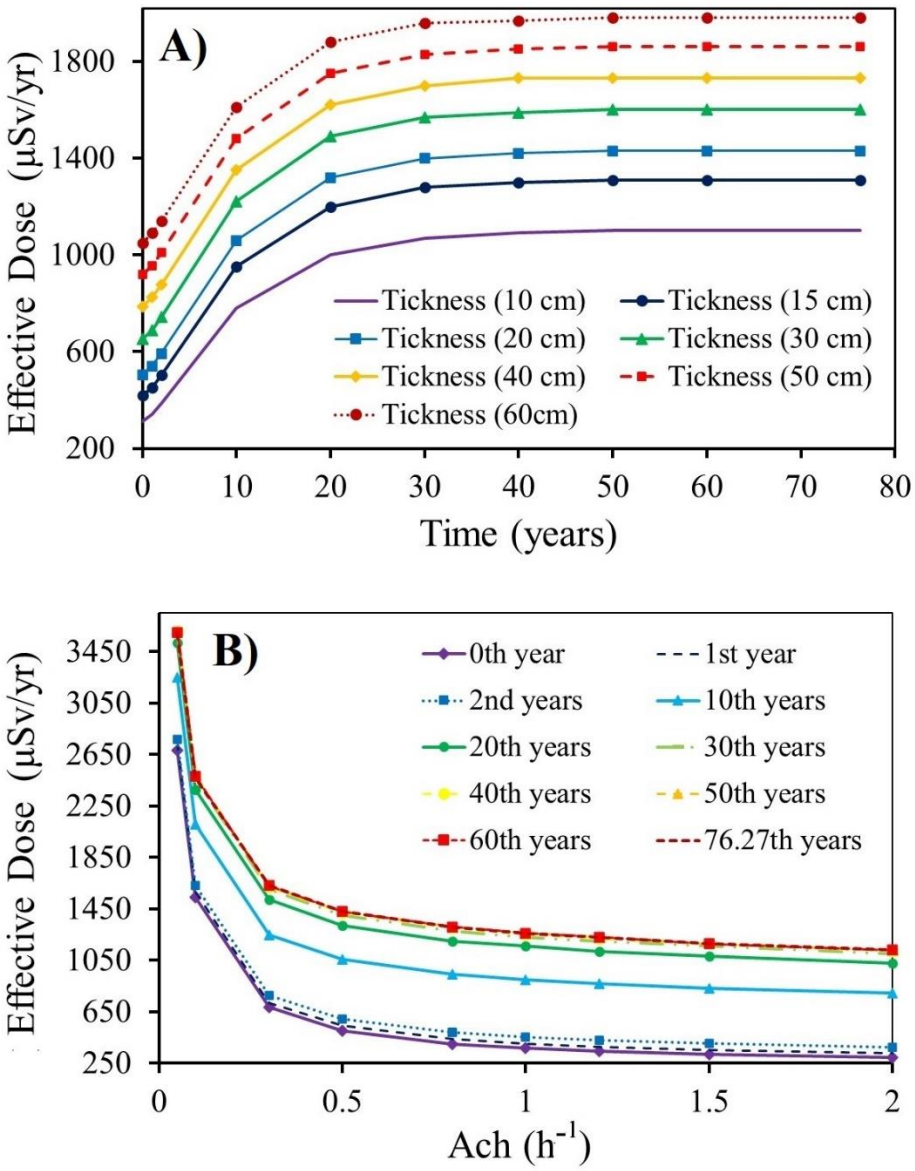

Figure 30. Effect of A) wall thickness and B) air exchange rate on the effective dose inhabitants of Mahallat, Iran are exposed to

3.3 Third case of study: Thermal bath in Dehloran, Iran

To determine the indoor radon and thoron concentrations in thermal spa of Dehloran, passive radon-thoron discriminative detectors, commercially known as RADUET were used. Such detectors were used to measure not only the concentrations of radon but thoron as well. These detectors consist of two diffusion chambers with different ventilation rates, each of which contains a CR-39 chip, the dimensions of which are 10 × 10 mm, to detect alpha particles emitted by radon and thoron as well as their decay products (Tokonami et al., 2005). The low diffusion rate chamber is comprised of an electrically conductive plastic with an inner volume of 30 cm^3. Six holes in the

wall of the high diffusion rate chamber, composed of the same material, are covered with a sponge material to prevent decay products of radon and thoron as well as aerosols from infiltrating into the chamber. While one chamber only measures radon, the other detects both radon and thoron levels. The concentration of thoron is then determined by subtracting the track densities.

Visitors and workers who use the baths served by the hot springs are also exposed to radiation through the inhalation of radon. During showering, water splashes and radon is released into the air resulting in possible inhalation exposure. In addition, the use of building materials and decorative stones is another source of indoor exposure. Figure 31 shows the concentration of radon for each bath and gallery. The concentrations of radon in the baths measured were between 1880±410 and 2450±530 Bq/m^3 with an average of 2010±440 Bq/m^3. Unfortunately, due to high radon concentrations, all the thoron concentration results were below the detection limit of the method. It is interesting to note that the radon concentrations in the galleries were less than those in the baths, ranging from 790±135 to 1050±120 Bq/m^3, as the ventilation system causes a reduction in the radon concentration in air. In addition, each of the baths in this thermal spa only has one small window, therefore, are characterized by high relative humidity due to the inability of the poor ventilation system to efficiently refresh the air inside the premises. In this thermal bath, no storage reservoirs for water are present, unlike in other modern spas. The radon concentrations are significantly higher when compared with those observed in modern spas elsewhere (Sohrabi, 1997; Radolić et al., 2005; Beitollahi et al., 2007; Ródenas et al., 2008; Nikolov et al., 2012; Karakaya et al., 2017; Wang et al., 2017).

In Figure 32, the concentrations of ^{40}K, ^{226}Ra and ^{228}Ra present in the soil samples are shown. The Minimum Detectable Concentrations (MDC) for particular radionuclides were calculated as 46 Bq/kg for ^{40}K, 1.3 Bq/kg for ^{226}Ra and 2.3 Bq/kg for ^{228}Ra. Soil samples D-01 to D-03 were collected from different areas of land where hot spring water was used for irrigation, while soil samples D-04 to D-06 were extracted from reference areas where another source of water was used. The results shown in Figure 30 reveal that the average concentration of ^{40}K is below the worldwide average, whereas the mean concentrations of ^{228}Ra (^{232}Th) and ^{226}Ra are much higher than it. Values of 400, 32 and 30 Bq/kg are the world average concentrations of ^{40}K, ^{226}Ra and ^{228}Ra in soil, respectively (UNSCEAR, 2008).

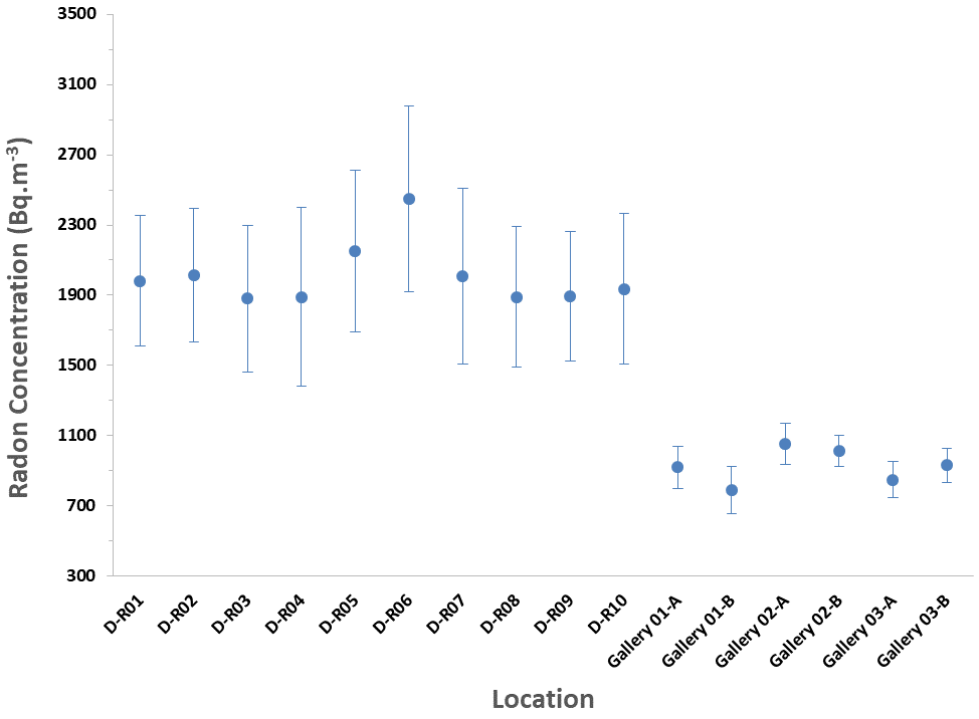

Figure 31. Activity concentrations of ^{222}Rn in thermal baths

For example, the mean concentration of ^{226}Ra in the soil samples is 8 times higher than the world average. The results show that a systematic relationship between the concentrations of ^{226}Ra and ^{228}Ra in the soil samples and sources of hot water. In fact, the soil samples which were collected from other areas of farming land supplied by different sources of water for irrigation close to the sampling area of this study consist of lower concentrations of ^{226}Ra and ^{228}Ra. Probably the reason for this was the presence of ^{228}Ra in the water (unfortunately, this was impossible to measure using gamma spectroscopy due to its detection limit). This is also why the concentration of ^{228}Ra but not ^{232}Th was presented, due to possible disequilibrium of the thorium series.

It is necessary to mention that due to time and budget limitations, measurements of the radon level in other locations in this area were omitted. However, it was found that enhanced radon concentrations were generated by ^{222}Rn dissolved in hot spring water and released in baths amongst other places. Secondly, the thermal water does not constantly run into baths but its flow depends on the usage of baths by clients. Results have shown correlations between the concentration of ^{222}Rn and the size of baths, the frequency of their use and their distance from a hot spring. It is evident that the concentration of radon in the indoor air of the Spa in Dehloran varied from one treatment room to another, due to the influence of several factors, e.g., its size, the ventilation

rate and water flow rate. The highest concentration of 2450±530 Bq/m^3 was measured in one of the baths.

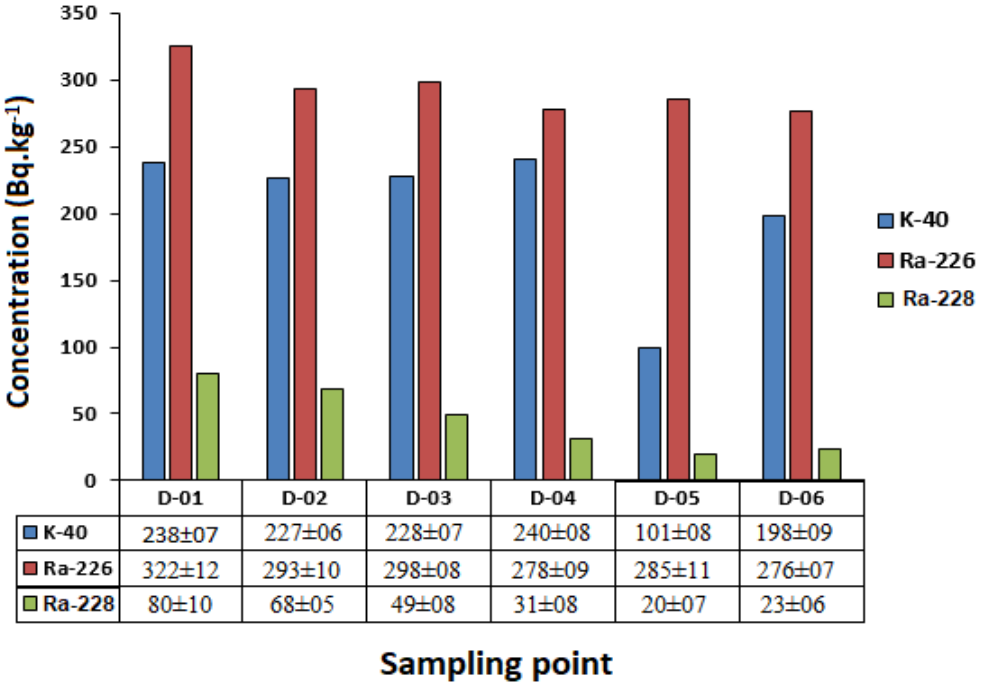

	D-01	D-02	D-03	D-04	D-05	D-06
K-40	238±07	227±06	228±07	240±08	101±08	198±09
Ra-226	322±12	293±10	298±08	278±09	285±11	276±07
Ra-228	80±10	68±05	49±08	31±08	20±07	23±06

Figure 32. Concentration of ^{40}K, ^{226}Ra and ^{228}Ra in soil samples irrigated by different sources of water

The maximum radiation dose for the members of staff at the spa as a result of inhaling radon was estimated based on the measured results and recommended maximum treatment duration (see Table 16). If the percentage of the spending time of staff in the bath area is 80%, the actual dose of radon received by staff was estimated to be within the range of 4.16 to 5.55 mSv/year with an average of 4.9 mSv/year. The minimum and maximum annual radiation doses originating from radon received by tourists was estimated to be 0.043 to 0.132 mSv/year, respectively, with an average of 0.086 mSv/year. It was also estimated that for the most frequent clients of the spa, the annual radiation dose should not exceed 10 % of the dose the staff are exposed to, i.e., 0.55 mSv/year.

On the other hand, the measured concentrations of ^{226}Ra in water samples are shown in Table 17. The concentrations of ^{226}Ra in the samples of thermal water were measured within the range of 408±200 to 423±180 mBq/l with an average of 419±170 mBq/l. Since the water source is the same for the baths and thermal pools, the concentration of ^{226}Ra fell approximately within the same range.

Table 16. The annual dose caused by radon with regard to tourists and staff at the spa

Location	C_{Radon} (Bq.m^{-3})	C_{Thoron} (Bq.m^{-3})	Dose (mSv.yr^{-1}) (UNCER DCF)		Dose (mSv.yr^{-1}) (ICRP DCF)	
			Tourist	Staffs	Tourist	Staffs
D-R01	1982±370	Below LLD	0.107	-	0.079	-
D-R02	2012±380	Below LLD	0.108	-	0.080	-
D-R03	1880±420	Below LLD	0.101	-	0.075	-
D-R04	1890±510	Below LLD	0.102	-	0.075	-
D-R05	2150±460	Below LLD	0.116	-	0.086	-
D-R06	2450±530	Below LLD	0.132	-	0.098	-
D-R07	2010±500	Below LLD	0.108	-	0.080	-
D-R08	1890±400	Below LLD	0.102	-	0.075	-
D-R09	1895±370	Below LLD	0.102	-	0.076	-
D-R10	1937±430	Below LLD	0.104	-	0.077	-
Gallery 01-A	920±120	Below LLD	0.049	4.86	0.036	3.62
Gallery 01-B	789±135	Below LLD	0.043	4.16	0.031	3.1
Gallery 02-A	1052±120	Below LLD	0.056	5.55	0.042	4.13
Gallery 02-B	1014±90	Below LLD	0.054	5.35	0.040	3.99
Gallery 03-A	850±100	Below LLD	0.045	4.49	0.034	3.34
Gallery 03-B	932±98	Below LLD	0.050	4.92	0.037	3.66

* LLD for thoron measurement was calculated to be 130 Bq/m^3

Table 17. ^{226}Ra concentrations in water samples

Location	^{226}Ra (mBq/l)	SD
D-R01	418	±180
D-R02	421	±170
D-R03	423	±160
D-R04	421	±165
D-R05	422	±180
D-R06	428	±188
D-R07	408	±200
D-R08	415	±145
D-R09	413	±130
D-R10	416	±183
Gallery 01	422	±190
Gallery 02	419	±170
Gallery 03	423	±180
Mean	**419.15**	**±171**

If these values are compared with the results reported indoor radon and ^{226}Ra activity concentrations in water in various spas around the world, it can be seen that the concentration of this radionuclide is elevated compared to typical levels in surface waters (Radolić et al., 2005; Ródenas et al., 2008; Bituh et al., 2009; Nikolov et al., 2012; Kasić et al., 2015; Karakaya et al., 2017; Wang et al., 2017) but similar to radium levels in other spas.

3.4 Development of RRI thoron calibration chamber based on a computational fluid dynamics simulation

As described previously, thoron gas has become increasingly recognized as a potential source of radiation exposure in dwellings, long-term levels of indoor exposure (passive measurements) and eventually the calibration of SSNTDs required to measure this have been highly recommended by different organizations to predict the exact concentration distribution of thoron inside a calibration chamber and determine the calibration factor of SSNTDs. This is vital in order to obtain an accurate dose assessment of exposure to radon and thoron. Therefore, in the following parts, the simulation results of calibration chamber at RRI are described by using different configurations of the inlet and outlet as well as at various flow rates to assess the applicability of RRI thoron calibration chamber for calibrating the SSNTDs.

3.4.1 Determining the optimized configuration

In this survey, the first step to design an initial version of a thoron calibration chamber for the purposes of measuring the activity concentration of thoron and calibrating the SSNTD was the development of simulation models for several chamber configurations using the FVM method implemented by ANSYS Fluent CFD code. ANSYS Fluent is an advanced industry-leading fluid simulation software known for its advanced physics modeling capabilities and unequalled accuracy. With ANSYS Fluent, many advanced physics models could be implemented and a variety of fluid phenomena analyzed. Given its parallel capabilities of meshing and equation solving, different CFD simulations have been performed taking into account the geometry of the chamber but not the tray (to reduce the amount of meshing as well as the convergence time) by varying flow rates as well as the positions of the inlet and outlet in order to determine their optimum locations. The results of the thoron transmission factors simulated the concentration distribution of thoron inside the chamber for various configurations at flow rates of between 5 and 100 l/min are presented in Table 18.

As expected, transmission factors were enhanced by flow rates for all chamber configurations. It can be seen that Configuration II (where the inlet and outlet were located symmetrically along the y axis at a distance of 10 cm from the center of the chamber) exhibits the best transmission factor. Therefore, this position of the inlet and outlet is used for the next step of the CFD simulation and is validated by experimental as well

as analytical results. According to Table 18, it can also be observed that the transmission factors are different for all configurations with similar flow rates because by changing the configuration, the profile of the airflow inside the calibration chamber varies resulting in differences in the profile of thoron distribution.

Table 18. Thoron transmission factor (C_{out}/C_{in}) for various chamber configurations at different flow rates (l/min) resulting from the CFD simulations

Flow rate (l/min)	**Thoron transmission factor (C_{out}/C_{in})**						**% Rel. Dev* with Config. II**
	Config. I	**Config. II**	**Config. III**	**Config. IV**	**Config. V**	**Analytical prediction**	
5	0.0233	0.0253	0.0240	0.0239	0.0231	0.0329	29.62
7.5	0.03534	0.0386	0.0371	0.0373	0.0337	0.0486	25.90
10	0.0518	0.0531	0.0512	0.0506	0.0452	0.0638	20.16
15	0.0784	0.0816	0.0785	0.0773	0.0737	0.0927	13.61
20	0.1012	0.1066	0.1023	0.102	0.1014	0.1199	12.47
25	0.1242	0.1351	0.1283	0.1282	0.1274	0.1455	7.71
50	0.2164	0.2410	0.2344	0.233	0.2317	0.2541	5.44
100	0.3815	0.3931	0.3842	0.3833	0.3813	0.4053	3.13

* The % Relative deviation between simulation results and the uniform mixing model was calculated using the following equation:

$$\%\ \text{Rel. Dev.} = \frac{|\text{simulation result} - \text{Analytical model prediction}|}{\text{simulation result}}$$

3.4.2 Results of CFD simulations

By setting up the input parameters in the CFD code, the contours concerning the concentration distribution of thoron (Bq/m^3) inside the chamber at different distances from the inlet and various airflow velocities for the optimized Configuration II were simulated and illustrated in Figures 31 to 33. From the CFD results, it can be noted that air enters into the calibration chamber as a jet flow and hits the opposite wall before spreading out in all directions, leading to a comparatively higher concentration near to the left-hand side wall and corner. When the flow rate was increased, the fluid hit the end of the chamber with a higher impulse causing the fluid to rapidly spread which can clearly be observed in Figures 33 to 35. Furthermore, the thoron concentration tended towards a uniform distribution under higher flow regimes due to thorough mixing of the thoron gas inside the chamber. Correspondingly, it could be concluded that the flow rate and turbulence played a critical function in the distribution as well as mixing of the thoron gas within the closed volume.

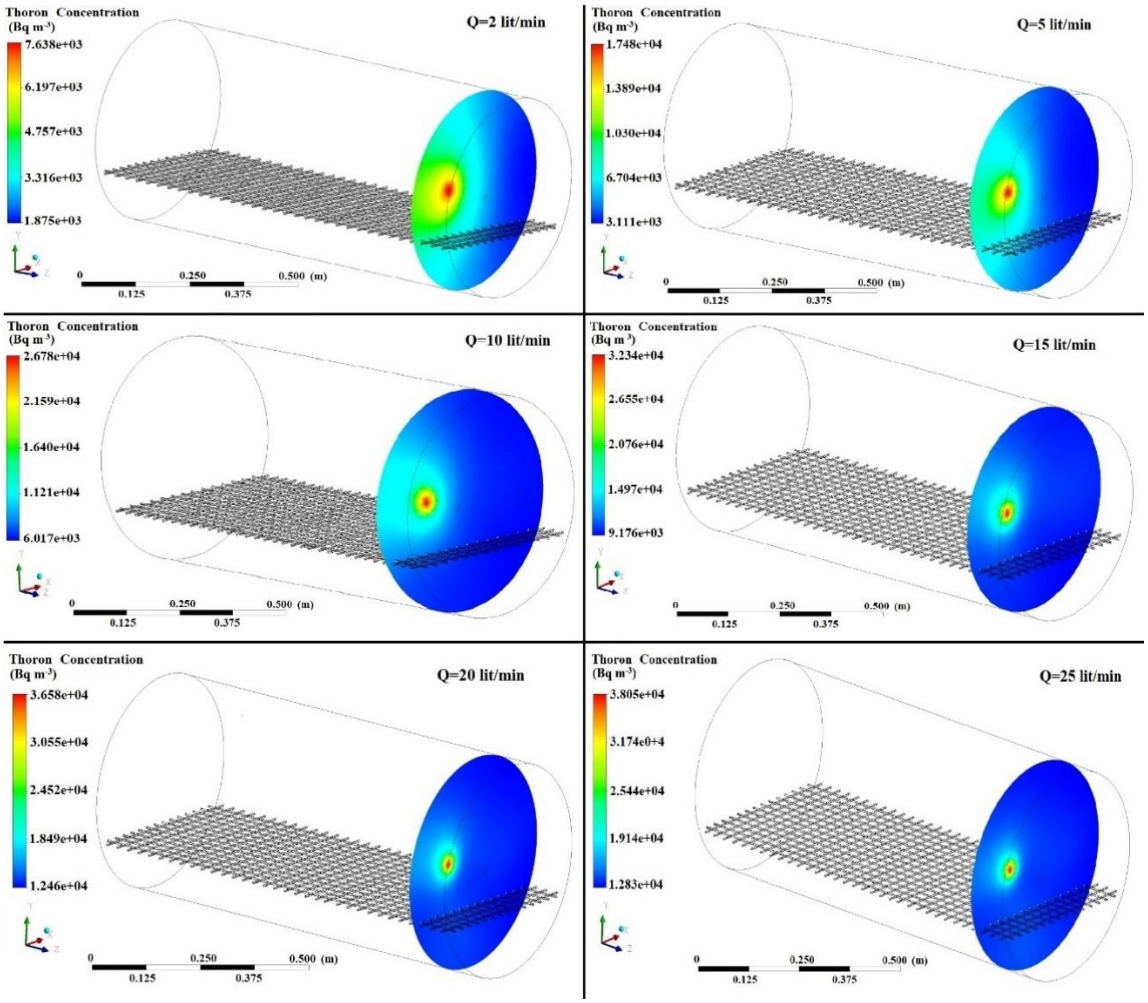

Figure 33. Concentration distribution of thoron (Bq/m^3) at Z=10 cm and different flow rates using the optimized Chamber Configuration II

The velocity pattern of thoron gas inside the chamber at different distances from the inlet and at two different flow rates of 5 and 20 l/min using the optimized Chamber Configuration II is presented in Figure 36. Accordingly, as a result of changes in the airflow rate, the concentration distribution of thoron inside the calibration chamber varied, affecting the transmission factor.

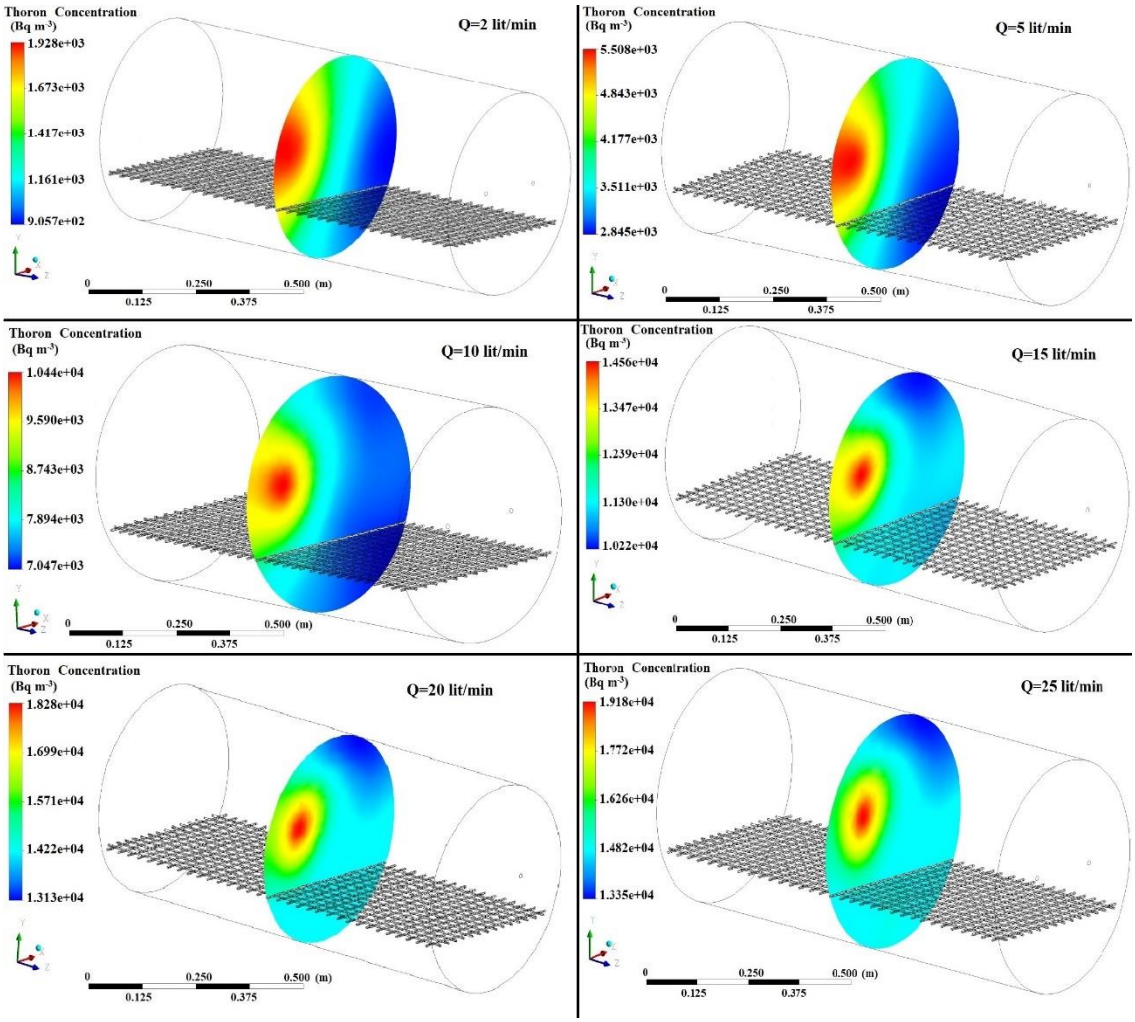

Figure 34. Concentration distribution of thoron (Bq/m^3) in the middle of the chamber (Z=50 cm) and at different flow rates using the optimized Chamber Configuration II

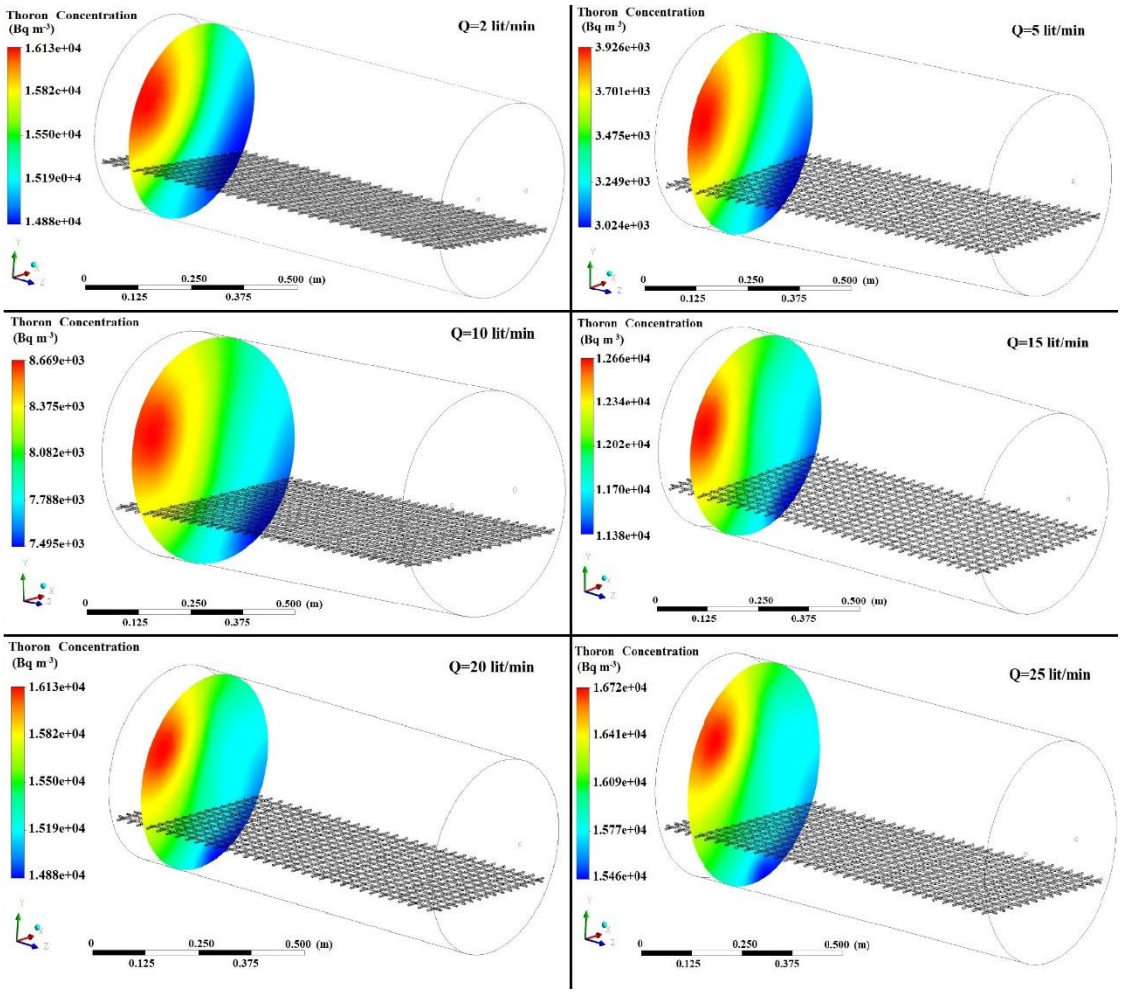

Figure 35. Concentration distribution of thoron (Bq/m^3) near the end of the chamber (Z=90 cm) and at different flow rates using the optimized Chamber Configuration II

3.4.3 Experimental observations and validation

Currently, three different sources of ceramic with different thorium contents are available at RRI (Jobbágy and Bety-Denissa, 2010) and previously performed experiments have shown that the sources are suitable for the purposes of research. Therefore, the investigations were continued along these lines (Csordás et al., 2015; Fábián et al., 2017) and concentrations of up to 19 KBq/m^{3}can be produced inside the chamber by different sources. The sources of ceramic were produced by Sibelco. Afterwards, the source was placed outside the chamber to obtain optimized Configuration II from the simulation step. Having passed through a drying column and filter, the air was pumped through the source before entering the chamber and mixed inside it by a fan. The air exiting via the outlet was recirculated through the source creating a closed loop. A schematic diagram of the experimental setup is shown in Figure 37.

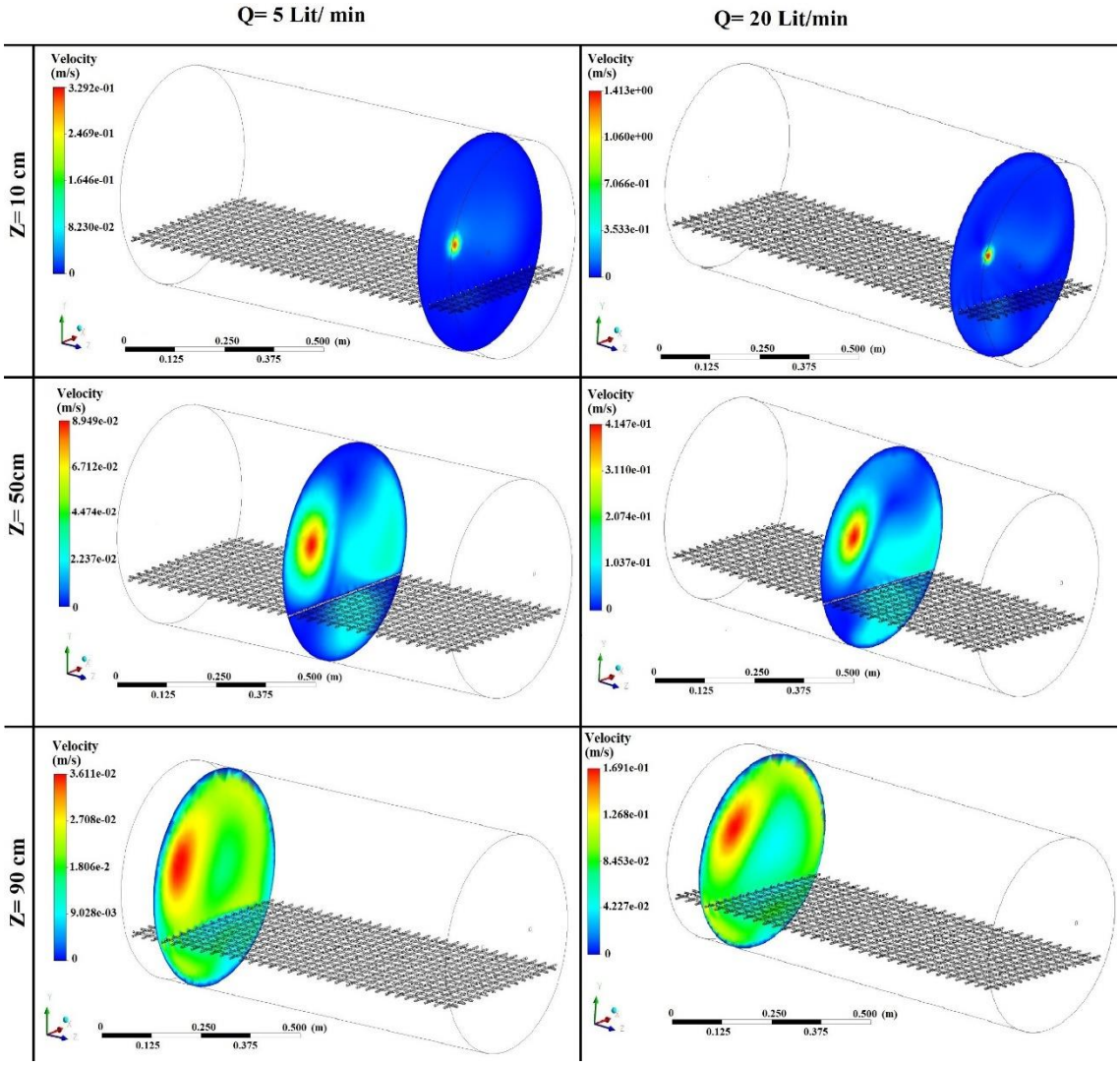

Figure 36. Velocity pattern of thoron gas inside the chamber at different distances and at two flow rates using the optimized Chamber Configuration II

The activity concentration of thoron gas was continuously measured at the inlet (C_{in}) and outlet (C_{out}) by using RAD7 radon/thoron detectors manufactured by DURRIDGE, USA. The measurements were done using the "thoron protocol" over a 5 minute-long repeating cycle. The detectors were placed outside the chamber and connected to it by plastic pipes. As the half-life of thoron is less than 1 min, measurements of the activity concentration of thoron gas must commence immediately after sampling. For the optimized chamber configuration and at different flow rates, five sets of experiment were carried out, the steady state C_{in} and C_{out} observed as well as the consequent transmission factor of thoron calculated.

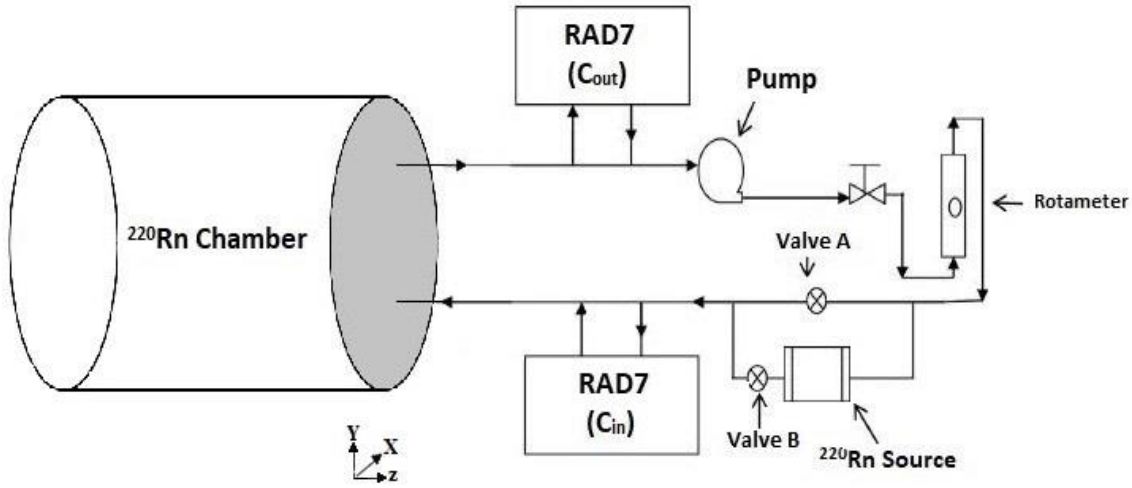

Figure 37. Experimental setup for measuring thoron activity concentrations in the thoron calibration chamber at RRI

The transmission factors of thoron (C_{out}/C_{in}) obtained from experiments, simulations and analytical models in the thoron calibration chamber at RRI at various flow rates between 2 and 25 l/min based on the optimized Configuration II are presented in Table 19. Accordingly, at lower flow rate of 2 l/min, the relative deviation between experimental observations and simulation results and also analytical model predictions were slightly high, namely 44.74% and 49.93%, respectively. By increasing the flow rates, this deviation reduced, which was expected owing to enhanced mixing as a result of a turbulence regime.

For example, the corresponding relative deviations were calculated to be 18% and 8% at flow rates of 5 l/min and 25 l/min, respectively. Furthermore, by computing the percentage difference between the estimated results according to ANSYS Fluent and the mixing model calculations at each flow rate, the differences were determined to be 31% and 9% at flow rates of 5 l/min and 25 l/min, respectively. Although our experiments were only performed at flow rates of up to 25 l/min, this deviation remained appreciable (at a maximum of approximately 9%). This validates the capability of the CFD technique for estimating the distribution of thoron gas inside the chamber while simulation results corresponded well with the experimental observations as well. Finally, in conclusion, our results clearly demonstrate the applicability of using the thoron calibration chamber at RRI when calibrating SSNTDs. Therefore, the calibration factors for CR-39 in case of thoron dose assessment is estimated with the optimum condition in RRI calibration chamber.

Table 19. Transmission factors of thoron obtained from experiments, simulations and analytical models

Flow rate (l/min)	Thoron transmission factor (C_{out}/C_{in})		Analytical method	Rel. Dev[1] (%)	Rel. Dev[2] (%)
	Config. II With Tray	Experimental			
2	0.0089	0.0062	0.0134	44.74	49.93
3	0.0142	0.0109	0.0201	30.13	41.11
4	0.0203	0.0158	0.0265	28.40	30.80
5	0.0250	0.0212	0.0329	18.22	31.31
7.5	0.0369	0.0317	0.0486	16.16	31.78
10	0.0524	0.0441	0.0638	18.98	21.75
12.5	0.0651	0.0559	0.0785	16.57	20.44
15	0.0808	0.0708	0.0927	14.14	14.79
20	0.1093	0.1001	0.1199	9.18	9.75
25	0.1332	0.1233	0.1456	8.05	9.26

[1] % Relative deviation between experimental observations and simulation results was calculated as follows: % Rel. Dev. = $\frac{|\text{Experimental observation} - \text{Simulation result}|}{\text{Experimental observation}}$

[2] % Relative deviation between simulation results and the uniform mixing model was calculated as follows: % Rel. Dev. = $\frac{|\text{simulation result} - \text{Analytical model prediction}|}{\text{simulation result}}$

SUMMARY

According to the radiation protection standards and health physics, which have also been introduced by difference organizations and explained in details in the first chapter of this thesis (ICRP, 1994; European commission, 1999; UNSCEAR, 2000, 2008; Council of the European union, 2014), in order to protect people against exposure to ionizing radiation, this is significant due to monitor and control the indoor exposure including exposure and inhalation of indoor radon and thoron concentration and its decay products in the dwelling and workplaces and also the external gamma radiation emanating from building materials which population is expose to. Therefore, not only exposure to such sources of radiation is a major public health concern (especially in high natural background radiation areas) but also because almost 80% of human life is spent indoors, knowing the dose limits for public exposure and measuring the levels of naturally occurring background radiation emanated from the building materials, ground, air, water inside of the buildings, etc. is essential for estimating the exposure of humans to natural sources of radiation.

Due to the lack of measurement data concerning the indoor radon and thoron concentrations as well as radioactivity data in building materials in some areas in IRAN specially HNBR of Mahallat, attempts have been made to the current thesis and divided the area of study into 3 major parts to estimate aforementioned data. Below a summary of the radiation results for each considered case study in Iran, assessed in this thesis, is given.

1. In case of indoor radon and thoron measurement in Mashhad dwellings, the average radon and thoron concentrations in summer and winter represent the annual radon and thoron concentration. The total exposure time was 90 days (two seasons). Indoor radon and thoron concentrations are measured in the living rooms of houses at ground level. It was also understood that thoron concentration would be strongly dependent on the distance from the source due to its short haft-life. As a result, it can be stated that the indoor ^{222}Rn and ^{220}Rn concentrations in the winter ranged from 75±11 to 376±24 Bq/m^3 with a mean value of 150±19 $Bq.m^3$ and from below the LLD to 166±10 Bq/m^3 with a mean value of 66±8 Bq/m^3, respectively. In the case of the summer, the indoor ^{222}Rn and ^{220}Rn concentrations ranged from 50±11 to 305±24 Bq/m^3 with a mean value of 114±18 Bq/m^3 and from below the LLD to 122±10 Bq/m^3 with a mean value of 48±6 Bq/m^3, respectively. In addition, the annual average indoor ^{222}Rn

and ^{220}Rn concentrations in the studied areas were 132±19 Bq/m^3 and 58±7 Bq/m^3, respectively. The corresponding annual effective dose from the inhalation of radon and thoron was calculated to be 3.7±0.5 mSv/year. The main source of indoor ^{222}Rn originates from soil gas infiltration, building materials and ventilation. Regarding the relationship between radon and thoron concentrations, no clear and strong correlation between was observed and thoron concentrations could not be predicted from widely available information concerning radon. However, indoor radon and thoron concentration might directly depend on the activity of ^{226}Ra and ^{232}Th (^{228}Th) in building materials, ground is the main entry path of radon at dwellings; therefore, it could say that the content of both ^{222}Rn and ^{220}Rn depends on the building materials and soil composition. Moreover, the soil-gas radon concentrations recorded in the studied area fell within the range of 1.07±0.28 to 8.02±0.65 kBq/m^3 with a mean value of 3.07±1.09 kBq/m^3. The activity concentrations of radon vary from location to location, possibly because of the physic geological properties of the types of soil studied, topographic differences, as well as geomorphology and meteorological conditions of the region.

Finally, the spatial distribution map of indoor radon concentrations in Mashhad dwellings were plotted by various interpolation techniques over a grid with the dimensions of 1 km×1 km using ArcGIS software version 10.7. The arithmetic mean was used over the grid cells to predict a mean indoor radon concentration on the ground-floor level of buildings in the grid cells where no data was available. Accordingly, radon concentrations were lower than standard values in eastern residential areas and were higher in central as well as southern districts. Nevertheless, when the spatial autocorrelation between cells was considered, predictions about radon concentrations using different methods range from 65 to 260 Bq/m^3. These values may be more realistic and similar to average values found in some dwellings in the region. IDW, which predicts unknown values using known values concerning their distance, was proven to be more suitable for predicting mean indoor radon concentrations.

Suggestion: In addition to the results and given the significant health impacts of radon and thoron, it is hoped that both indoor radon and thorn gases will be studied more seriously in Iran and these techniques as well as complementary procedures used to minimize its concentration. Hence, it is recommended that

radon gas concentrations as well as soil-gas radon and soil permeability should be measured in all regions of the country by numerous devices supplied by the Atomic Energy Organization of Iran (AEOI). As a result, it would be possible to compile a radon map of Iran to estimate the concentration and number of radon-induced incidences of cancer as well as decide how to distribute the population. This would aid to reduce the number of cases of lung cancer and other radon-induced human health problems.

2. The radiological survey has been also conducted to monitor radioactivity of most common building materials in Semnan Province, Iran and HNBR of Mahallat to assess the corresponding radiation risk. Therefore, the NORMs activity concentrations of the studied building materials in Semnan province were measured by HPGe gamma spectrometry as: ^{226}Ra activity concentration was found to vary from 7±1 to 44±9 with mean value of 27±5 Bq/kg. The concentration of ^{226}Ra was the highest in tile and the lowest in marble sample. The activity concentrations of ^{232}Th in the measured samples ranged from 6±1 (in marble sample) to 60±11 Bq/kg with mean value of 23±4 Bq/kg. Granite had the highest concentration of ^{232}Th. The activity concentration of ^{40}K also were measured to be between 28±3 (in marble sample) and 1085±113 Bq/kg (in granite sample). The average activity concentration of ^{40}K was 322±41 Bq/kg. Higher activities of ^{226}Ra, ^{232}Th and ^{40}K were recorded in various building materials such as tiles, ceramic, bricks and granite but, with the exception of the granite samples, did not remarkably exceed the worldwide average values. By analyzing the frequency distribution of all corresponded radionuclides, the histogram of ^{226}Ra and ^{232}Th indicates a normal distribution (bell-shaped). While ^{40}K revealed in some level of multi-modality. This multimodal feature of ^{40}K demonstrates the complexity of minerals in building materials. By applying multivariate statistical approach (Pearson correlation, cluster, and PCA), the radiological health hazard parameters were analyzed to obtain similarities and correlations between the various samples. The Pearson correlation showed that the ^{226}Ra distribution in the samples is controlled by changing the ^{232}Th concentration. The variance of 95.58% obtained from PCA resulted that the main radiological health hazard parameters exist due to the concentration of ^{226}Ra and ^{232}Th. The resulting dendrogram of cluster analysis also shows a well coincidence with the correlation analysis.

Regarding the studied building materials in HNBR of Mahallat, the average activity concentration of ^{226}Ra, ^{232}Th and ^{40}K in the samples measured were 34±6, 27±6 and 276±58 Bq/kg, respectively. It can be seen that concentrations measured were, in most cases, below worldwide average values. In most of the studied building materials in Mahallat, there is also a positive correlation between ^{226}Ra and ^{232}Th. The strongest linear relationship is observed between ^{226}Ra and ^{232}Th in Sand and Gravel, and Ceramic; since ^{226}Ra series and ^{232}Th series are usually found together in nature, and good correlation between them is indicative of common sources, which, in general, are associated with a mineralogical component. The radioactivity index, was less than 1 for all of the samples. However, even for the samples with low radioactivity indexes - due to the absence of national regulations in Iran- to monitor and control the radioactivity of building materials, such measurements are necessary. Also, simulations were carried out using the computer code RESRAD-BUILD and a pathway analysis model designed to evaluate the potential radiological dose incurred by an individual who lives in a building contaminated with radioactive material in Mahallat, Iran for three case studies with different building materials. The maximum long-term Effective Dose rate was recorded from the case study two (tiled cement floor), which varied from 504 to 1433 μSv/year and was below the recommended maximum limit set by the ICRP.

Suggestion: As from the studied building materials, it can be concluded that most results fell below the average values for building materials worldwide, therefore, in terms of their inhabitants, buildings constructed from such materials are radiologically safe; but the results draw specific attention to the use of granite, brick, ceramic, and tile in the construction of dwellings. Therefore, firstly, the legislation of a national standard into the Iranian legal system describing the requirements for the radiological examination of building materials, is necessary before their introduction on the market. Secondly, a wide national study is highly recommended to measure the radioactivity in different building materials for the country specially the local products. Thirdly, it is also recommended to measure radioactivity in by-product and industrial raw materials which are widely used in the production of some building materials, like Portland cement, concrete, bricks and so on. Lastly, since the radon exhalation study (mass and surface exhalation rates) is important for understanding

the relative contribution of the corresponding materials to the total radon concentration found inside the dwellings, so it is better to measure and estimate it. Finally, investigate the applicability and appropriate concentration of such by-products and raw materials in construction of dwelling to be considered more safely for inhabitants according to the relevant regulations.

3. Regarding the thermal baths at a spa in Dehloran (Iran), the concentrations of radon and thoron inside the spa were investigated. The concentrations of dissolved ^{226}Ra in samples of water from thermal baths were also measured. Additionally, the activity concentrations of abundant naturally occurring radionuclides in farmland soils irrigated with water from hot springs was measured and compared with other soil samples irrigated with water from other sources to estimate possible radioecological effects of natural radiation staff, patients and tourists at the spa are exposed to. In addition, the search for a link between the concentration of naturally occurring radionuclides in soil and the use of water from hot springs for irrigation was one of the main goals of the study. The activity concentrations of three major naturally occurring radionuclides in soil samples were measured; the ranges for ^{40}K, ^{226}Ra and ^{228}Ra were 101 ± 8 to 240 ± 12, 276 ± 7 to 322 ± 12 and 20 ± 7 to 80 ± 10 Bq/kg, respectively. Higher activity concentrations of ^{226}Ra and ^{228}Ra were recorded in soil samples irrigated with hot spring water. The water from the same spring was used in all thermal baths so concentrations of dissolved ^{226}Ra in water samples from different thermal baths were approximated to also be 0.42 ± 0.20 Bq/l. The indoor radon concentrations in the private thermal baths over a period of 45 days (including both occupied and vacant time) were measured to be between 1880 ± 410 and 2450 ± 530 Bq/m^3 and the radon concentrations in the spa galleries were measured to be between 790 ± 135 and 1050 ± 120 Bq/m^3, however, thoron concentrations were below the detection limit. The ventilation and centralized heating systems at the spa under investigation are inefficient so the radon concentrations in the therapy rooms and baths are high. The maximum radiation doses originating from the inhalation of radon for tourists and the staff were estimated to be 0.13 and 5.5 mSv/year, respectively, which is slightly over the national limit in Iran (5 mSv/year).

   Suggestion: This shows the importance of determining the dose workers are exposed to and for whom the radiation hazard of radon is more significant than

for tourists. Therefore, it is necessary to mitigate this dose by increasing ventilation and/or aerating the spring water to remove radon. Since the maximum estimated dose for members of staff was close to the national dose limit, environmental radon monitoring at the spa must be implemented with the provision of personal dosimetry for the members of staff most at risk. Given the results of this thesis, the implementation of a regulation for monitoring radon concentrations is highly recommended in popular public places such as thermal baths and caves.

4. As long-term indoor exposure of thoron concentration (passive measurement) and subsequently SSNTDs calibration methods for its measurement have been developed and becomes an important topic to be determined, in this thesis, I have also developed the thoron calibration chamber in the RRI facility, by applying the CFD technique. RRI thoron exposure calibration chamber was designed and simulated established on the CFD approach implemented in ANSYS FLUENT 2020 R1 code R1 based on the finite volume method. The thoron behavior and its spatial distribution inside the RRI thoron calibration chamber in the presence of a different flow rates were predicated and discussed. Then, the simulation results are compared with analytical calculations as well as experimental measurement. The obtained results indicated that the measured transmission factors were depending on the flow rate as well as the positions of the inlet and outlet. Our results clearly demonstrate the applicability of the thoron calibration chamber at RRI for the purposes of calibrating monitoring instruments. Furthermore, the CFD-based predictions were in strong agreement with the results from experimental and analytical models due to the corresponding appreciable relative deviation (with a maximum of approximately 9%).

   Suggestion: This study extends the applicability of the CFD technique for acquiring an in-depth understanding of issues related to the ^{220}Rn concentration profile, improving measurement protocol, etc. This study also paves the way for simulations targeting real-scale field problems. Therefore, a CFD simulation approach could be carried out to study the concentration profile of radon and thoron and their decay products in a flow-through scintillation cell and its performance could be improved in terms of alpha production efficiency for long run indoor environments measurements. In addition, to follow this study,

it is highly recommended that the CFD simulation results should compare with another experimental work by sampling from different distance from inlet of thoron calibration chamber to see the exact behavior of thoron gas inside the chamber.

Also, since inaccurate dosimetric assessments based on the limited approach of the point measurements can be improved by the validated CFD technique in the near future. CFD could assist the radon and thoron visualization and may also supplement the regulation codes, presently enforced or to be laid down in the future, for the construction of buildings. Hence, it is suggested to perform the measurements and computational fluid dynamics investigation of the indoor radon and thoron distribution in a typical naturally and mechanically ventilated room and compare it with the results of passive and active detectors in order to find out the indoor radon and thoron distribution.

List of Papers included

This thesis is based on the following papers, which are referred into the text by the name of authors:

I. Adelikhah, M., Shahrokhi, A., Chalupnik, S., Tóth-Bodrogi, E. and Kovács, T., 2020. High level of natural ionizing radiation at a thermal bath in Dehloran, Iran. Heliyon, 6(7), p.e04297. (**Q1, IF=3.776**)

II. Adelikhah, M., Shahrokhi, A., Imani, M., Chalupnik, S. and Kovács, T., 2021. Radiological assessment of indoor radon and thoron concentrations and indoor radon map of dwellings in Mashhad, Iran. International Journal of Environmental Research and Public Health, 18(1), p.141. (**Q1, IF=4.614**)

III. Imani, M., Adelikhah, M., Shahrokhi, A., Azimpour, G., Yadollahi, A., Kocsis, E., Toth-Bodrogi, E. and Kovács, T., 2021. Natural radioactivity and radiological risks of common building materials used in Semnan Province dwellings, Iran. Environmental Science and Pollution Research, 28(30), pp.41492-41503. (**Q2, IF=5.190**)

IV. Adelikhah, M., Imani, M., Hegedűs, M. and Kovács, T., 2022. Modelling of indoor external and internal exposure due to different building materials containing NORMs in the vicinity of a HNBRA in Mahallat, Iran. Heliyon, p.e08909. (**Q1, IF=3.776**)

V. Shahrokhi, A., Adelikhah, M., Chalupnik, S., Kocsis, E., Tóth-Bodrogi, E. and Kovács, T., 2020. Radioactivity of building materials in Mahallat, Iran -an area exposed to a high level of natural background radiation -attenuation of external radiation doses. Materiales de Construcción, Vol. 70, issue 340, p. 2233. (**Q2, IF=2.13**).

BIBLIOGRAPHY

Abbasi, A., 2013. Calculation of gamma radiation dose rate and radon concentration due to granites used as building materials in Iran. Radiation protection dosimetry, 155(3), pp.335-342. https://doi.org/10.1093/rpd/nct003

Abdullahi, S., Ismail, A.F., Yasir, M.S., 2020. Radiological hazard analysis of Malaysia's ceramic materials using generic and RESRAD-BUILD computer code approach. J. Radioanal. Nucl. Chem. 324, 301–315. https://doi.org/10.1007/s10967-020-07070-3

Adelikhah, M., Imani, M., Hegedűs, M. and Kovács, T., 2022. Modelling of indoor external and internal exposure due to different building materials containing NORMs in the vicinity of a HNBRA in Mahallat, Iran. Heliyon, p.e08909.https://doi.org/10.1016/j.heliyon.2022.e08909

Adelikhah, M., Shahrokhi, A., Imani, M., Chalupnik, S. and Kovács, T., 2021. Radiological assessment of indoor radon and thoron concentrations and indoor radon map of dwellings in Mashhad, Iran. International Journal of Environmental Research and Public Health, 18(1), p.141. https://doi.org/10.3390/ijerph18010141

Adelikhah, M., Shahrokhi, A., Chalupnik, S., Tóth-Bodrogi, E. and Kovács, T., 2020. High level of natural ionizing radiation at a thermal bath in Dehloran, Iran. Heliyon, 6(7), p.e04297. https://doi.org/10.1016/j.heliyon.2020.e04297

Agarwal, T.K., Sahoo, B.K., Gaware, J.J., Joshi, M. and Sapra, B.K., 2014. CFD based simulation of thoron (^{220}Rn) concentration in a delay chamber for mitigation application. Journal of environmental radioactivity, 136, pp.16-21.https://doi.org/10.1016/j.jenvrad.2014.05.003

Agarwal, T.K., Sahoo, B.K., Joshi, M., Mishra, R., Meisenberg, O., Tschiersch, J. and Sapra, B.K., 2019. CFD simulations to study the effect of ventilation rate on ^{220}Rn concentration distribution in a test house. Radiation Physics and Chemistry, 162, pp.82-89. https://doi.org/10.1016/j.radphyschem.2019.04.018

Agbalagba, E.O., Osakwe, R.O.A. and Olarinoye, I.O., 2014. Comparative assessment of natural radionuclide content of cement brands used within Nigeria and some countries in the world. Journal of Geochemical Exploration, 142, pp.21-28.https://doi.org/10.1016/j.gexplo.2013.12.002

Agung, H. and Lucas, D.S., 2015. Tectonic setting of adang volcanic complex in Mamuju region, West Sulawesi Province. Eksplorium, 36(1), pp.31-44. https:// doi. org/ 10. 17146/ ekspl orium. 2015. 36.1. 2769 DOI:10.17014/ijog.3.3.195-214

Alexander, D.L., Tropsha, A. and Winkler, D.A., 2015. Beware of R 2: simple, unambiguous assessment of the prediction accuracy of QSAR and QSPR models. Journal of chemical information and modeling, 55(7), pp.1316-1322. https://doi.org/10.1021/acs.jcim.5b00206

Al Mugahed, M. and Bentayeb, F., 2019. Studying of Radon Gas Concentrations in Soil Qaa Al-Hakel Agricultural Area, Ibb, Yemen. Materials Today: Proceedings, 13, pp.525-529. https://doi.org/10.1016/j.matpr.2019.04.009

Al-Sewaidan, H.A., 2019. Natural radioactivity measurements and dose rate assessment of selected ceramic and cement types used in Riyadh, Saudi Arabia. Journal of King Saud University-Science, 31(4), pp.987-992. https://doi.org/10.1016/j.jksus.2019.04.001

Al-Sulaiti, H., Alkhomashi, N., Al-Dahan, N., Al-Dosari, M., Bradley, D.A., Bukhari, S., Matthews, M., Regan, P.H. and Santawamaitre, T., 2011. Determination of the natural radioactivity in Qatarian building materials using high-resolution gamma-ray spectrometry. Nuclear Instruments and Methods in Physics Research Section A: Accelerators, Spectrometers, Detectors and Associated Equipment, 652(1), pp.915-919. https://doi.org/10.1016/j.nima.2011.01.020

Amatullah, S., Rahman, R., Ferdous, J., Siraz, M.M.M., Khandaker, M.U. and Mahal, S.F., 2021. Assessment of radiometric standard and potential health risks from building materials used in Bangladeshi dwellings. International Journal of Environmental Analytical Chemistry.
Amini Birami, F., Moore, F., Faghihi, R. and Keshavarzi, B., 2019. Distribution of natural radionuclides and assessment of the associated radiological hazards in the rock and soil samples from a high-level natural radiation area, Northern Iran. Journal of Radioanalytical and Nuclear Chemistry, 322(3), pp.2091-2103. https://doi.org/10.1007/s10967-019-06912-z
Anjos, R.M., Okuno, E., Gomes, P.R.S., Veiga, R., Estellita, L., Mangia, L., Uzeda, D., Soares, T., Facure, A., Brage, J.A.P. and Mosquera, B., 2003. Radioecology teaching: evaluation of the background radiation levels from areas with high concentrations of radionuclides in soil. European journal of physics, 25(2), p.133. https://doi.org/10.1088/0143-0807/25/2/001
Asaduzzaman, K., Mannan, F., Khandaker, M.U., Farook, M.S., Elkezza, A., Amin, Y.B.M., Sharma, S. and Abu Kassim, H.B., 2015. Assessment of natural radioactivity levels and potential radiological risks of common building materials used in Bangladeshi dwellings. PLoS one, 10(10), p.e0140667. https://doi.org/10.1371/journal.pone.0140667
Ashrafi, S. and Jahanbakhsh, O., 2019. Measurement of natural radioactivity of Iranian granite samples using beta–gamma coincidence spectrometer and maximum likelihood method. Environmental Earth Sciences, 78(15), pp.1-8. https://doi.org/10.1007/s12665-019-8434-6
Bahtijari, M., Nafezi, G., Hodolli, G. and Kadiri, S., 2022. Radon activity assessment of thermal water in Spas of Kosovo by using different methods. International Journal of Radiation Research, 20(1), pp.229-233. https://dx.doi.org/10.52547/ijrr.20.1.35
Baptista, E., Pereira, A.J., Domingos, F.P. and Sêco, S.L., 2022. Radon and thoron concentrations in the southwest region of Angola: dose assessment and implications for risk mapping. Environmental Geochemistry and Health, pp.1-22. https://doi.org/10.1007/s10653-022-01226
Bátor, G., Csordás, A., Horvath, D., Somlai, J. and Kovács, T., 2015. A comparison of a track shape analysis-based automated slide scanner system with traditional methods. Journal of Radioanalytical and Nuclear Chemistry, 306(1), pp.333-339. https://doi.org/10.1007/s10967-
Bavarnegin, E., Fathabadi, N., Moghaddam, M.V., Farahani, M.V., Moradi, M. and Babakhni, A., 2013. Radon exhalation rate and natural radionuclide content in building materials of high background areas of Ramsar, Iran. Journal of environmental radioactivity, 117, pp.36-40.
Bé, M.-M.; Chechev, V.P.; Dersch, R.; Helene, O.A.M.; Helmer, R.G.; et al., 2007. Update of x ray and gamma ray decay data standards for detector calibration and other applications, volume 2: data selection assessment and evaluation procedures. International Atomic Energy Agency. Vienna
Becker, K., 2003. Health effects of high radon environments in central Europe: another test for the LNT hypothesis? Nonlinearity in biology, toxicology, medicine, 1(1), p.15401420390844447. https://doi.org/10.1080/15401420390844447
Beitollahi, M., Ghiassi-Nejad, M., Esmaeli, A., Dunker, R., 2007. Radiological studies in the hot spring region of Mahallat, central Iran. Radiation Protection Dosimetry, Vol. 123, No. 4, pp. 505–508. https://doi.org/10.1093/rpd/ncl524
Beretka, J. and Matthew, P.J., 1985. Natural radioactivity of Australian building materials, industrial wastes and by-products. Health physics, 48(1), pp.87-95. DOI: 10.1097/00004032-198501000-00007
Bivand, R.S., Pebesma, E.J., Gómez-Rubio, V. and Pebesma, E.J., 2008. Applied spatial data analysis with R (Vol. 747248717, pp. 237-268). New York: Springer.
Boice Jr, J.D., Hendry, J.H., Nakamura, N., Niwa, O., Nakamura, S. and Yoshida, K., 2010. Low-dose-rate epidemiology of high background radiation areas. Radiation research, 173(6), pp.849-854. https://doi.org/10.1667/RR2161.1

Bouzarjomehri, F., Ehrampoosh, M.H., 2008. Radon level in dwellings basement of Yazd-Iran. Iran. J. Radiat. Res., 6: 141-144. http://ijrr.com/article-1-483-en.html
Chen, J. and Ford, K.L., 2017. A study on the correlation between soil radon potential and average indoor radon potential in Canadian cities. Journal of environmental radioactivity, 166, pp.152-156. https://doi.org/10.1016/j.jenvrad.2016.01.018
Cetin, E., Altinsoy, N. and Örgün, Y., 2012. Natural radioactivity levels of granites used in Turkey. Radiation Protection Dosimetry, 151(2), pp.299-305. https://doi.org/10.1093/rpd/ncs
Chen, J., 2022. Assessment of thoron contribution to indoor radon exposure in Canada. Radiation and Environmental Biophysics, pp.1-7. https://doi.org/10.1007/s00411-021-00956-
Chauhan, N., Chauhan, R.P., Joshi, M., Agarwal, T.K., Aggarwal, P. and Sahoo, B.K., 2014. Study of indoor radon distribution using measurements and CFD modeling. Journal of Environmental Radioactivity, 136, pp.105-111. https://doi.org/10.1016/j.jenvrad.2014.05.020
Cinelli, G., Tositti, L., Capaccioni, B., Brattich, E. and Mostacci, D., 2015. Soil gas radon assessment and development of a radon risk map in Bolsena, Central Italy. Environmental geochemistry and health, 37(2), pp.305-319. https://doi.org/10.1007/s10653-014-9649-9
Cosma, C., Cucoş-Dinu, A., Papp, B., Begy, R. and Sainz, C., 2013. Soil and building material as main sources of indoor radon in Băiţa-Ştei radon prone area (Romania). Journal of environmental radioactivity, 116, pp.174-179. https://doi.org/10.1016/j.jenvrad.2012.09.006
Csordás, A., Fábián, F., Horváth, M., Hegedűs, M., Somlai, J. and Kovács, T., 2015. Preparation and characterization of ceramic-based thoron sources for thoron calibration chamber. Radiation protection dosimetry, 167(1-3), pp.151-154. https://doi.org/10.1093/rpd/ncv234
De Cort, M., Gruber, V., Tollefsen, T., Bossew, P. and Janssens, A., 2011. Towards a European Atlas of natural radiation: goal, status and future perspectives. Radioprotection 46, S737–S743. https://doi.org/10.1051/radiopro/20116871s
Dey, G.K. and Das, P.K., 2012. Estimation of radon concentration in dwellings in and around Guwahati. Journal of earth system science, 121(1), pp.237-240. https://doi.org/10.1007/s12040-012-0136-3
Dubois, G., 2005. An overview of radon surveys in Europe. EUR 21892 EN.
Dubois, G., Bossew, P., Tollefsen, T. and De Cort, M., 2010. First steps towards a European atlas of natural radiation: status of the European indoor radon map. Journal of environmental radioactivity, 101(10), pp.786-798. https://doi.org/10.1016/j.jenvrad.2010.03.007
Duggal, V., Rani, A. and Mehra, R., 2014. Measurement of soil-gas radon in some areas of northern Rajasthan, India. Journal of Earth System Science, 123(6), pp.1241-1247. https://doi.org/10.1007/s12040-014-0473-5
DURRIDGE Company Inc., 2018. BIG BOTTLE SYSTEM - High Sensitivity Radon in Water Accessory for the RAD7 With Aerator Cap Revision C: User Manual.
Eappen, K.P., Sapra, B.K. and Mayya, Y.S., 2007. A novel methodology for online measurement of thoron using Lucas scintillation cell. Nuclear Instruments and Methods in Physics Research Section A: Accelerators, Spectrometers, Detectors and Associated Equipment, 572(2), pp.922-925. https://doi.org/10.1016/j.nima.2006.11.074
Elío, J., Crowley, Q., Scanlon, R., Hodgson, J. and Long, S., 2017. Logistic regression model for detecting radon prone areas in Ireland. Science of The Total Environment, 599, pp.1317-1329. https://doi.org/10.1016/j.scitotenv.2017.05.071
European Commission, 1999. Radiation Protection 112: Radiological Protection Principles Concerning the Natural Radioactivity of Building Materials. Directorate-General, Environment, Nuclear Safety and Civil Protection. 5-16.
El-Taher, A., 2010. Gamma spectroscopic analysis and associated radiation hazards of building materials used in Egypt. Radiation protection dosimetry, 138(2), pp.166-173.

Faheem, M. and Mati, N., 2007. Seasonal variation in indoor radon concentrations in dwellings in six districts of the Punjab province, Pakistan. Journal of Radiological Protection, 27(4), p.493.
Fahiminia, M., Fard, R.F., Ardani, R., Naddafi, K., Hassanvand, M.S., Mohammadbeigi, A., 2016. Indoor radon measurements in residential dwellings in Qom, Iran. International Journal of Radiation Research. 14(4):331-9.
Fathabadi, N., Farahani, M.V., Amani, S., Moradi, M. and Haddadi, B., 2011. Evaluation of occupational exposure to naturally occurring radioactive materials in the Iranian ceramics industry. Radiation protection dosimetry, 145(4), pp.400-404.
Fathivand, A.A. and Amidi, J., 2007. Assessment of natural radioactivity and the associated hazards in Iranian cement. Radiation protection dosimetry, 124(2), pp.145-147.
Fluent, I., 2006. FLUENT 6.3 User's Guide: Lebanon. NH: Fluent Inc.
Gaware, J.J., Sahoo, B.K., Sapra, B.K. and Mayya, Y.S., 2011. Development of online radon and thoron monitoring systems for occupation and general environments. BARC News Lett, 318(318), pp.45-51.
Ghiassi-Nejad, M., Mortazavi, S.M.J., Cameron, J.R., Niroomand-Rad, A. and Karam, P.A., 2002. Very high background radiation areas of Ramsar, Iran: preliminary biological studies. Health physics, 82(1), pp.87-93.
Hadad, K., Doulatdar, R., Mehdizadeh, S., 2007. Indoor radon monitoring in northern Iran using passive and active measurements. Journal of Environmental Radioactivity, 95: 39-52.
Hadad, K., Hakimdavoud, M.R. and HASHEMI, T.M., 2011. Indoor radon survey in Shiraz-Iran using developed passive measurement method.
Hadad, K., Mokhtari. J., 2015. Indoor radon variations in central Iran and its geostatistical map. Atmospheric Environment. 102:220-7.
Hassan, N.M. and Chae, J.S., 2019. Radioactivity and radiological impact of industrial raw materials in Korea. International Journal of Environmental Science and Technology, 16(12), pp.8073-8080.
Health Canada, 2016. Radon: Reduction Guide for Canadians, http://www.hc-sc.gc.ca/ewh-semt/pubs/radiation/radon_canadians-canadiens/index-eng.php
Hendry, J.H., Simon, S.L., Wojcik, A., Sohrabi, M., Burkart, W., Cardis, E., Laurier, D., Tirmarche, M. and Hayata, I., 2009. Human exposure to high natural background radiation: what can it teach us about radiation risks?. Journal of Radiological Protection, 29(2A), p.A29.
Hoffmann, M., Aliyev, C.S., Feyzullayev, A.A., Baghirli, R.J., Veliyeva, F.F., Pampuri, L., Valsangiacomo, C., Tollefsen, T. and Cinelli, G., 2017. First map of residential indoor radon measurements in Azerbaijan. Radiation protection dosimetry, 175(2), pp.186-193.
Hosoda, M., Nugraha, E.D., Akata, N., Yamada, R., Tamakuma, Y., Sasaki, M., Kelleher, K., Yoshinaga, S., Suzuki, T., Rattanapongs, C.P. and Furukawa, M., 2021. A unique high natural background radiation area–Dose assessment and perspectives. Science of The Total Environment, 750, p.142346.
Hosoda, M., Tokonami, S., Omori, Y., Sahoo, S.K., Akiba, S., Sorimachi, A., Ishikawa, T., Nair, R.R., Jayalekshmi, P.A., Sebastian, P. and Iwaoka, K., 2015. Estimation of external dose by car-borne survey in Kerala, India. PLoS One, 10(4), p.e0124433.
IAEA (International Atomic Energy Agency), 2004. Radiation, people and the environment. Vienna: IAEA.
IAEA (International Atomic Energy Agency), 2014. Radiation Protection and Safety of Radioactive Sources: International Basic Safety Standards. General Safety Report Part 3. No. GSR Part 3. International Atomic Energy Agency, Vienna.

ICRP (International Commission on Radiological Protection), 1994. Protection Against ^{222}Rn at home and at work. ICRP Publication-65. Pergamon Press, Oxford.
ICRP (International Commission on Radiological Protection), 2007. The 2007 Recommendations of the International Commission on Radiological Protection. ICRP Publication 103. Ann. ICRP 37 (2-4).
ICRP (International Commission on Radiological Protection), 2010. Lung Cancer Risk from radon and Progeny and Statement on Radon; Annals of the ICRP: New York, NY, USA.
ICRP (International Commission on Radiological Protection), 2014. Radiological protection against radon exposure. ICRP Publication 126. Ann. ICRP 43(3).
ICRP (International Commission on Radiological Protection), 2017. Occupational intakes of radionuclides, Part 3. ICRP Publication 137. Ann. ICRP 46(3/4).
Imani, M., Adelikhah, M., Shahrokhi, A., Azimpour, G., Yadollahi, A., Kocsis, E., Toth-Bodrogi, E. and Kovács, T., 2021. Natural radioactivity and radiological risks of common building materials used in Semnan Province dwellings, Iran. Environmental Science and Pollution Research, 28(30), pp.41492-41503.
Institute of Standards and Industrial Research of Iran (ISIRI), 2005. Protection against ionizing radiation and the safety of radiation sources-Basic standards. ISIRI 7751, 1st edition.
Irlinger, J., 2015. Development of an electronic monitor for the determination of individual radon and thoron exposure (Doctoral dissertation).
Ismail, A.H. and Jaafar, M.S., 2010, June. Indoor radon concentration and its health risks in selected locations in Iraqi Kurdistan using CR-39 NTDs. In 2010 4th International Conference on Bioinformatics and Biomedical Engineering (pp. 1-8). IEEE.
Janik, M., Ishikawa, T., Omori, Y. and Kavasi, N., 2014. Invited Article: Radon and thoron intercomparison experiments for integrated monitors at NIRS, Japan. Review of Scientific Instruments, 85(2), p.022001.
Jobbágy, V., Kávási, N., Somlai, J., Dombovári, P., Kardos, R., Kovács, T., 2010. Radioanalytical investigations of uranium concentrations in natural spring, mineral, spa and drinking waters in Hungary. Journal of Radioanalytical Nuclear Chemistry, 286(2), 417-422.
Kapdan, E. and Altinsoy, N., 2012. A comparative study of indoor radon concentrations between dwellings and schools. Radiation Physics and Chemistry, 81(4), pp.383-386.
Karakaya, M.Ç., Doğru, M., Karakaya, N., Kuluöztürk, F. and Nalbantçılar, M.T., 2017. Radioactivity and hydrochemical properties of certain thermal Turkish spa waters. Journal of water and health, 15(4), pp.591-601.
Kardos, R., Sas, Z., Hegedűs, M., Shahrokhi, A., Somlai, J. and Kovács, T., 2015. Radionuclide content of NORM by-products originating from the coal-fired power plant in Oroszlány (Hungary). Radiation protection dosimetry, 167(1-3), pp.266-269.
Kasić, A. and Kasumović, A., 2022. Indoor radon levels, dose and health risk assessments in spas of Bosnia and Herzegovina. Journal of Radioanalytical and Nuclear Chemistry, 331(1), pp.231-239.
Kayakökü, H., Karatepe, Ş. and Doğru, M., 2016. Measurements of radioactivity and dose assessments in some building materials in Bitlis, Turkey. Applied Radiation and Isotopes, 115, pp.172-179.
Kikaj, D., Jeran, Z., Bahtijari, M. and Stegnar, P., 2016. Radon in soil gas in Kosovo. Journal of environmental radioactivity, 164, pp.245-252.
Kim, Y., Chang, B.U., Park, H.M., Kim, C.K., Tokonami, S., 2011. National radon survey in Korea. Radiation protection dosimetry. 146(1-3):6-10.

Kocsis, E., Tóth-Bodrogi, E., Peka, A., Adelikhah, M. and Kovács, T., 2021. Radiological impact assessment of different building material additives. Journal of Radioanalytical and Nuclear Chemistry, 330(3), pp.1517-1526.
Kotrappa, P. and Steck, D., 2010. Electret ion chamber-based passive radon–thoron discriminative monitors. Radiation protection dosimetry, 141(4), pp.386-389.
Krieger, R., 1981. Radioactivity of construction materials. Betonwerk Fertigteil Techn, 47(8), pp.468-473.
Kudo, H., Tokonami, S., Omori, Y., Ishikawa, T., Iwaoka, K., Sahoo, S.K., Akata, N., Hosoda, M., Wanabongse, P., Pornnumpa, C. and Sun, Q., 2015. Comparative dosimetry for radon and thoron in high background radiation areas in China. Radiation protection dosimetry, 167(1-3), pp.155-159.
Kunovska, B., Ivanova, K., Stojanovska, Z., Vuchkov, D. and Zaneva, N., 2013. Measurements of radon concentration in soil gas of urban areas, Bulgaria. Romanian Journal of Physics, 58(S), pp.S172-S179.
Kuzmanović, P., Todorović, N., Filipović Petrović, L., Mrđa, D., Forkapić, S., Nikolov, J. and Knežević, J., 2020. Radioactivity of building materials in Serbia and assessment of radiological hazard of gamma radiation and radon exhalation. Journal of Radioanalytical and Nuclear Chemistry, 324(3), pp.1077-1087.
Launder, B.E. and Spalding, D.B., 1983. The numerical computation of turbulent flows. In Numerical prediction of flow, heat transfer, turbulence and combustion (pp. 96-116). Pergamon.
Lecomte, J.F., Solomon, S., Takala, J., Jung, T., Strand, P., Murith, C., Kiselev, S., Zhuo, W., Shannoun, F. and Janssens, A., 2014. ICRP publication 126: radiological protection against radon exposure. Annals of the ICRP, 43(3), pp.5-73.
Lee, K.Y., Hwang, S., Kim, Y. and Ko, K.S., 2019. Measurement of NORM in geologic and building materials by pair measurement–gamma spectrometry. Journal of Radioanalytical and Nuclear Chemistry, 322(3), pp.1791-1795.
Lu, X., Yang, G. and Ren, C., 2012. Natural radioactivity and radiological hazards of building materials in Xianyang, China. Radiation Physics and Chemistry, 81(7), pp.780-784.
Lu, X., Chao, S. and Yang, F., 2014. Determination of natural radioactivity and associated radiation hazard in building materials used in Weinan, China. Radiation Physics and Chemistry, 99, pp.62-67.
Mirbag, A., Shokati Poursani, A., 2019. Indoor radon measurement in residential/commercial buildings in Isfahan city, J. Air Pollut. Heal. 3, 209–218, doi: http://dx.doi.org/10.18502/japh.v3i4.404.
Mirzaee, S.Y., Chitszan, M., Peiri, Z. and Karimi, H., 2019. Hydrogeochemical study and determination of Pollution Source of Dehloran Sargrou Spring. Journal of Advanced Applied Geology 9 (3): 357-373. DOI: 10.22055/AAG.2019.28116.1917
Mortazavi, S.M.J. and Mozdarani, H., 2012. Is it time to shed some light on the black box of health policies regarding the inhabitants of the high background radiation areas of Ramsar? International Journal of Radiation Research, 10(3/4), p.111.
Mowlavi, A.A., Fornasier, M.R., Binesh, A. and De Denaro, M., 2012. Indoor radon measurement and effective dose assessment of 150 apartments in Mashhad, Iran. Environmental monitoring and assessment, 184(2), pp.1085-1088. https://doi.org/10.1007/s10661-011-2022-x
Nagy, K., Kavasi, N., Kovacs, T. and Somlai, J., 2008. Radon therapy and speleotherapy in Hungary. Press Therm Climat, 145, pp.219-225.

Nagy, K., Berhés, I., Kovács, T., Kávási, N., Somlai, J., Kovacs, and Bender, T., 2009. Study on endocronological effects of radon speleotherapy on respiratory diseases. International journal of radiation biology, 85(3), pp.281-290. https://doi.org/10.1080/09553000802512550
Nair, R.R.K., Rajan, B., Akiba, S., Jayalekshmi, P., Nair, M.K., Gangadharan, P., Koga, T., Morishima, H., Nakamura, S. and Sugahara, T., 2009. Background radiation and cancer incidence in Kerala, India—Karanagappally cohort study. Health physics, 96(1), pp.55-66.
NEA-OECD (Organization for Economic Co-operation and Development), 1979. Exposure to radiation from radioactivity in building materials. Report by a Group of Experts of The OECD Nuclear Energy Agency.
Nikolov, J., Todorovic, N., Pantic, T.P., Forkapic, S., Mrdja, D., Bikit, I., Krmar, M. and Veskovic, M., 2012. Exposure to radon in the radon spa Niška Banja, Serbia. Radiation Measurements, 47(6), pp.443-450. https://doi.org/10.1016/j.radmeas.2012.04.006
Nowak, J., Chau, D. and Rajchel, L., 2012. Natural radioactive nuclides in the thermal waters of the Polish Inner Carpathians. Geologica Carpathica, 63(4), p.343. doi: 10.2478/v10096-012-0027-1
Nuccetelli, C., Leonardi, F. and Trevisi, R., 2015. A new accurate and flexible index to assess the contribution of building materials to indoor gamma exposure. Journal of environmental radioactivity, 143, pp.70-75. https://doi.org/10.1016/j.jenvrad.2015.02.011
Nugraha, E.D., Hosoda, M., Tamakuma, Y., Kranrod, C., Mellawati, J., Akata, N. and Tokonami, S., 2021. A unique high natural background radiation area in Indonesia: A brief review from the viewpoint of dose assessments. Journal of Radioanalytical and Nuclear Chemistry, 330(3), pp.1437-1444. https://doi.org/10.1007/s10967-021-07908-4
Omori, Y., Tokonami, S., Sahoo, S.K., Ishikawa, T., Sorimachi, A., Hosoda, M., Kudo, H., Pornnumpa, C., Nair, R.R.K., Jayalekshmi, P.A. and Sebastian, P., 2016. Radiation dose due to radon and thoron progeny inhalation in high-level natural radiation areas of Kerala, India. Journal of Radiological Protection, 37(1), p.111. https://doi.org/10.1088/1361-6498/37/1/111
Özdiş, B.E., Çam, N.F. and Canbaz Öztürk, B., 2017. Assessment of natural radioactivity in cements used as building materials in Turkey. Journal of Radioanalytical and Nuclear Chemistry, 311(1), pp.307-316. https://doi.org/10.1007/s10967-016-5074-0
Özen, S.A., Celik, N., Dursun, E. and Taskın, H., 2018. Indoor and outdoor radon measurements at lung cancer patients' homes in the dwellings of Rize Province in Turkey. Environmental geochemistry and health, 40(3), pp.1111-1125. https://doi.org/10.1007/s10653-017-9991-9
Park, J.H., Lee, C.M., Lee, H.Y. and Kang, D.R., 2018. Estimation of seasonal correction factors for indoor radon concentrations in Korea. International journal of environmental research and public health, 15(10), p.2251. https://doi.org/10.3390/ijerph15102251
Preston, D.L., Ron, E., Tokuoka, S., Funamoto, S., Nishi, N., Soda, M., Mabuchi, K. and Kodama, K., 2007. Solid cancer incidence in atomic bomb survivors: 1958–1998. Radiation research, 168(1), pp.1-64. https://doi.org/10.1667/RR0763.1
Rabi, R., Oufni, L. and Amrane, M., 2017. Modeling of indoor ^{222}Rn distribution in ventilated room and resulting radiation doses measured in the respiratory tract. Journal of Radiation Research and Applied Sciences, 10(3), pp.273-282.https://doi.org/10.1016/j.jrras.2017.05.003
Radolić, V., Vuković, B., Šmit, G., Stanić, D. and Planinić, J., 2005. Radon in the spas of Croatia. Journal of Environmental Radioactivity, 83(2), pp.191-198. https://doi.org/10.1016/j.jenvrad.2005.02.016
Rafique, M., Rehman, H., Malik, F., Rajput, M.U., Rahman, S.U. and Rathore, M.H., 2011. Assessment of radiological hazards due to soil and building materials used in Mirpur Azad Kashmir; Pakistan. https://pesquisa.bvsalud.org/portal/resource/pt/emr-113755

Rahman, S., Mati, N. and Ghauri, B.M., 2007. Seasonal indoor radon concentration in the North West Frontier Province and federally administered tribal areas—Pakistan. Radiation measurements, 42(10), pp.1715-1722. https://doi.org/10.1016/j.radmeas.2007.07.002

Ravisankar, R., Vanasundari, K., Suganya, M., Raghu, Y., Rajalakshmi, A., Chandrasekaran, A., Sivakumar, S., Chandramohan, J., Vijayagopal, P. and Venkatraman, B., 2014. Multivariate statistical analysis of radiological data of building materials used in Tiruvannamalai, Tamilnadu, India. Applied Radiation and Isotopes, 85, pp.114-127. https://doi.org/10.1016/j.apradiso.2013.12.005

Righi, S. and Bruzzi, L., 2006. Natural radioactivity and radon exhalation in building materials used in Italian dwellings. Journal of environmental radioactivity, 88(2), pp.158-170. https://doi.org/10.1016/j.jenvrad.2006.01.009

Roshandel, G., Ghanbari-Motlagh, A., Partovipour, E., Salavati, F., Hasanpour-Heidari, S., Mohammadi, G., Khoshaabi, A., Davanlou, M., Tavangar, S.M. and Abadi, H., 2019. Cancer incidence in Iran in 2014: results of the Iranian National Population-based Cancer Registry. Cancer epidemiology, 61, pp.50-58. https://doi.org/10.1016/j.canep.2019.05.009

Röttger, A., Honig, A., Dersch, R., Ott, O. and Arnold, D., 2010. A primary standard for activity concentration of ^{220}Rn in air. Applied Radiation and Isotopes, 68(7-8), pp.1292-1296.

Sabot, B., Pierre, S., Cassette, P., Michielsen, N. and Bondiguel, S., 2015. Development of a primary thoron activity standard for the calibration of thoron measurement instruments. Radiation protection dosimetry, 167(1-3), pp.70-74. https://doi.org/10.1093/rpd/ncv221

Sainz-Fernandez, C., Fernandez-Villar, A., Fuente-Merino, I., Gutierrez-Villanueva, J.L., Martin-Matarranz, J.L., Garcia-Talavera, M., Casal-Ordas, S. and Quindós-Poncela, L.S., 2014. The Spanish indoor radon mapping strategy. Radiation protection dosimetry, 162(1-2), pp.58-62. https://doi.org/10.1093/rpd/ncu218

Saphymo, 2016. AlphaGUARD: professional Radon monitor from Saphymo.

Saputra, M.A., Nugraha, E.D., Purwanti, T., Arifianto, R., Laksmana, R.I., Hutabarat, R.P., Hosoda, M. and Tokonami, S., 2020. Exposures from radon, thoron, and thoron progeny in high background radiation area in Takandeang, Mamuju, Indonesia. Nukleonika, 65.

Sas, Z., Somlai, J., Szeiler, G. and Kovács, T., 2015. Usability of clay mixed red mud in Hungarian building material production industry. Journal of Radioanalytical and Nuclear Chemistry, 306(1), pp.271-275. https://doi.org/10.1007/s10967-015-3966-z

Schauer, D.A. and Linton, O.W., 2009. NCRP report No. 160, ionizing radiation exposure of the population of the United States, medical exposure—are we doing less with more, and is there a role for health physicists? Health physics, 97(1), pp.1-5.

Schötzig, U. and Debertin, K., 1983. Photon emission probabilities per decay of ^{226}Ra and ^{232}Th in equilibrium with their daughter products. The International Journal of Applied Radiation and Isotopes, 34(2), pp.533-538. https://doi.org/10.1016/0020-708X(83)90275-2

Serge Didier, T.S., Saïdou, Tokonami, S., Hosoda, M., Suzuki, T., Kudo, H. and Bouba, O., 2019. Simultaneous measurements of indoor radon and thoron and inhalation dose assessment in Douala City, Cameroon. Isotopes in environmental and health studies, 55(5), pp.499-510. https://doi.org/10.1080/10256016.2019.1649258

Shahbazi-Gahrouei, D., 2003. Natural background radiation dosimetry in the highest altitude region of Iran. Journal of radiation research, 44(3), pp.285-287. https://doi.org/10.1269/jrr.44.285

Shahbazi Sehrani, M., Boudaqpoor, S. and Mirmohammadi, M., 2019. Measurement of indoor radon gas concentration and assessment of health risk in Tehran, Iran. International Journal of Environmental Science and Technology, 16(6), pp.2619-2626. https://doi.org/10.1007/s13762-018-1715-x

Shahrokhi, A., Nagy, E., Csordás, A., Somlai, J. and Kovács, T., 2016. Distribution of indoor radon concentrations between selected Hungarian thermal baths. Nukleonika, 61(3), pp.333-336. DOI: https://doi.org/10.1515/nuka-2016-0055

Shahrokhi, A., Adelikhah, M., Chalupnik, S., Kocsis, E., Toth-Bodrogi, E. and Kovács, T., 2020. Radioactivity of building materials in Mahallat, Iran–an area exposed to a high level of natural background radiation–attenuation of external radiation doses. Materiales de Construcción, 70(340), pp. e233-e233. https://doi.org/10.3989/mc.2020.03820

Shetty, P.K. and Narayana, Y., 2010. Variation of radiation level and radionuclide enrichment in high background area. Journal of environmental radioactivity, 101(12), pp.1043-1047. https://doi.org/10.1016/j.jenvrad.2010.08.003

Shikha, D., Kaur, R., Gupta, R., Kaur, J., Sapra, B.K., Singh, S.P. and Mehta, V., 2021. Estimation of indoor radon and thoron levels along with their progeny in dwellings of Roopnagar District of Punjab, India. Journal of Radioanalytical and Nuclear Chemistry, 330(3), pp.1365-1381. https://doi.org/10.1007/s10967-021-07993-5

Singh, P., Singh, P., Singh, S., Sahoo, B.K., Sapra, B.K. and Bajwa, B.S., 2015. A study of indoor radon, thoron and their progeny measurement in Tosham region Haryana, India. Journal of Radiation Research and Applied Sciences, 8(2), pp.226-233.

Sohrabi, M., 1993, August. Recent radiological studies of high-level natural radiation areas of Ramsar. In Proceedings of an international conference on high levels of natural radiation, Ramsar, Iran (pp. 39-47).

Sohrabi, M., Babapouran, M., 2005. New public dose assessment from internal and external exposures in low and elevated-level natural radiation areas of Ramsar, Iran, Int. Congr. Ser.1276, 169–174. http://dx.doi.org/10.1016/j.ics.2004.11.102.

Sohrabi, M., 2013. World high background natural radiation areas: Need to protect public from radiation exposure. Radiation Measurements, 50, pp.166-171.

Sohrabi, M.M., Beitollahi, M.M., Lasemi, Y. and Amin, S.E., 1996, October. Origin of a new high level natural radiation area in hot spring region of Mahallat, Central Iran. In Proceedings of the 4th International Conference on High Levels of Natural Radiation. Vienna.

Solak, S., Turhan, Ş., Uğur, F.A., Gören, E., Gezer, F., Yeğingil, Z. and Yeğingil, İ., 2014. Evaluation of potential exposure risks of natural radioactivity levels emitted from building materials used in Adana, Turkey. Indoor and Built Environment, 23(4), pp.594-602. https://doi.org/10.1177/1420326X12448075

Somlai, J., Torma, Á., Dombovári, P., Kávási, N., Nagy, K. and Kovács, T., 2007. Contribution of 222 Rn, 226 Ra, 234 U and 238 U radionuclides to the occupational and patient exposure in Heviz-spas in Hungary. Journal of Radioanalytical and Nuclear Chemistry, 272(1), pp.101-106. https://doi.org/10.1007/s10967-006-6837-9

Song, G., Zhang, B., Wang, X., Gong, J., Chan, D., Bernett, J. and Lee, S.C., 2005. Indoor radon levels in selected hot spring hotels in Guangdong, China. Science of the total environment, 339(1-3), pp.63-70. https://doi.org/10.1016/j.scitotenv.2004.06.026

Sorimachi, A., Tokonami, S., Omori, Y. and Ishikawa, T., 2012. Performance test of passive radon–thoron discriminative detectors on environmental parameters. Radiation measurements, 47(6), pp.438-442. https://doi.org/10.1016/j.radmeas.2012.04.003

Stoulos, S., Manolopoulou, M. and Papastefanou, C., 2003. Assessment of natural radiation exposure and radon exhalation from building materials in Greece. Journal of Environmental Radioactivity, 69(3), pp.225-240. https://doi.org/10.1016/S0265-931X(03)00081-X

Syaeful, H., Sukadana, I.G. and Sumaryanto, A., 2014. Radiometric mapping for naturally occurring radioactive materials (NORM) assessment in Mamuju, West Sulawesi. Atom Indonesia, 40(1), pp.33-39. https://doi. org/10.17146/aij. 2014. 263

Szabó, K.Z., Jordan, G., Horváth, Á. and Szabó, C., 2014. Mapping the geogenic radon potential: methodology and spatial analysis for central Hungary. Journal of environmental radioactivity, 129, pp.107-120. https://doi.org/10.1016/j.jenvrad.2013.12.009

Szeiler, G., Somlai, J., Ishikawa, T., Omori, Y., Mishra, R., Sapra, B.K., Mayya, Y.S., Tokonami, S., Csordás, A. and Kovács, T., 2012. Preliminary results from an indoor radon thoron survey in Hungary. Radiation protection dosimetry, 152(1-3), pp.243-246. https://doi.org/10.1093/rpd/ncs231

Szerbin, P., Köteles, G. and Stúr, D., 1994. Radon concentrations in Rudas thermal bath, Budapest. Radiation Protection Dosimetry, 56(1-4), pp.319-321. https://doi.org/10.1093/oxford

The Council of European union, 2014. Council directive 2013/59/EURATOM, Official Journal of the European Union. L13, 1-73.

Tanasković, I., Golobocanin, D. and Miljević, N., 2012. Multivariate statistical analysis of hydrochemical and radiological data of Serbian spa waters. Journal of Geochemical Exploration, 112, pp.226-234. https://doi.org/10.1016/j.gexplo.2011.08.014

Tokonami, S., Yang, M. and Sanada, T., 2001. Contribution from thoron on the response of passive radon detectors. Health physics, 80(6), pp.612-615. DOI:10.1097/00004032-200106000-00014

Tokonami, S., 2020. Characteristics of thoron (^{220}Rn) and its progeny in the indoor environment. International Journal of Environmental Research and Public Health, 17(23), p.8769. https://doi.org/10.3390/ijerph17238769

Turhan, Ş. and Varinlioğlu, A., 2012. Radioactivity measurement of primordial radionuclides in and dose evaluation from marble and glazed tiles used as covering building materials in Turkey. Radiation protection dosimetry, 151(3), pp.546-555. https://doi.org/10.1093/rpd/ncs041

Tuo, F., Peng, X., Zhou, Q. and Zhang, J., 2020. Assessment of natural radioactivity levels and radiological hazards in building materials. Radiation Protection Dosimetry, 188(3), pp.316-321. https://doi.org/10.1093/rpd/ncz289

UNSCEAR, 1993. Sources, effects and risks of ionizing radiation. United Nations Scientific Committee on the Effects of Atomic Radiation, United Nations New York

UNSCEAR, 2008. Sources and effects of ionizing radiation. New York (NY): United Nations Publications. Scientific Committee on the Effects of Atomic Radiation.

UNSCEAR 2000. Sources and effects of ionizing radiation: sources (Vol. 1). United Nations Publications.

U.S. Environmental Protection Agency (EPA)., 2003. EPA assessment of risks from radon in homes. Office of Radiation and Indoor Air, Washington DC, EPA 402-R-03-003.

Vaeth, M. and Pierce, D.A., 1990. Calculating excess lifetime risk in relative risk models. Environmental Health Perspectives, 87, pp.83-94. https://doi.org/10.1289/ehp.908783

Valentin, J., International Commission on Radiological Protection., 2007. The 2007 recommendations of the International Commission on Radiological Protection. Annals of the ICRP.

Vaupotič, J., Gregorič, A., Kobal, I., Žvab, P., Kozak, K., Mazur, J., Kochowska, E. and Grządziel, D., 2010. Radon concentration in soil gas and radon exhalation rate at the Ravne Fault in NW Slovenia. Natural hazards and earth system sciences, 10(4), pp.895-899.

Walczak, K., Olszewski, J. and Zmyslony, M., 2016. Estimate of radon exposure in geothermal spas in Poland. International Journal of Occupational Medicine and Environmental Health, 29(1), p.161. http://dx.doi.org/10.13075/ijomeh.1896.00404

Wang, S., Ye, C., Liu, J., Lin, P., Liu, K., Dong, P., Sun, Y., Liu, Y., Wang, L. and Wang, G., 2017. Natural radioactivity of geothermal water in Beijing, China. Journal of Radioanalytical and Nuclear Chemistry, 314(3), pp.1547-1555. https://doi.org/10.1007/s10967-017-5541-2

Wei, L.X. and Yuan, Y.L., 1998. Problems concerning dose assessments in epidemiology of high background radiation areas of Yangjiang, China. Radiation protection dosimetry, 77(1-2), pp.113-117. https://doi.org/10.1093/oxfordjournals.rpd.a032281

WHO, 2009. WHO handbook on indoor radon: a public health perspective. Geneva: WHO.

Yarahmadi, M., Shahsavani, A., Mahmoudian, M.H., Shamsedini, N., Rastkari, N., Kermani, M., 2016. Estimation of the residential radon levels and the annual effective dose in dwellings of Shiraz, Iran, in 2015, Electron. Phys. 8, 2497–2505. Doi: 10.19082/2497

Yu, C., LePoire, D.J., Cheng, J.J., Gnanapragasam, E., Kamboj, S. and Arnish, J., 2003. User's manual for RESRAD-BUILD Ver. 3. ANL/EAD/03-1. Argonne, Illinois. https://doi.org/10.2172/813697

Zhang, L.; Wu, J.; Guo, Q. and Zhuo, W., 2010. Measurement of thoron gas in the environment using a Lucas scintillation cell. Journal of Radiological Protection, 30(3), p. 597. doi:10.1088/0952-4746/30/3/013

Zhao, C., Zhuo, W., Chen, B. and Zhang, H., 2010. Characteristic and performance of a simple thoron chamber. Radiation protection dosimetry, 141(4), pp.444-447. https://doi.org/10.1093/rpd/ncq250

Zölzer, F., Hon, Z., Skalická, Z.F., Havránková, R., Navrátil, L., Rosina, J. and Škopek, J., 2013. Micronuclei in lymphocytes from radon spa personnel in the Czech Republic. International archives of occupational and environmental health, 86(6), pp.629-633. https://doi.org/10.1007/s00420-012-0795-z